5-2015

Altitudinal Variability of Quiet-Time Plasma Drifts in the Equatorial Ionosphere

Debrup Hui
Utah State University

ALTITUDINAL VARIABILITY OF QUIET-TIME PLASMA DRIFTS IN THE EQUATORIAL IONOSPHERE

by

Debrup Hui

A dissertation submitted in partial fulfillment
of the requirements for the degree

of

DOCTOR OF PHILOSOPHY

in

Physics

Approved:

Bela Fejer Major Professor	Robert Schunk Committee Member
Michael Taylor Committee Member	Ludger Scherliess Committee Member
David Geller Committee Member	Mark McLellan Vice President for Research and Dean of the School of Graduate Studies

UTAH STATE UNIVERSITY
Logan, Utah

2015

ABSTRACT

Altitudinal Variability of Quiet-time Plasma Drifts
in the Equatorial Ionosphere

by

Debrup Hui, Doctor of Philosophy
Utah State University, 2015

Major Professor: Bela Fejer
Department: Physics

The plasma drifts or electric fields and their structures in the ionosphere affect the accuracy of the present-day space-based systems. For the first time, we have used ionospheric plasma drift data from Jicamarca radar measurements to study the climatology of altitudinal variations of vertical and zonal plasma drifts in low latitudes during daytime. We used data from 1998 to 2014 to derive these climatological values in bimonthly bins from 150 km to 600 km. For the vertical plasma drifts, we observed the drifts increasing with altitudes in the morning and slowly changing to drifts decreasing with altitude in the afternoon hours. The drifts change mostly linearly from E- to F-region altitudes except in the morning hours of May-June when the gradients are very small. The zonal drifts show a highly nonlinear increase in the westward drifts at the lower altitudes and then increase slowly at the higher altitudes. We see a break in the slopes at lower altitudes during the morning hours of March-April and May-June. The E-region zonal drifts, unlike vertical drifts, show a very large variability compared to F-region drifts. We also explored the altitudinal profiles of vertical drifts during late afternoon and evening hours when the electrodynamic properties in the ionosphere change rapidly. For the first time using drifts up to 2000 km, we have shown the drifts increase and decrease below and above the F-region peak before becoming height independent. These structures arise to satisfy the curl-free condition of electric fields

in low latitudes. The altitudinal gradients of vertical drifts are balanced by a time derivative of the zonal drifts to satisfy the curl-free condition of electric fields. We have shown how these structures evolve with local time around the dusk sector and change with solar flux. During solar minimum, the peak region can go well below 200 km. The present-day electric field models do not incorporate these gradients, particularly in the evening sectors when they change very rapidly. Very often their results do not match with the observations. Including these gradients along with proper magnetic field models will improve the model results and accuracy of our navigation, communication, and positioning systems.

(113 pages)

PUBLIC ABSTRACT

Altitudinal Variability of Quiet-time Plasma Drifts in the Equatorial Ionosphere

In the modern world, we increasingly depend on space-based systems for our communication, positioning, and navigation systems. These systems depend on electromagnetic waves propagating through the ionosphere. The ionosphere is the medium in the upper atmosphere where, due to presence of the charged atomic and molecular particles and electrons collectively known as plasma, it influences the traveling electromagnetic waves following laws of electrodynamics. Improved models for predicting space weather conditions require improved knowledge of the drifts of these plasmas in the ionosphere. This study is focused on climatology of the altitudinal variations of these plasma drifts in the equatorial latitudes. We used vertical and zonal plasma drift data measured by Jicamarca radars from 150 km to about 600 km altitude in bimonthly bins. One of the objectives of this study is to understand the relationship between E- and F-region drifts during the daytime. The vertical drifts, in general increase with altitude in the morning hours and decrease with altitude in the afternoon. The vertical drifts change mostly linearly from E- to F-region altitudes except in the morning hours of May-June when the gradients are very small. The zonal drifts, on the other hand, show large nonlinear decrease with altitude at the lower altitudes and then slowly decrease with increasing height. We also observed occasional exceptions to these general patterns, especially in the morning hours of March-April and May-June. The E-region zonal drifts show more day-to-day variability compared to higher altitudes. The altitudinal variations during the special periods, known as sudden stratospheric warming periods, have also been studied. While the altitudinal variations do not change much for vertical drifts, the sudden stratospheric events do not seem to affect zonal drifts much.

We also presented altitudinal variations of vertical plasma drifts during late afternoon and evening time when these variations change more rapidly compared to the daytime. For the first time, we presented observations of drifts up to 2000 km altitude. We found that

during the evening prereversal enhancement, the drifts increase with altitude up to the F-region peak, above which the drifts decrease with altitude until a height from where they become height independent. This transition from height-dependent to height-independent drifts seems to increase with increasing solar flux. We also addressed the relationship between the vertical and zonal plasma drifts and how the time derivatives of zonal drifts balance the altitudinal gradients of vertical plasma drifts. Neglecting these altitudinal variations would violate the curl-free condition of the electric field in the ionosphere; and thus, these variations are important to be incorporated in the present ionospheric models to improve space weather predictions.

Debrup Hui

To my mother who first taught me to look at the stars . . .

ACKNOWLEDGMENTS

This dissertation, which documents my PhD research work, would not have been possible without the support of many people during my graduate studies. On completion of my degree, I take this opportunity to recognize their contributions in my own way. I would like to express my deepest gratitude to my research advisor, Prof. Bela G. Fejer, who not only guided me every day throughout this period to get the results presented in this dissertation, but also taught me how to keep a strong vision in my professional life. Thank you, Bela.

I also thank my other committee members, Prof. Robert Schunk, Prof. Mike Taylor, Prof. Ludger Scherliess, and Prof. David Geller for their time and advice from time to time. I feel highly indebted to Prof. Schunk and Prof. Taylor for their immense support during my initial days as a graduate student in the Physics Department. I would like to express special thanks to Prof. Scherliess and Dr. Vince Eccles for their valuable discussions and guidance from time to time on my research.

I take this opportunity to express appreciation to the staff of the Jicamarca Radio Observatory for their immense effort in collecting the data I used for my work. This research work was supported by the Aeronomy Program, Division of Atmospheric Sciences of the National Science Foundation through grant AGS-1068104 and by NASA through grant NNH12CF02C. I would also like to thank Prof. Dibyendu Chakrabarty from the Physical Research Laboratory, India, for numerous discussions on basic materials for an understanding of the subject.

When I was busy working on my research and presentations in my lab, the staff of the Center for Atmospheric and Space Sciences and the Physics Department kept my administrative requirements smooth and almost invisible. Thank you Shawna, Melanie, Karalee, and Sharon.

Being away from my family, I must thank my parents and family for allowing me the opportunity to travel and explore what I wanted when they took care of all responsibilities back home. Their constant support and inspiration kept me motivated. I miss my

elder brother and sister, who are not with me today to see and share this day; but, their inspirations and sacrifices for me will keep me going throughout my life.

Last, but not least, I am very thankful to my colleagues, Dr. Michael Olson and Brian Tracy, and my friends Prajwal Kasturi , Amrita Ghosh Dastidar, and Ashish Raj for their constant support and company in all seasons.

Debrup Hui

CONTENTS

LIST OF TABLES

LIST OF FIGURES

CHAPTER 1

INTRODUCTION

1.1. The Earth's Atmosphere

The Earth's atmosphere is the gaseous region surrounding the solid or ocean surface and extending up to a few hundred kilometers. From ground to about 90 km is a very dense and homogeneous mixture of various gases.

The neutral atmosphere can be stratified into different sublayers depending on the changing temperature gradients. From ground up to around 10 km is called the troposphere, where the temperature reduces with height at the lapse rate of 7 K/km. The troposphere ends at the tropopause, an overlapping region, which separates the troposphere from the layer above. From 10 km to up to 50 km is a region of increasing temperature, called the stratosphere, mainly because of absorption of solar ultraviolet radiation by the ozone layer, which maximizes at around 50 km. The stratopause marks the end of the stratosphere. The region up to around 90 km is called the mesosphere. Here the temperature again reduces with height because of radiative cooling. The mesopause separates the mesosphere from its overlying layer, the thermosphere, where again the temperature rises exponentially because of absorption of higher energetic parts of solar radiation until the temperature reaches a steady value of above 1000 K at an altitude of around 500 km. Figure 1.1, adopted from *Kelley* [2009], shows such a midlatitude atmospheric temperature profile.

From 90 km to 500 km is a region of increasing temperature called the thermosphere. Here neutral particles maintain diffusive equilibrium, which means the vertical distribution of the neutrals is governed by respective masses (under gravity) of the species. The region around 90 km, which separates the lower homogeneous atmosphere from the thermosphere, is called the turbopause. Below the turbopause, the neutral atmosphere is mostly homogeneous because of the turbulent mixing of gases.

1.2. Ionosphere

The solar radiation penetrates the topside of the atmosphere and gets absorbed by the

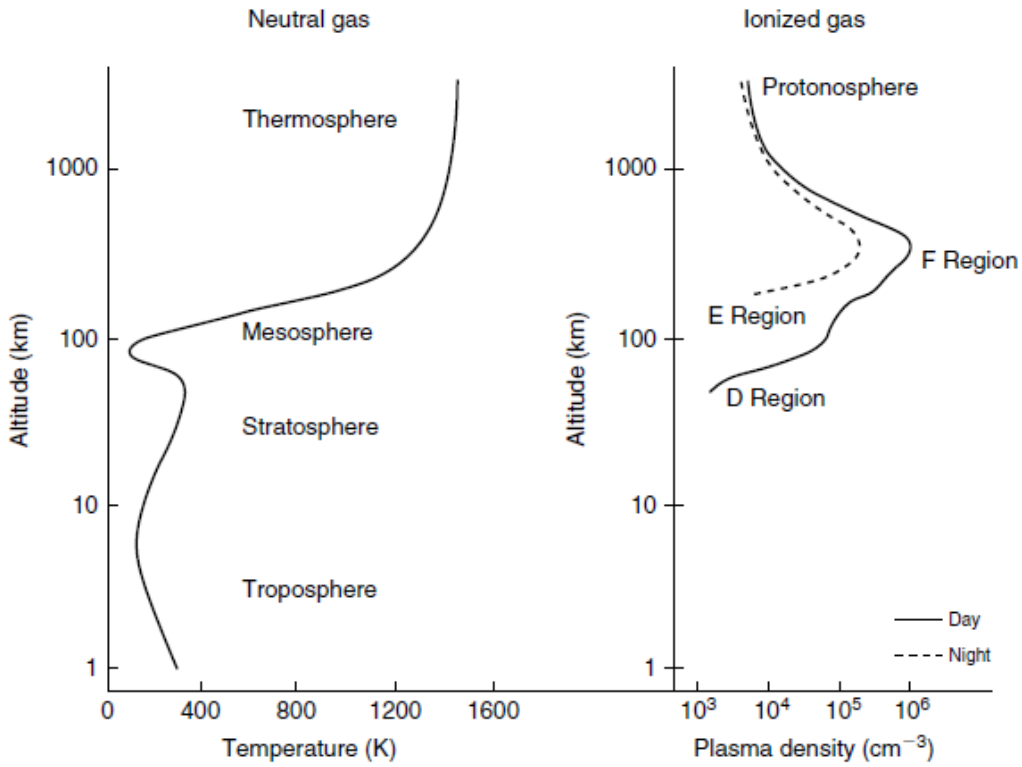

Figure 1.1. Typical temperature profile of neutral atmosphere with height (left). Plasma density profile of day and nighttime ionosphere (right) reproduced from *Kelley* [2009].

constituent gases at different altitudes. The solar radiations, for example, cause heating and photoionization. Above 60 km, such ionization produces charged particles, referred to as plasma. This region from around 60 km to 1000 km, where the plasma, in spite of having very small population (compared to neutrals), can alter the behavior of this part of the atmosphere and affect radio communications, is generally referred to as the Ionosphere. Because of absorption of different parts of solar radiation spectra at different altitudes, which produces equilibrium with electron-ion recombination and diffusive transport, the ionosphere can be divided into different layers with individual peak densities and dominant ion species. Traditionally the ionosphere is divided into D (60-90 km), E (95-150 km), and F ($>$ 150 km) regions. The F region is often split into F_1 and F_2 regions on the day side. On the night side, in the absence of the ionizing solar radiation and for reasons explained later, the D region disappears, the E region eagerly fades away, and F_1 and F_2 combine to

form a single F layer. Typical midlatitude plasma profiles of day and night-side ionosphere are shown in Figure 1.1 (right).

It is important to note that throughout the ionosphere, though the number of neutrals is more than ions or electrons, the number density of positive ions is equal to the number density of electrons, thus maintaining a charge-neutrality condition [*Kelley*, 2009]. All the plasma parameters (e.g., density, peak density height, and plasma temperature) mentioned above show substantial variations with latitude, longitude, local time, season, solar cycle, and magnetic activities. The day-to-day variability of the ionosphere can go up to 30% of climatological averages from standard models like the International Reference Ionosphere (IRI) model even during magnetically quiet conditions [*Bilitza et al.*, 1988].

When neutral winds carry charged ions and electrons along with it across the Earth's magnetic field (**B**), it produces a (e.m.f.) current following Faraday's law and, the process is called ionospheric dynamo. Such processes exist in both E and F layers of the ionosphere, but the E- and F-region dynamos operate in rather different ways [*Rishbeth*, 1997], as we will discuss in Chapter 3. These dynamo processes cause plasma to drift in directions perpendicular to the Earth's **B** field. Just like geographical coordinates on the ground, it is conventional to divide and distinguish between the high-, mid- and low-geomagnetic latitudes of the ionosphere because of the different processes dominating electrodynamics in these different regions. High latitudes (above 60^0) are exposed to the outer magnetosphere through open magnetic field lines at the poles. Momentum and energy dominating the electrodynamic processes in this region come mostly from the outer magnetosphere through particle precipitation and the connecting electric field. These drive the high-latitude convections and currents and cause phenomena like Joule heating and aurora in the high latitudes. The mid (from 60^0 to 30^0) and low latitudes (below 30^0) are shielded from magnetospheric energy dynamics at ordinary times, but during geomagnetic disturbances, magnetospheric perturbations penetrate down to equatorial latitudes. During geomagnetic quiet times, the neutral wind-driven dynamos, mentioned above, dominate the electrodynamics in the mid and low latitudes. The E- and F-region dynamos, connected to each other through the

Earth's magnetic field lines, cause the plasma to drift in the direction perpendicular to the Earth's magnetic fields in the F region with a velocity given by

$$(\mathbf{V_i})_\perp = \frac{\mathbf{E} \times \mathbf{B}}{B^2}, \tag{1.1}$$

where $\mathbf{V_i}$, $\mathbf{E}$, and $\mathbf{B}$ are plasma drift velocity, electric, and magnetic field vectors, respectively. So by measuring the perpendicular drifts, we can get the ambient electric field as

$$\mathbf{E}_\perp = -\mathbf{V_i} \times \mathbf{B}. \tag{1.2}$$

The special feature of the equatorial region is that the Earth's magnetic field lines are horizontal to the Earth's surface; and as a result, the perpendicular to $\mathbf{B}$ drifts are vertically upward drifts and zonal (east-west) drifts. This dissertation focuses mainly on distributions and flow of ionospheric plasmas in the equatorial latitudes and their variations with altitudes.

Low-latitude drifts have been studied over the last four decades by ground-based [*Abdu*, 1997; *Fejer*, 1991; *Fejer et al.*, 1979, 1981; *Woodman*, 1970] and space-based systems [*Coley et al.*, 2014; *Fejer et al.*, 1995, 2013; *Hartman and Heelis*, 2007; *Immel et al.*, 2004; *Scherliess and Fejer*, 1999]. These drifts depend on season, solar activity, magnetic activity, longitude, time of the day, and altitude (as we will see in this study). Empirical models have also been developed for these drifts [*Fejer et al.*, 2005; *Scherliess and Fejer*, 1999]. Detailed knowledge about these drifts/electric fields with respect to local time, season, solar activity, and varying geomagnetic conditions is important to determine ionospheric effects on space-based communication, navigation, and positioning systems.

1.3. An Overview of This Work

In the previous section, we have seen how we can derive electric fields by measuring plasma drifts perpendicular to magnetic field. This dissertation focuses on studying how this low-latitude electric field varies with altitude with respect to local time and season. Only geomagnetically quiet-time ($K_p \leq 3$) studies are investigated in this study. Effects of high-

latitude electrodynamics, which especially influence plasma distribution and transportation during geomagnetically active conditions, have not been considered. Post-sunset irregularity process, like equatorial spread F (ESF), has not been included for the present study.

For this present study, we have used data from incoherent scatter radar (ISR) at Jicamarca, Lima, Peru, which measures plasma drifts from 200 to 800 km and from about 150 km derived from Doppler echoes measured by Jicamarca Unattended Longtime Ionosphere and Atmospheric (JULIA) radar. Details of measurement techniques and specifications are discussed in detail in Chapter 3.

This dissertation is divided into six chapters. Chapter 2 introduces the most important features of the low-latitude ionosphere. It describes the background physics of the electrodynamics of the equatorial and low-latitude plasma relevant to this research work. Chapter 3 includes the description of the measurement techniques, summary of the previous observations, and theoretical work, as well as the mathematical relationship between vertical and zonal drifts. Chapter 4 describes the climatology of daytime vertical and zonal drifts with altitude combining data from Incoherent Scattered Radar (ISR) and Jicamarca Unattended Long-term Ionosphere and Atmosphere (JULIA) radar at Jicamarca, Peru. We will focus on 150 km region JULIA drifts and their differences from F-region drifts. In Chapter 5, we discuss the evening time altitudinal variations of equatorial plasma drifts. We will present the first observations of the top side (up to about 2000 km) drifts and discuss the special features of these evening time drifts and the relationship between vertical and zonal drifts in light of previous work. Chapter 6 summarizes the most important results and the importance of altitudinal gradients in the vertical and zonal plasma drifts in the ionosphere. The importance of incorporating these corrections in the present ionospheric electric field models and their effect on the space-based communication, navigation, and positioning systems are briefly discussed. Some suggestions for future work are included at the end.

CHAPTER 2

LOW-LATITUDE IONOSPHERE

The ionosphere is made up of charged particles produced by the absorption of solar radiation at different regions in the atmosphere. The production, loss, and transport processes of this ionospheric plasma dictate the electrodynamic properties of the ionospheric plasmas. While production and loss are primarily radiative and chemical processes, transportation is driven by neutral winds, electric fields, and diffusion.

This chapter focuses on the chemical composition of the ionosphere, the most important production and loss processes of ionospheric plasma, and the physical processes responsible for their transportation. We will discuss how the neutral winds drive the plasma across magnetic field lines by dynamo actions and the role played by the Earth's magnetic field lines at different altitudes and different latitudes.

2.1. Production, Loss and Transport in Ionosphere-Thermosphere System (ITS)

2.1.1. Production and Loss Processes

Figure 2.1 shows a typical daytime composition of ions and neutrals in the ionosphere-thermosphere system. From ground up to 120 km, N_2 and O_2 maintain a ratio of 4:1. Atomic O number density crosses O_2 density at 120 km and that of N_2 at 250 km. From the base of the thermosphere NO^+ and O_2^+ dominate the ion population up to around 150 km where O^+ becomes the most dominant ion species. From about 900 km H^+ becomes the most dominant ion species followed by He^+ and O^+. More details about the temperature and compositional structure of the ionosphere can be found in *Kelley* [2009].

The D region is created when NO absorbs solar X-ray (0.1-0.8 nm), H Ly α (121.6 nm) and by cosmic rays. Solar X-ray (0.8-14 nm) and UV radiation (79.6-102.7 nm) ionize the neutral particles to form the E region. F region is produced mainly by radiation in the range of 14-79.6 nm. On the dayside, the F region is split into two sublayers, F_1 and F_2 depending on its major constituents. Beyond the direct photoionization of neutral particles

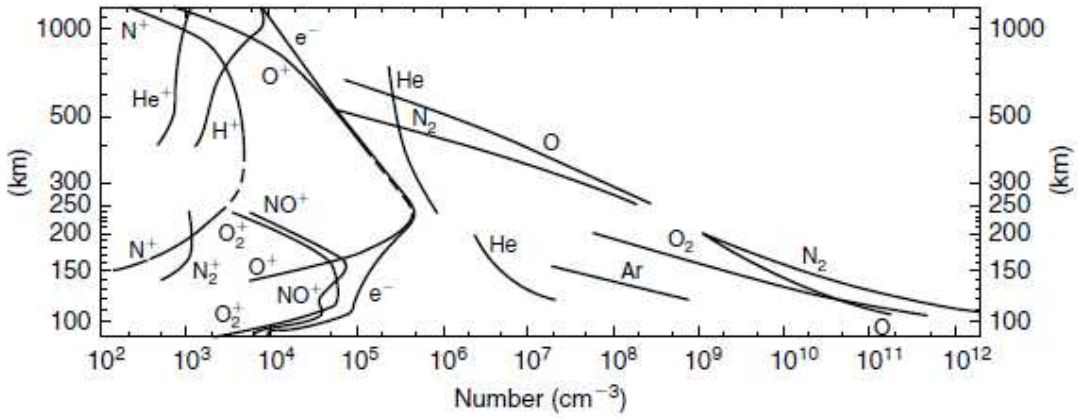

Figure 2.1. Typical daytime composition of IT system during solar quiet year (after *Johnson*, 1969 with permission).

by solar UV and x-ray spectrum, the next important process is the creation of ions through interaction of ions, neutrals, and electrons.

Molecular ions like NO^+ and O_2^+, which dominate the E and lower F regions (below 200 km) are produced by the following reactions:

$$N_2 + O^+ \rightarrow NO^+ + N. \tag{2.1}$$

$$N_2^+ + O \rightarrow NO^+ + N. \tag{2.2}$$

$$O_2 + O^+ \rightarrow O_2^+ + O. \tag{2.3}$$

O^+ is most dominant above the F-region peak up to about 900 km. In the molecular ion-dominated regions, ion-neutral chemistry and electron-ion recombination are the dominant processes, and the loss rate follows square law (loss is proportional to the square of neutral density), whereas the upper F region, where diffusion rate becomes comparable with chemical loss rate, follows linear loss rate. This transition from the square to the linear loss process takes place around 160-200 km. On the dayside, when F layer splits into F_1 and F_2 layers, F_1 is dominated by molecular ions, whereas F_2 consists mainly of atomic ions. Few important characteristics of different ionospheric layers are summarized in Table 2.1.

Table 2.1. Important Characteristics of Different Ionospheric Layers

Layer	Altitude (km)	Major Ion	Production
D	60-90	NO^+ , O_2^+	Ly α , x-rays
E	90-150	NO^+ , O_2^+	Ly β , soft x-rays
F_1	150-200	O^+ ,NO^+	He II, UV
F_2	200-400	O^+ ,N^+	He II, UV

The D region disappears on the night side in the absence of ionizing solar radiation and because of recombination effects. The molecular ions have faster (about 1000 times) recombination rates than higher altitude atomic ions. The two most important ion loss reactions in the ionosphere are:

$$NO^+ + e^- \rightarrow N + O \quad (below 200km), \tag{2.4}$$

and

$$O^+ + e^- \rightarrow O + photon \quad (above 200km). \tag{2.5}$$

This explains the fading away of D- and E-region plasma densities after sunset when O^+, having longer lifetime, survives the night in F-region altitudes. The E-region plasma density decreases by a factor of 10 soon after sunset before reaching a minimum equilibrium. The F_1 layer, if present, fades away into the F_2 region after sunset to form a single F region. The F_2 layer, on the other hand, has a peak density at around 300 km during the day and at higher altitudes at night. Because of transport processes, the peak density of the F region increases shortly after sunset before decreasing to a nighttime value [*Rich and Basu*, 1985].

Above F-region peak, charge exchange reactions like

$$O^+ + H \leftrightarrow O + H^+ \tag{2.6}$$

become important. Details of important photoionization and ionospheric chemistry reactions can be found in *Hudson* [1971], *Torr* [1979], and *Schunk and Nagy* [2009].

Above F-region peak, generally referred to as Topside Ionosphere, the plasma density

decreases exponentially with height. The middle and low latitudes (below 60^0 magnetic latitudes) trap the ions, especially hydrogen, along the geomagnetic fields and thus, the ionosphere extends further out in space. This region is called the plasmasphere [*Carpenter and Park*, 1973].

The temporal variation of plasma throughout the Ionosphere-Thermosphere system depends upon production, loss, and transportation processes, which in turn are functions of solar radiation, local time, geomagnetic field, latitude, longitude, season, and solar activity.

2.1.2. Transport Processes

Neutral Wind Effects

Because of the vast horizontal extent of the atmosphere compared to vertical extent, neutral motions and thus, upper atmospheric winds, are mostly constrained in the horizontal (zonal and meridional winds) direction; vertical winds contribute only about 1% of the total winds in the atmosphere. The primary driving force for thermospheric winds is the diurnal absorption of solar UV rays, which expands the day side thermosphere and creates a day-to-night pressure gradient [*Richmond*, 1995]. The meridional winds can move the plasma up and down the magnetic field lines because of the collisional drag between neutrals and plasma [*Rishbeth*, 1977, 1998]. Thus the meridional winds can shift the F region up or down in the off-magnetic equatorial latitudes where the field lines are not horizontal [*Krishna Murthy et al.*, 1990]. During daytime, meridional winds blow from the hotter magnetic equator toward poles and in the reverse direction at night. The zonal winds, on the other hand, are westward during the day and eastward during night. At E-region altitudes the ions move freely with the neutral winds across the Earth's magnetic field, thereby creating a dynamo action. This is called E-region dynamo and is active only during the day. The resulting electric fields can drive **E x B** plasma drifts in both E and F regions [*Evans*, 1978]. During nighttime, because of fast recombination of molecular ions with electrons in E region, the E region has negligible charge density and thus, no current flows. The E- and F-region dynamo will be described in more detail in section 2.2.

Ionospheric currents associated with the neutral wind-driven dynamo actions have regular, smooth, daily variations. The main part of these currents is called Sq (solar quiet) or solar regular. A steady wind and atmospheric tides contribute to this Sq current. *Sabben* [1962] first showed that a steady ionospheric wind can produce Sq-like currents. Further studies indicate the steady winds contribution to the ionospheric currents is very small [*Kato*, 1957; *Richmond et al.*, 1976] and the bulk of Sq is produced by atmospheric tides of different modes. Atmospheric tides [*Chapman and Lindzen*, 1970; *Kato*, 1980] are periodic global oscillations particularly of period one (diurnal) or half (semi-diurnal) of a solar day forced by a regular periodic source like the sun or the moon. The solar tides are generated because of differential thermal heating by sun, whereas lunar tides are mostly due to gravitational forces. Such tides propagate vertically and grow in amplitude, as the atmospheric density reduces, before breaking down and transferring their energy and momentum into the medium. They modulate the flow of plasma in the lower thermosphere. From a detailed study on atmospheric tides and their effects on ionospheric currents, *Richmond et al.* [1976] showed atmospheric tides with modes (1, -2)* and (2, 4) can account for practically all the Sq currents. Mode (1, -2)* is a diurnal tide, which originates at the equator because of local heating. They discuss simulation results of how (1,-2)* mode tidal wind pattern generate different current functions at different latitudes. These simulations take into consideration the height-integrated ionospheric conductivities along with ion drag, viscosity, and wind velocities. (2, 4) tidal mode is observed from the temperature and velocity variations in the E region [*Bernard and Spizzichino*, 1971; *Murphy and Bull*, 1968]. Dissipative forces as ion drag and viscosity are not important like (1, -2)* because of lower altitude origin (refer to *Richmond et al.* [1976] for detail). A few important horizontal uniform atmospheric tides of different modes and of solar ($S_{m,n}$) and lunar ($L_{m,n}$) origin are given in Table 2.2 (here subscripts m refers to longitudinal wave number and n refers to an index for latitudinal structure). Since the atmosphere is not uniform, in reality different complicated combinations of these modes can exist. *Forbes and Vial* [1989, 1991] have calculated such realistic structures. Detailed study of different modes of atmospheric tides and their effect can be

found in *Hines* [1965], *Richmond* [1995], *Richmond et al.* [1976], and *Volland* [1997]. More recent studies based on NCAR thermosphere ionosphere electrodynamics general circulation model (TIEGCM) describe how diurnal, semi-diurnal, migrating, and nonmigrating tides affect the transportation of plasma in ionosphere (e.g., *Fesen et al.*, 2000; *Hagan et al.*, 2007; *Liu and Richmond*, 2013; *Liu et al.*, 2013).

Table 2.2. Different Types of Tides that Produce Currents in the Ionosphere

Modes	Symmetry about equator	Vertical Propagation	Comments
$S_{1,-2}$	Symmetric	No	Driven by local heating. Largest winds at the high altitudes
$S_{1,-1}$	Anti-symmetric	No	Driven by local heating
$S_{1,1}$	Symmetric	Yes	Largest winds at low latitude. Vertical wavelength 24 km
$S_{2,2}$	Symmetric	above 110 km	Winds larger at low latitudes
$S_{2,3}$	Anti-symmetric	Yes	Vertical wavelength(VW) 60 km
$S_{2,4}$	Symmetric	Yes	Larger at upper mid-latitudes. VW 45 km
$L_{2,2}$	Symmetric	Yes	Period :12.42 h. Similar to $S_{2,2}$

Smaller-scale tidal waves called gravity waves with a period of few hours have also been detected, which also propagate and release their energy into the lower thermosphere on nonlinear breakdown. Atmospheric gravity waves can affect low-latitude F-region electrodynamics [*Chakrabarty et al.*, 2004; *Nicolls and Kelley*, 2005]. Planetary waves with time periods of 2, 5, and 16 days have also been found to modulate plasma drifts in the ionosphere too. *Hagan et al.* [1993] show through modeling that such waves can penetrate well into the dynamo region.

Electrodynamic Effect of Geomagnetic Fields

The variations in ionospheric parameters like density, plasma temperature, peak heights,

and currents mentioned before result not only from ionosphere-thermosphere coupling mechanisms, but also due to ionospheres coupling to solar-terrestrial system including sun, magnetosphere, and interplanetary regions. When solar radiation remains the primary source of energy, the magnetospheric electric fields, particle precipitation, and consequent joule heating at high latitudes also affect the distribution of ionospheric plasmas. The solar wind dynamic pressure and orientation of interplanetary magnetic field dictates the magnetospheric effect on ionosphere. Such magnetospheric processes not only affect the high-latitude ionosphere through open field lines, but also middle- and low-latitude ionosphere, especially during geomagnetic storms. Also upward propagating gravity waves and tides from the bottom-side thermosphere modulate the plasma densities. These different external driving mechanisms combined with the chemical, radiative, and electrodynamical processes within the ionosphere determine the global distribution of plasma densities, temperatures, and drifts [*Schunk and Nagy*, 2009].

The effect of geomagnetic field on different ionospheric layers is also important. In the D region, collision frequency for both ions and electrons with neutrals is more than gyro frequency and thus, collision becomes more important than magnetic field. In the E region, electrons have higher gyro frequency and thus, respond to the geomagnetic field; whereas, ions having higher collision frequency than gyro frequency are still dominated by collisions. In the F region, both ions and electrons have higher gyro frequencies than collision frequency and both are strongly affected by magnetic field effects [*Rishbeth*, 1997].

The latitudinal variation of the strength of Earth's magnetic field (the equatorial field is almost half of the strength at the poles) and orientation (at the magnetic equatorial region the magnetic field lines are horizontal to the Earth's surface, but at the poles they are almost vertical) has great influence in the dynamical processes, thereby modifying the spatial distribution of ionospheric plasma. The ionosphere and thermosphere variables are inherently connected through a feedback mechanism driven by ion-neutral chemistry, winds, waves, and electric and magnetic fields.

2.2. E- and F-Region Dynamos

The ionospheric dynamo theory was first suggested by Balfour Stewart in 1882 to explain the daily variation of geomagnetic fields, which was further developed by A. Schuster in 1908. A good understanding of ionospheric conductivity is made through works of many scientists [*Chapman*, 1956; *Cowling*, 1945; *Maeda*, 1952]. The dynamo theory is explained in many books and review articles like *Maeda and Kato* [1966], *Matsushita* [1969], *Rishbeth and Garriott* [1969], and most recently in *Kelley* [2009].

When neutral winds carry charged ions and electrons along with it across the Earth's magnetic field, it produces a (e.m.f.) current and the process is called ionospheric dynamo process. Such processes exists in both E and F layers of the ionosphere, but the E- and F-region dynamos operate in rather different ways [*Rishbeth*, 1997]. This difference arises because of conductivities, which depend on the ratio of collision frequency to gyro frequency (ν/ω) at different altitudes and on the nature of neutral winds, which drive the drifts, currents, and polarization fields in the ionosphere. During daytime most of the currents flow in the E region at 100-130 km height, but during nighttime the E-region ionization almost disappears and the F-region dynamo at around 300 km carries most of the currents despite small values of $(\nu/\omega)_i$ at these heights.

The conductivity tensor in Cartesian coordinates with geomagnetic field pointing in the third axis is usually defined as [*Rishbeth*, 1997]

$$[\sigma_P] = \begin{pmatrix} \sigma_P & -\sigma_H & 0 \\ \sigma_H & \sigma_P & 0 \\ 0 & 0 & \sigma_0 \end{pmatrix} , \tag{2.7}$$

where σ_0, σ_P and σ_H are called direct or longitudinal conductivity, the Pedersen or transverse conductivity, and the Hall conductivity. Including both ion and electron (subscripts i and e) currents, they are mathematically given by

$$\sigma_0 = (\frac{N_e}{m_e \nu_e} + \frac{N_i}{m_i \nu_i})e^2. \tag{2.8}$$

$$\sigma_P = \Big[\frac{N_e}{m_e\nu_e}\cdot\frac{\nu_e^2}{(\nu_e^2+\omega_e^2)} + \frac{N_i}{m_i\nu_i}\cdot\frac{\nu_i^2}{(\nu_i^2+\omega_i^2)}\Big]e^2. \tag{2.9}$$

$$\sigma_P = \Big[\frac{N_e}{m_e\nu_e}\cdot\frac{\omega_e^2\nu_e^2}{(\nu_e^2+\omega_e^2)} + \frac{N_i}{m_i\nu_i}\cdot\frac{\omega_i^2\nu_i^2}{(\nu_i^2+\omega_i^2)}\Big]e^2. \tag{2.10}$$

σ_0 is in the direction parallel to the geomagnetic field, **B**, and increases exponentially upwards, though limited, at great heights by ion-electron collisions. The Pedersen conductivity, σ_P, in the direction parallel to **E** and perpendicular to **B** peaks at a level where $(\nu/\omega)_i \approx (\nu/\omega)_e \approx 1$, which usually happens at around 125 km. σ_H in the direction perpendicular to both **E** and **B** is mainly carried by electrons moving in the **E x B** direction and peaks at around 105 km [*Richmond*, 1995; *Rishbeth*, 1997]. To calculate the total current flow, which is valid in low and middle latitudes, height-integrated Pedersen and Hall conductivities defined as $\sum P = \int \sigma_P\, dh$ and $\sum H = \int \sigma_H\, dh$ are generally used.

The neutral-air wind velocity, **U**, blowing across the geomagnetic field, **B**, produces an induced electric field $\mathbf{E_I}$ in **U x B** direction, which is upwards in the magnetic equator. There also exists an electrostatic polarization field, $\mathbf{E_P}$, associated with a distribution of electrostatic charges. The major contributors to this polarization fields are i) fields arising from magnetospheric processes, which enter the Earth's ionosphere through high latitudes and at times of geomagnetic storms, influences mid and low latitudes in a great way, and also from ii) fields originating at remote points to satisfy the current continuity in the dynamo circuit [*Rishbeth*, 1997]. The polarization charges build continuously and adjust themselves to ensure the total current, **J**, is divergence free (div **J** = 0). The current density equation can be written as

$$\mathbf{J} = [\sigma]\cdot(\mathbf{E_I} + \mathbf{E_P}). \tag{2.11}$$

The dynamo action can be described both as a voltage generator (low-impedance sources) or a current generator (high-impedance sources) mechanism. Here voltage generator description is summarized from *Rishbeth* [1997]. The neutral wind, **U**, induces an electric field $\mathbf{E_I} = \mathbf{U\ x\ B}$ as mentioned before. This induced field drives a current,

$\mathbf{J} = [\sigma] \cdot (\mathbf{UxB})$. In general, this current is not divergence free everywhere and electric charges build up whenever div $(\mathbf{J}) = 0$. To satisfy Poisson's law, the charge produces a polarization electric field, $\mathbf{E_P}$, which continuously adjusts itself to make the total current divergence free so that $div([\sigma] \cdot (\mathbf{E_I} + \mathbf{E_P})) = 0$ everywhere. The $\mathbf{E_P}$ makes ions and electrons drift at $\mathbf{V} = \mathbf{E_P} \times \mathbf{B}/|\mathbf{B}|^{\mathbf{2}}$. Though both voltage- and current-generator descriptions of dynamos in principle could be applied for both E and F regions, the voltage-generator description suits more to the E region (low-impedance region) and a current-generator description suits more to the F region (a region with high impedance). In the E layer the induced and polarized fields are comparable in magnitude. During daytime, because of high conductivities in presence of large number of charge carriers, the E-region dynamo dominates (short circuiting the F-region dynamo). At night, in absence of charge carriers, the Hall conductivity decreases more drastically than Pedersen conductivity. As a result, even though the polarization field is maintained, the E-region dynamo becomes very weak at night. At night, the F region has higher (Pedersen) conductivity and thus, the F-region dynamo becomes active at night. The E- and F-region dynamos are linked through geomagnetic field lines. Because of high parallel conductivity along equipotential field lines, any divergence in local currents in F region is shorted by highly conducting E region during daytime. Thus the F-region dynamo is short-circuited by the highly conducting E region. After sunset, however, polarization field builds up in the F region such that drift velocity, $\mathbf{V}$, approaches wind speed, $\mathbf{U}$, thereby opposing dynamo action. Because of the special geometry of the magnetic field lines in the magnetic equatorial region, maximum polarization field is developed, which increases the eastward wind speed at night [*Rishbeth*, 1971].

The neutral wind-driven E- and F-region dynamos interact with each other through the equipotential field lines and create vertical and east-west (zonal) electric field [*Fejer et al.*, 1979]. Due to electrodynamic effects of such fields during daytime, the plasma moves upward in the equatorial latitudes, which diffuse down magnetic field lines to 15^0 magnetic latitude. This phenomenon of upward movement of plasma at equatorial latitudes is known as Fountain effect and the high density at 15^0 is called Appleton anomaly.

Figure 2.2 demonstrates the fountain effect and diffusion along the magnetic field lines (top) and a typical calculated electron density as a function of altitude and dip latitudes at 2000 LT in December solstice conditions (bottom). These fields also drive the equatorial electrojet [*Kelley*, 2009] and F-region plasma motion, thereby affecting the thermosphere neutral winds and composition of low-latitude ionosphere and protonosphere. They are also responsible for generation of E- and F-region plasma irregularities in the post-sunset sector, generally referred as Equatorial Spread F (ESF).

In the F region, because of the field lines, the neutral winds cannot move the electrons with them ($\nu << \omega$), but the electric fields make them drift in the Hall (perpendicular to **E** and **B**) direction. In fact, the plasma drift velocity perpendicular to **B** is given by equation 3.1 in *Kelley* [2009]:

$$(\mathbf{V_i})_\perp = \Big[\mathbf{E} - \Big(\frac{k_B T_i}{q_i}\Big)\frac{\nabla n}{n} + \Big(\frac{M}{q_i}\Big)g\Big] \times \Big[\frac{\mathbf{B}}{B^2}\Big], \tag{2.12}$$

which includes contributions from electric field (1st term), the pressure (2nd term), and the gravity (3rd term). But at a typical height in F region, both pressure and gravity term contribute too small compared to electric field (See Chapter 3 in *Kelley* [2009] for details). As a result, it is mainly the ambient perpendicular electric field that causes the drift

$$\mathbf{E}_\perp = -\mathbf{V_i} \times \mathbf{B}. \tag{2.13}$$

Since this drift is perpendicular to both **E** and **B**, in short, it is referred as **E x B** drift in literature. In the F region, the zonal electric field causes the plasma to drift upward during the day and downward during the night in the low latitudes and the vertical electric field causes zonal drifts, westward during the day and eastward during the night. These electric fields and drifts play very important roles in the ionospheric and plasmaspheric electrodynamic processes. Such fields and drifts can get significantly perturbed by lower atmospheric gravity waves and planetary waves, even during magnetically quiet periods and by magnetospheric processes through high-latitude ionosphere during magnetically dis-

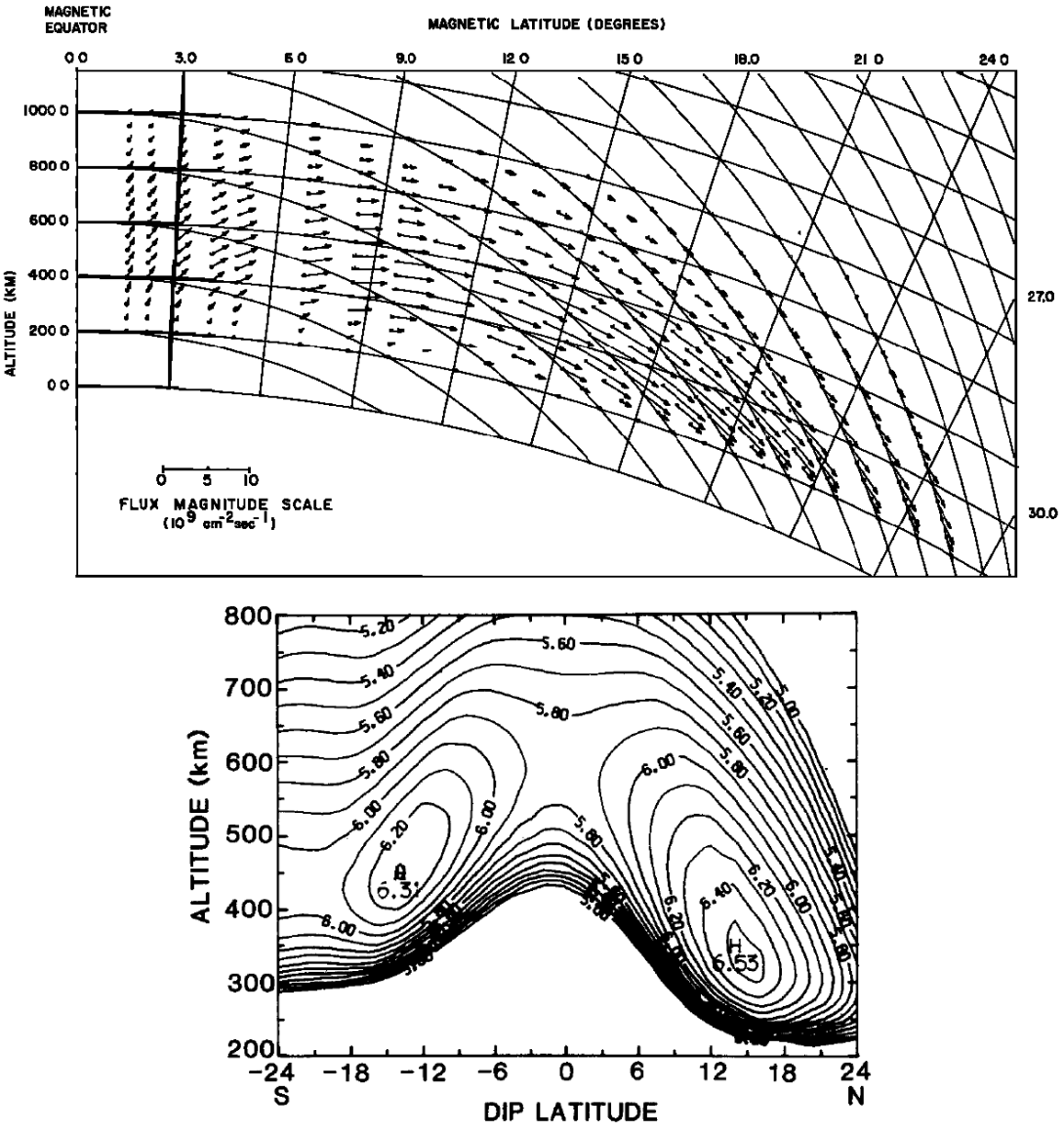

Figure 2.2. (top) Fountain effect and diffusion along the magnetic field lines (after *Hanson and Moffett*, 1966). (bottom) Calculated electron density contours ($\log_{10} e$) as a function of altitude and dip latitude (after *Anderson and Roble*, 1981).

turbed period [*Fejer*, 1997]. Specific knowledge about these drifts is fundamental to the accuracy of the increasing space-based systems [*Fejer*, 2011].

CHAPTER 3
LOW-LATITUDE PLASMA DRIFTS

3.1. Introduction

The **E x B** plasma drifts play very important roles in the electrodynamics and distribution of the plasma in the low latitudes. During day time, the vertical drift (zonal electric field) driven by dynamo action and fountain effect controls the equatorial anomaly crest latitude and density. Around sunset hours, when the electrodynamics and conductivity in the ionosphere changes rapidly causing prereversal enhancement, it controls the altitude of peak F layer, thus influencing the formation of Equatorial Spread F (ESF). These ionospheric electrodynamic processes affect space-based communication and navigation systems.

Low-latitude vertical **E x B** drifts have been studied over the last few decades from ground observations [*Abdu*, 1997; *Fejer*, 1991; *Fejer et al.*, 1979, 1981; *Woodman*, 1970] and space-based systems [*Coley et al.*, 2014; *Fejer et al.*, 1995, 2013; *Hartman and Heelis*, 2007; *Immel et al.*, 2004; *Scherliess and Fejer*, 1999], and their climatology, particularly in the F region, has been well studied [*Fejer*, 1991; *Fejer et al.*, 2008; *Scherliess and Fejer*, 1999]. Most of the ground-based measurements of such drifts at ionospheric heights have been done using Incoherent Scatter Radars (ISR). The Jicamarca incoherent scatter radar (ISR) has been used since 1968 to study these drifts [*Woodman*, 1970].

Low-latitude zonal plasma drifts have also been measured using Jicamarca ISR, but not as often as the vertical drifts. *Fejer and Scherliess* [2001]; *Fejer et al.* [1985, 2005] describe the climatology of zonal plasma drifts using the Jicamarca ISR data on the basis of season, local time, and solar flux. *Valladares et al.* [1996] and *Sheehan and Valladares* [2004] also studied the zonal drifts at nighttime in the Peruvian sector. *Fejer et al.* [2013] describe their longitudinal features during the last solar minimum periods using C/NOFS satellite data. Section 3.2 discusses the climatology of these drifts in detail.

3.2. Quiet-Time Low-Latitude Plasma Drifts

Low-latitude plasma drifts originate as a result of ionospheric electric dynamo process

when neutral winds flow across the horizontal magnetic fields of the Earth. These drifts depend on season, solar activity, magnetic activity, longitude, altitude, and time of the day. The incoherent scatter radar (ISR) at Jicamarca Radio Observatory (JRO) at Lima, Peru (11.9^0N, 76.8^0W, magnetic dip 1^0N) has been used since 1968 to study these drifts [*Woodman*, 1970]. It provides the most extensive plasma drifts database for low latitudes. It consists of three 1.5 MW transmitters and an antenna array of 18,432 dipole elements covering an area of about 85,000 square meters. The radar operates at 50 MHz. The magnetic dip angle of 1^0 for JRO changes with year and altitude. The radar can determine the direction of Earth's magnetic field, **B**, accurately and can make measurements perpendicular to **B** at any altitude in the ionosphere (source: JRO website). The measurement technique is described in detail by *Woodman* [1970, 1971], but the old technique was replaced by a more accurate and novel technique in 1996 as described in *Kudeki et al.* [1999]. The ISR measures F-region (typically between 200-800 km altitude) vertical and zonal plasma drifts with a time resolution of 1-5 min and height resolution of 15-25 km. The data is most accurate near the F-region peak where the signal-to-noise ratio is highest. The typical errors in vertical and zonal drifts are 1 m/s and 10 m/s, respectively, during day and larger at night. Over Jicamarca an upward (eastward) drift of 40 m/s corresponds to an electric field of 1 mV/m in the eastward (downward) direction [*Fejer*, 2011]. The climatology of quiet-time, low-latitude F-region drifts has been studied using Jicamarca data by many [e.g., *Fejer* 1991, 2011; *Fejer et al.* 1979, 1981, 2005; *Scherliess and Fejer* 1999]. These drifts have large day-to-day variability at all local times even during geomagnetically quiet times [*Fejer*, 2011; *Fejer et al.*, 1979]. *Fejer et al.* [1979, 1991] reported seasonal variations of these drifts in both high (sunspot maximum) and low solar flux (sunspot minimum) periods.

3.2.1. Low-Latitude Vertical Drifts

Figure 3.1 (top) reproduced from *Scherliess and Fejer* [1999] shows, using Jicamarca ISR data, the seasonal variations of the vertical plasma drifts at different solar flux conditions during magnetic quiet conditions. The vertical bars show the scatter in the data and the continuous line shows the quiet-time empirical model values from *Scherliess and Fejer*

[1999]. A similar study from AE-E satellite Ion-drift meter data from *Fejer et al.* [1995] is also shown in Figure 3.1 (bottom) for comparison. There is a good agreement between these two datasets. A detailed comparison of AE-E data with Jicamarca is discussed in *Fejer et al.* [1995].

The drifts, to the first order, are upward during the day and downward during the night with typical value of 25 m/s. The daytime average drift maximizes at around 1100 LT with the largest values during equinox and the smallest during summer solstices [*Fejer et al.*, 1991]. The daytime drifts do not depend much on solar flux, except near sunset and sunrise. The upward daytime drift increases around dusk terminator before reversing to downward direction after sunset hours. This enhancement in upward drifts, called evening prereversal enhancement (PRE), strongly increase with increasing solar flux [*Fejer et al.*, 1979, 1991, 1995] during equinox and December solstice with typical peak values of 60 m/s and 10 m/s during solar maximum and minimum, respectively. During the June solstice, the peak values of prereversal enhancements during solar maximum are around 20 m/s and are very small in solar minimum [*Fejer*, 2011] except in the Pacific region where prereversal velocities increase by 40 m/s for an increase of 100 units in solar flux [*Scherliess and Fejer*, 1999].

The variation of prereversal enhancement peak drift velocities with solar flux for different seasons is reproduced here from *Fejer et al.* [1991] in Figure 3.2.

Longitudinal Variations

Data collected from different ionosondes and satellites [*Coley et al.*, 1990] show the equatorial F-region vertical drifts exhibit large longitudinal variations. This is believed to be largely because of the displacement of the geographic and geomagnetic equators and the large differences in declination angles and strength all along the magnetic equator [*Scherliess and Fejer*, 1999]. *Fejer et al.* [1995], using data from Ion Drift Meter onboard AE-E satellite for period 1977-1979, for the first time showed that for moderate to high solar flux conditions the longitudinally averaged satellite data indicates large longitudinal variations during June solstice. For equinox and December solstice, the satellite data is in good agree-

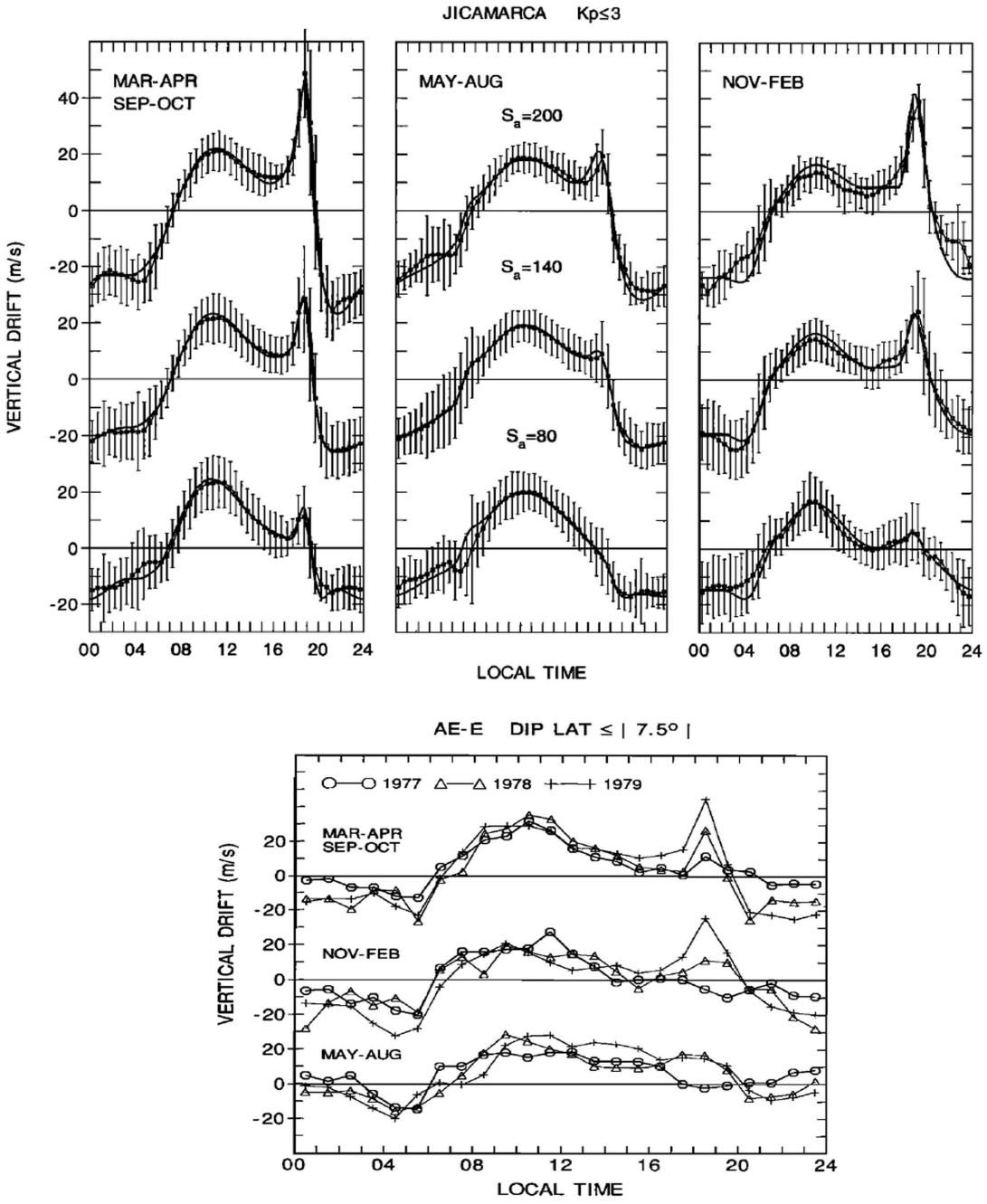

Figure 3.1. (top): Average vertical plasma drifts during Equinox (Mar-Apr, Sep-Oct), Summer (May-Aug), and Winter (Nov-Feb) at high (∼200), moderate (∼140), and low (∼80) solar flux conditions (after *Scherliess and Fejer*, 1999). (bottom): Average vertical drift from AE-E satellite data for high (1979), moderate (1978), and low (1977) solar flux conditions (after *Fejer et al.*, 1995).

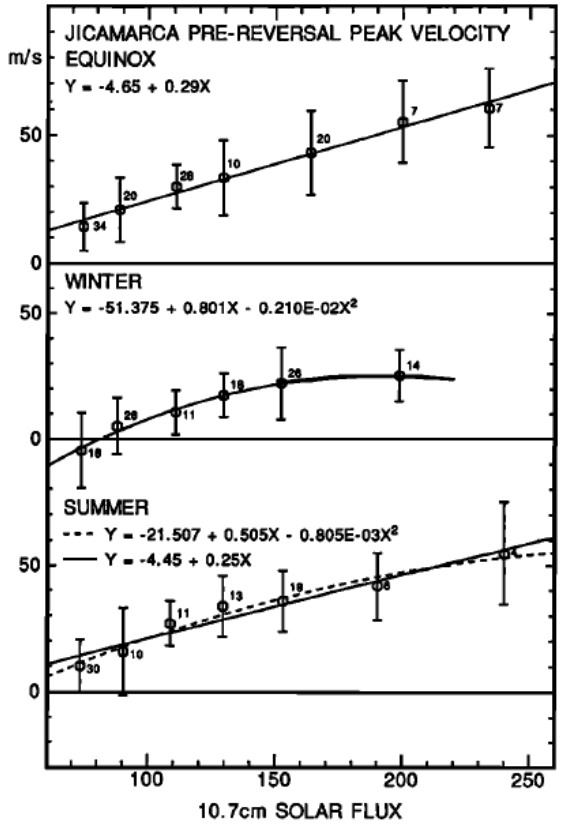

Figure 3.2. Variations in peak prereversal drift velocities with increasing solar flux for different seasons. The standard deviations and number of data points are marked (after *Fejer et al.*, 1991).

ment with Jicamarca ISR data. *Scherliess and Fejer* [1999] is the first detailed season and solar cycle-dependent global empirical model, and shows large longitudinal variations in the evening prereversal enhancement velocities and reversal times during solar maximum conditions. *Fejer et al.* [2008] analyzed the ROCSAT-1 satellite plasma drift data for different longitude sectors. A plot for the local time and longitude variation in eight different longitude sectors for moderate (130 sfu) to high (200 sfu) solar flux conditions is reproduced here from the paper in Figure 3.3. From the figure, it can be seen that the afternoon and evening upward and nighttime downward drifts during equinox and December solstice increase with solar flux. Longitudinal variations of prereversal peak velocity magnitudes during the solstices and of drift reversal time can also be seen clearly. The evening reversal times do not depend much on solar flux except in the American sector during June solstice.

The morning reversal times occur earlier with decreasing solar flux values.

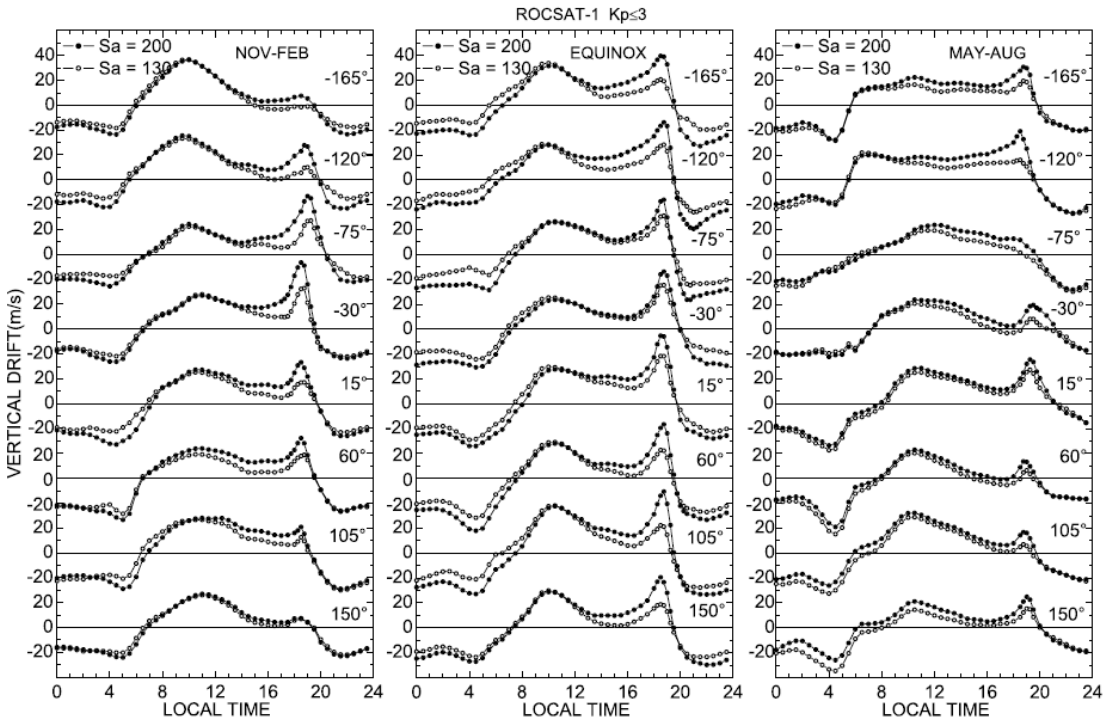

Figure 3.3. Local time and longitude variation of equatorial vertical plasma drift from ROCSAT-1 satellite in eight longitude sectors for moderate (130 sfu) to high (200 sfu) solar flux conditions (after *Fejer et al.*, 2008).

The equinox and June solstice data for equatorial vertical drifts show strong wave number four longitudinal modulations. These wave number four modulations have been confirmed by different studies of nighttime equatorial anomalies [*Sagawa et al.*, 2005], and noon time equatorial electrojet [*England et al.*, 2006; *Lühr et al.*, 2008], and are found to be strongest during equinox [*Hartman and Heelis*, 2007; *Scherliess et al.*, 2008]. This wave number four structure is believed to be primarily because of modulation of zonal electric field by eastward propagating diurnal tide with zonal wave number s = -3, otherwise called DE3 [*Fejer*, 2011; *Hagan et al.*, 2007].

3.2.2. Low-Latitude Zonal Drifts

The east west neutral winds drag plasma along with them in the east west direction,

which creates the vertical electric field as mentioned before. This vertical electric field plays an important role in distribution of plasma in nighttime low-latitude F region, generation of post sunset irregularities [*Fejer et al.*, 2013; *Su et al.*, 2009], and decoupling of local time and universal time experienced by magnetic flux tubes [*Murphy and Heelis*, 1986]. Jicamarca ISR has been measuring these zonal drifts since 1970 [*Fejer et al.*, 1979, 1985, 1991; *Woodman*, 1970], but less frequently than the vertical drifts. These zonal plasma drifts are westward during the daytime and eastward during the night. The zonal drifts show large day-to-day variability, even during magnetic quiet times. At the low latitudes, the daytime peak value is around 40 m/s and does not change much with solar flux and season. The nighttime eastward drifts increase with solar flux and have peak values from 90 m/s during solar minimum to 150 m/s in June solstice, and around 190 m/s during December solstice and equinox during solar maximum. The peak value shifts to earlier local time with increasing solar flux [*Fejer et al.*, 2005]. The peak value at night is reached at around 2100-2200 LT and then decreases towards dawn. Figure 3.4, reproduced from *Fejer et al.* [2005], shows these climatological characteristics of zonal plasma drifts.

Zonal drifts have also been studied using satellites [*Coley and Heelis*, 1989; *Maynard et al.*, 1988] and spaced receiver techniques [*Sheehan and Valladares*, 2004; *Valladares et al.*, 1996] and using air-glow measurements [*Chapagain et al.*, 2011; *Sobral et al.*, 2011] in relation to thermospheric zonal winds. Using DE 2 satellite data, *Maynard et al.* [1988] reported sudden eastward turning of the zonal drifts in the middle of the day, whereas *Valladares et al.* [1996] found the evening drifts are similar to ISR, but have bigger magnitudes and stronger solar flux dependence. In recent studies, *Coley et al.* [2014], *Fejer et al.* [2013], and *Huang et al.* [2010] have discussed the longitudinal characteristics of zonal drifts from satellite data from topside F region. *Fejer et al.* [2013] and *Coley et al.* [2014] found the zonal drifts tend to be more westward on the top side.

At daytime, the E-region dynamo winds dominate the F-region zonal drifts, and the weak F-region dynamo only modify the local conditions to reach a steady state. The F-region zonal drifts are much smaller than the zonal winds at E-region altitudes. At night

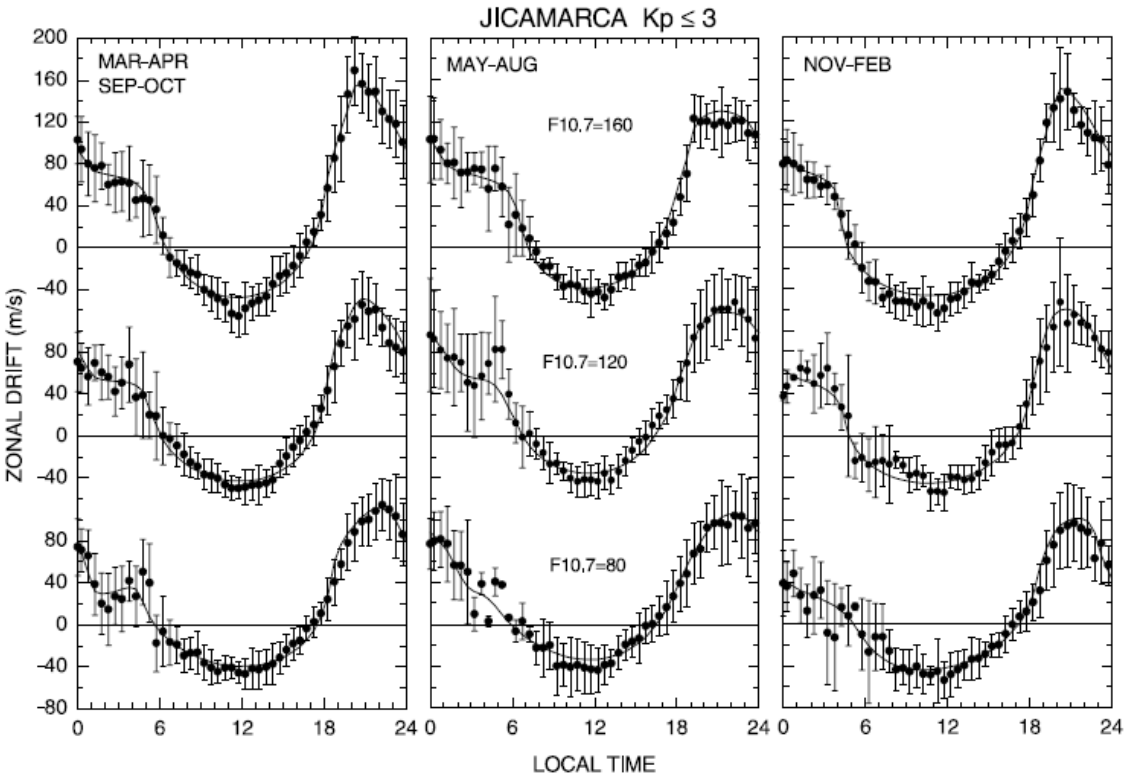

Figure 3.4. Climatological values of quiet-time zonal plasma drifts from Jicamarca observations with empirical model in solid curves (after *Fejer et al.*, 2005).

when the E-region conductivity decreases drastically, the coupling between E and F region becomes weaker and F-region dynamo dominates. The F-region zonal drifts approach values near F-region neutral winds [*Coley and Heelis*, 1989; *Woodman*, 1971].

The evening zonal drifts or vertical electric fields are very important in creating the prereversal enhancement and generation of post-sunset irregularities. Around the dusk terminator and after sunset, there is a strong shear below F-region peak density height. The drifts above F peak are eastward, whereas on the bottom side, the drifts are still in a westward direction [*Fejer et al.*, 1985; *Kudeki and Bhattacharyya*, 1999]. This creates a vortex-like pattern and is responsible for generation of post-sunset spread F or irregularity. The eastward drifts on the top side decrease with altitude [*Fejer et al.*, 2005]. This has been discussed further in Chapter 4.

3.3. 150 Km Region Echoes

Historically, 150 km echoes have been observed on a campaigning basis over Jicamarca since the 1960s [*Balsley*, 1964; *Chau and Woodman*, 2004; *Fawcett*, 1999]. But since 1996, these echoes have been monitored more frequently at Jicamarca to measure both vertical and zonal drifts of the plasma at 150 km region [*Alken*, 2009]. Since 2001, the vertical and zonal plasma drifts have been routinely measured from an E-region height of around 150 km from Doppler measurements or radar echoes at JRO using the Jicamarca Unattended Long-term Ionosphere and Atmosphere (JULIA) radar system. This system was made to observe equatorial plasma irregularities and neutral atmospheric waves for extended periods of time. It makes use of some of the exciter stages of Jicamarca ISR radar, along with the main antenna array. It is an MST/coherent scatter radar with a pair of 30 kW peak power, pulsed transmitters driving a 290 m^2 modular antenna array (source: JRO website). To observe the so-called 150 km region drifts, it samples between altitudes of 90-168 km. These 150 km echoes are present only during the daytime and their measurements are very precise because of high signal strength and narrowness of their spectra. The source of such echoes is believed to be from E-region irregularities, but the mechanism is not very well understood. *Chau and Kudeki* [2013] discuss two different types of 150 km echoes and suggested they are caused by naturally enhanced incoherent scattering and the unstable growth of field-aligned irregularities, respectively.

Kudeki and Fawcett [1993], from their observations of 150 km echoes and their correlation with ground magnetic field perturbations, suggested the vertical Doppler velocities of 150 km echoes could well represent the F-region **E x B** drifts in the ionosphere. *Woodman and Villanueva* [1995] suggested the Doppler velocities of 150 km echoes are indeed a representation of F-region plasma drifts. *Chau and Woodman* [2004] did simultaneous measurement in the F-region vertical and zonal plasma drifts using ISR system, and the 150 km Doppler-shifted velocities using the JULIA system at Jicamarca Radio Observatory. They observed that if the altitudinal drift profiles from 800 km to 200 km are extrapolated linearly from ISR data downward up to 150 km, the linearly extrapolated values of

ISR measurements match closely with the 150 km Doppler velocities measured by JULIA. These altitude gradients vary not only from day to day, but also with local time. Very good agreement between the ISR measured F-region vertical drifts with 150 km vertical Doppler-shifted velocities were found, whereas poor to good agreement for the zonal drifts was observed.

With the discovery of very good correlation between the 150 km Doppler-shift measurements and the F-region drifts, these coherent radar measurements have been used to measure vertical equatorial drifts at multiple longitudes along the magnetic equator around the globe [*Blanc et al.*, 1996; *Kudeki et al.*, 1998; *Patra et al.*, 2012]. *Alken* [2009] developed a 150 km vertical drift model for the Peruvian sector from the JULIA data. The model shows good agreement with observations from 0800 to 1600 LT typically when JULIA makes these measurements. More discussions on these 150 km echoes and JULIA observations are done in Chapters 4 and 5.

3.4. Altitudinal Variations of Vertical and Zonal Drifts

The vertical plasma drifts show gradients with altitude in the F region and this altitudinal gradient is related to the longitudinal gradient of the zonal drifts, as mathematically shown in *Moffett et al.* [1975] and *Murphy and Heelis* [1986] and proven with observations from Jicamarca data by *Pingree and Fejer* [1987]. This relationship between vertical and zonal drift arises from the curl-free condition of electric field. Thus, to satisfy the curl-free electric field condition in low-latitude ionosphere, the altitude gradients of the equatorial plasma drifts should not be neglected [*Murphy and Heelis*, 1986]. They show that for the curl-free electric fields condition at the low-latitude equatorial ionosphere, the altitudinal gradients of vertical plasma drifts are dependent on the longitudinal gradients of zonal plasma drifts through the relation in equation (3.1). The curl-free condition i.e., curl $\mathbf{E} = 0$ can be written as

$$\frac{1}{r}\frac{\partial v_\phi}{\partial \phi} - 2\frac{v_r}{r} + \frac{\partial v_r}{\partial r} = 0 \tag{3.1}$$

where, r is the radial distance from the Earth's center, ϕ is the longitude in spherical coordinate system, and v_ϕ and v_r are zonal and vertical plasma drifts.

Pingree and Fejer [1987] used Jicamarca ISR vertical drift data from 200 km to 700 km during low solar flux conditions to study these altitudinal gradients. They pointed out that though the gradients are highly variable from day to day, they are usually positive (increase with altitude) during the morning and negative during the afternoon hours. These gradients change very rapidly around dusk.

Pingree and Fejer [1987] argued the time and longitudinal variations of the zonal drifts are interchangeable because the local time variation at a longitude over a day will look like an instant snapshot of the drift around the globe in the magnetic equator (thus neglecting the longitudinal variations as an approximation). The time variation of the zonal drifts is then equal to the first term on the left side of the above equation. The second and third terms relate to the altitudinal gradients of vertical drifts.

Using data from Jicamarca, they show the above equation is satisfied and thus, the electric field is irrotational in the geomagnetic equatorial region, at least in the medium solar flux conditions. Figure 3.5 shows how different terms in the equation balance each other to make the E field curl free. The relatively small height gradients in the vertical plasma drifts during the daytime indicate the driving zonal electric fields vary weakly with latitude [*Fejer*, 2011].

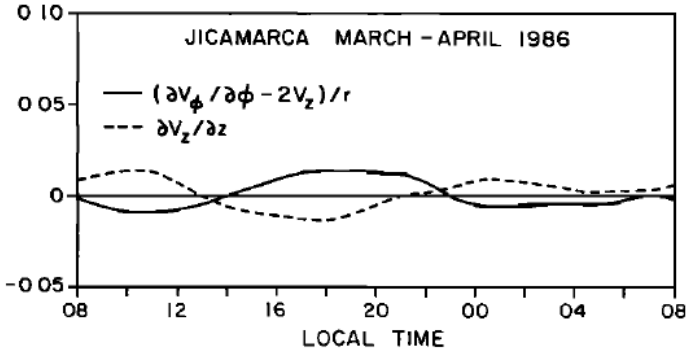

Figure 3.5. Comparison of different terms in equation 3.1 to show curl-free E field (after *Pingree and Fejer*, 1987).

The altitudinal variations in the plasma drifts during dusk are large and change more rapidly than during the daytime. In the post-sunset hours, the drifts at lower altitudes are still westward, whereas at higher altitude they turn eastward, thus giving rise to a vortex-like pattern in the plasma flow [*Kudeki and Bhattacharyya*, 1999]. Recently, using numerical simulation, *Rodrigues et al.* [2012] has shown such drift patterns in the post-sunset sector. Figure 3.6., reprinted from *Rodrigues et al.* [2012], shows how the vertical, zonal, and 2-D velocity vectors change with altitude and local time. These altitudinal variations of plasma drifts change very rapidly with time, as shown by *Fejer et al.* [2014].

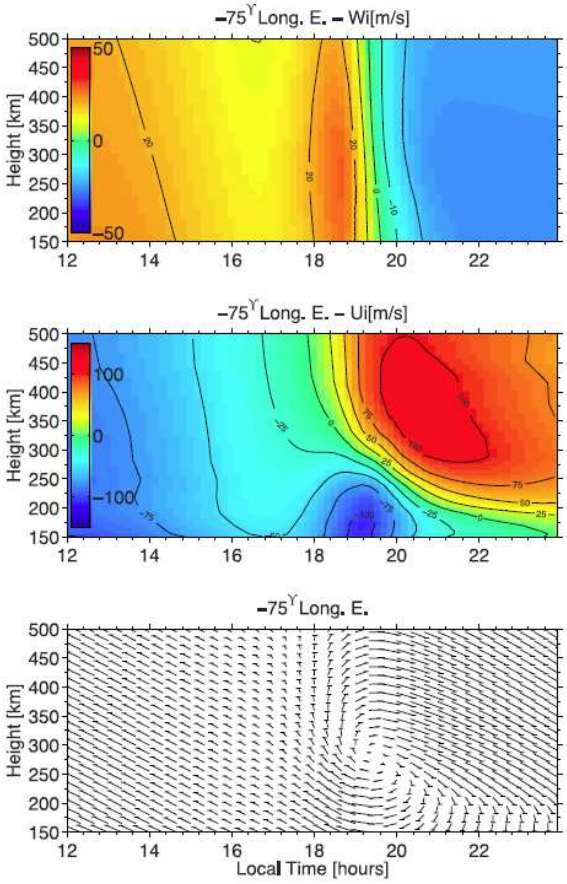

Figure 3.6. Simulation results for vertical (top), zonal (middle) plasma drifts, and 2-D plasma velocity vectors (bottom) around sunset as a function of altitude and local time (after *Rodrigues et al.*, 2012).

CHAPTER 4
ALTITUDINAL VARIATIONS OF DAYTIME EQUATORIAL PLASMA DRIFTS

In the previous chapter, we studied how the plasma drifts in the low-latitude ionosphere are responsible for different physical electrodynamic processes. The height-averaged climatology and the importance of the altitudinal variations of these plasma drifts were also discussed. In this chapter, we will study the climatology of the altitudinal variations of these plasma drifts during quiet times.

In this chapter, we will first focus on the climatology of the quiet-time daytime altitudinal variations of the vertical plasma drifts from 150 km to up to about 600 km combining the Jicamarca ISR and JULIA radar system data. We will then investigate the zonal drifts and their quiet-time daytime climatology in detail and describe their daytime climatological altitudinal variations. The climatology is usually studied in seasonal, four monthly (November-February, May-August, and equinoxial months-April, May, September, and October) bins. In this chapter, however, we will bin the data in a higher resolution bin of bimonthly periods. We will study how the vertical and zonal drifts vary with altitudes and discuss why these gradients are so variable in light of the wind systems, which drive the E- and F-region dynamo. We will also compare our results with observations made by others whenever available.

4.1. Data

We use data from the ISR and JULIA systems at Jicamarca Radio Observatory (JRO). The ISR and JULIA systems and their measurement techniques have been described very well in *Chau and Woodman* [2004] and *Fejer* [2011]. Though the description of ISR and JULIA is given in Chapter 3, section 3.2 and 3.3, respectively, we will briefly review the most important points. The ISR measures F-region (typically between 200-800 km altitudes) vertical, and zonal plasma drifts with a time resolution of 1-5 min and height resolution of 15-25 km. The data is most accurate near the F-region peak where the signal-to-noise

ratio is highest. The typical errors in vertical and zonal drifts are 1 m/s and 10 m/s, respectively, during day and larger at night. Over Jicamarca, an upward (eastward) drift of 40 m/s corresponds to an electric field of 1 mV/m in the eastward (downward) direction [*Fejer*, 2011]. These drifts have large day-to-day variability at all local times, even during very quiet times [*Fejer*, 2011; *Fejer et al.*, 1979]. For this study, we used ISR vertical and zonal drift data from 1997 to 2014, after a more advanced method of data collection and processing was adopted at JRO in 1996 [*Kudeki et al.*, 1999]. Over this period, we have used about 214 days of data for analysis of vertical drifts and 185 days of data for zonal drifts. This is done in such a way that each bimonthly period has a solar flux of about 110 solar flux units (sfu). The JULIA system measures 150 km region plasma drifts from Doppler shift measurements of the coherent echoes present during daytime. The JULIA data, as mentioned before, is very accurate because of narrowness of its spectra, but is available only in the daytime. We have used 1036 days of vertical and 509 days of zonal JULIA drift data from 2001 to 2013 for this analysis. The solar flux level for each bimonthly period has been adjusted to be close to that of the ISR data. All the data used are from magnetically quiet times ($K_p \leq 3$).

4.1.1. Data Selection

The database for this study uses 5 min averages from both facilities. The ISR data used has altitudinal resolution of 15 km, the JULIA data correspond to height-averaged (over 140 to 170 km altitude) values. The number of days of data in different bimonthly bins is given in Table 4.1. These data sets are publicly available at the Jicamarca webpage (http://jro.igp.gob.pe/madrigal/).

The error restrictions are chosen keeping in mind that, for ISR data, the signal-to-noise ratios are highest around F-region peak (around 350-400 km) and the signal strength drops with altitude. ISR zonal drifts data used for this study uses less strict constraints because of two reasons: firstly, they have larger errors, and secondly, the zonal drift database is smaller than that of vertical drifts. So to maintain sizable statistics, we have to relax on error values for the zonal drifts. For the vertical drifts, we used an error limit of 5 m/s up

Table 4.1. Distribution of Days of Data Used for this Study

	Zonal		Vertical	
	ISR	JULIA	ISR	JULIA
Jan-Feb (SSW)	30	21	36	54
Jan-Feb(No-SSW)	9	105	15	154
Mar-Apr	37	42	42	71
May-Jun	34	38	39	109
Jul-Aug	22	143	22	220
Sep-Oct	21	109	38	207
Nov-Dec	17	55	25	204
Total	170	513	217	1019

to 500 km and 10 m/s above 500 km, whereas for the zonal drifts, we used an error limit of 50 m/s up to 500 km and 80 m/s above 500 km. ISR data from 200 to 600 km is used as during low solar flux, the signal-to-noise ratio decreases faster due to rapidly decreasing plasma density above the F-region peak. In the topside, the low solar flux data has low accuracy and are more accurate only during high solar flux periods. JULIA measurements have higher accuracy, but a cap of 5 m/s error on measurement is used. For the present study, due to limited data in each altitude bin and to maintain sizable statistics, we could not divide them in terms of different solar flux levels. So the distribution is done so each bimonthly dataset has an average moderate solar flux level of around 110 sfu.

4.2. Results

Figure 4.1 shows examples of the variations of vertical (top panel) and zonal (bottom panel) plasma drifts with altitudes during a September equinox low solar flux period (71 sfu). This figure shows 30 min average drift profiles at three local times centered at 1015 LT, 1215 LT, and 1415 LT. Different colors represent different days from 14 to 23 September, 2009. General trends can be seen over the daytime for both vertical and zonal drifts. The characterististics and climatological trends of such altitude variations will be discussed later. This figure only stresses the fact that though we see large variations in the drift values from day to day, on any individual day, the drifts change with altitudes and these variations are

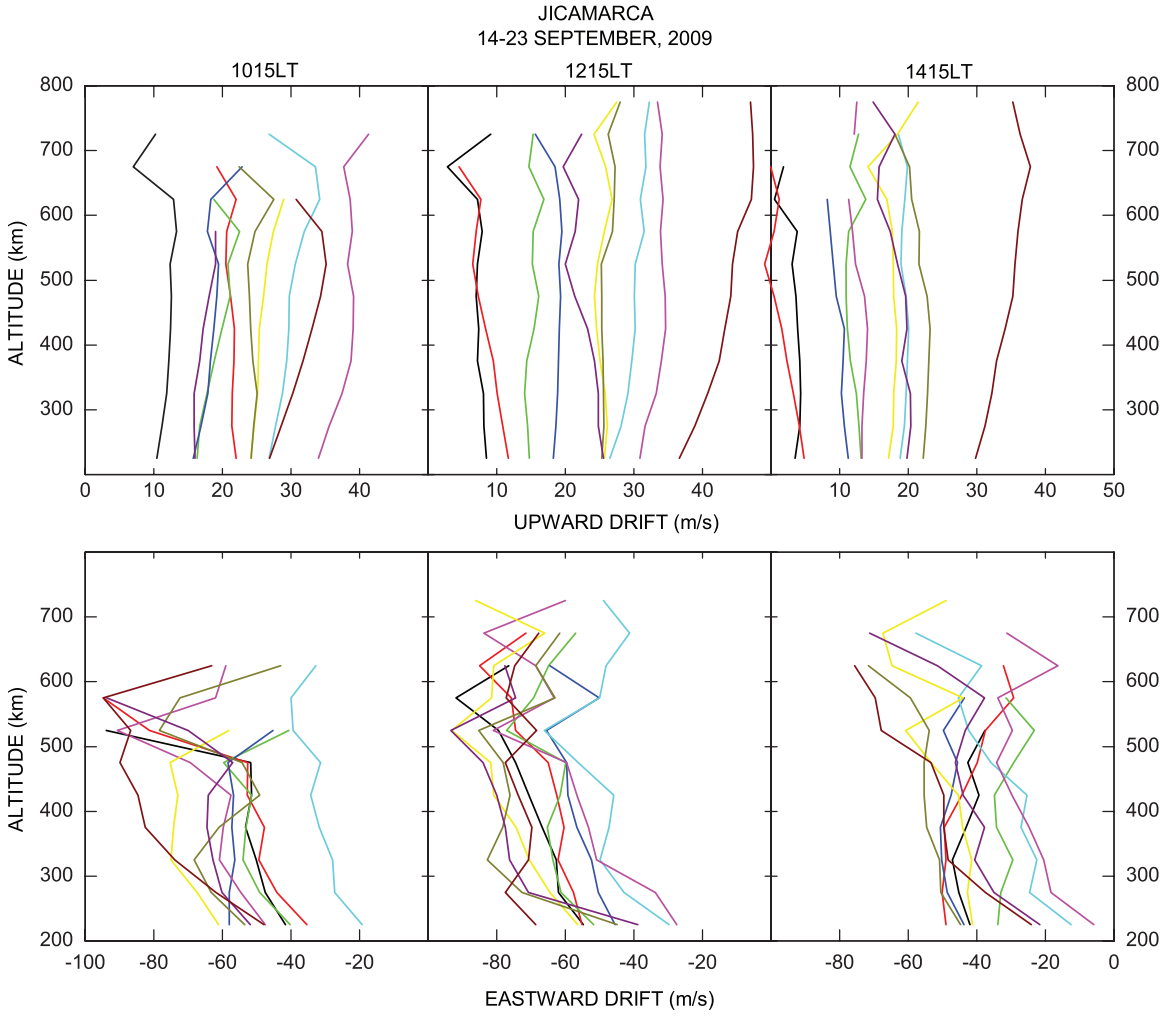

Figure 4.1. Examples of the variations of vertical (top) and zonal plasma (bottom) drifts with altitude. The different colors denote different days.

functions of local time.

Sample scatter plots of ISR and JULIA quiet-time plasma drifts during the months of September-October are shown in Figure 4.2. Each thin black line represents drifts from individual days, whereas the red lines show the means. ISR data has been averaged every 100 km centered at 250 km, 350 km, 450 km, and 550 km, whereas JULIA data shows averaged drifts around 150 km. The JULIA data has good statistics from 0800 LT to 1600 LT, but the statistics of ISR data usually decrease with altitude. As we can see, the undulations in zonal drifts at 550 km are results of poor statistics and are, hence, eliminated during further analysis. The vertical drifts are usually upward, and zonal drifts are westward during the

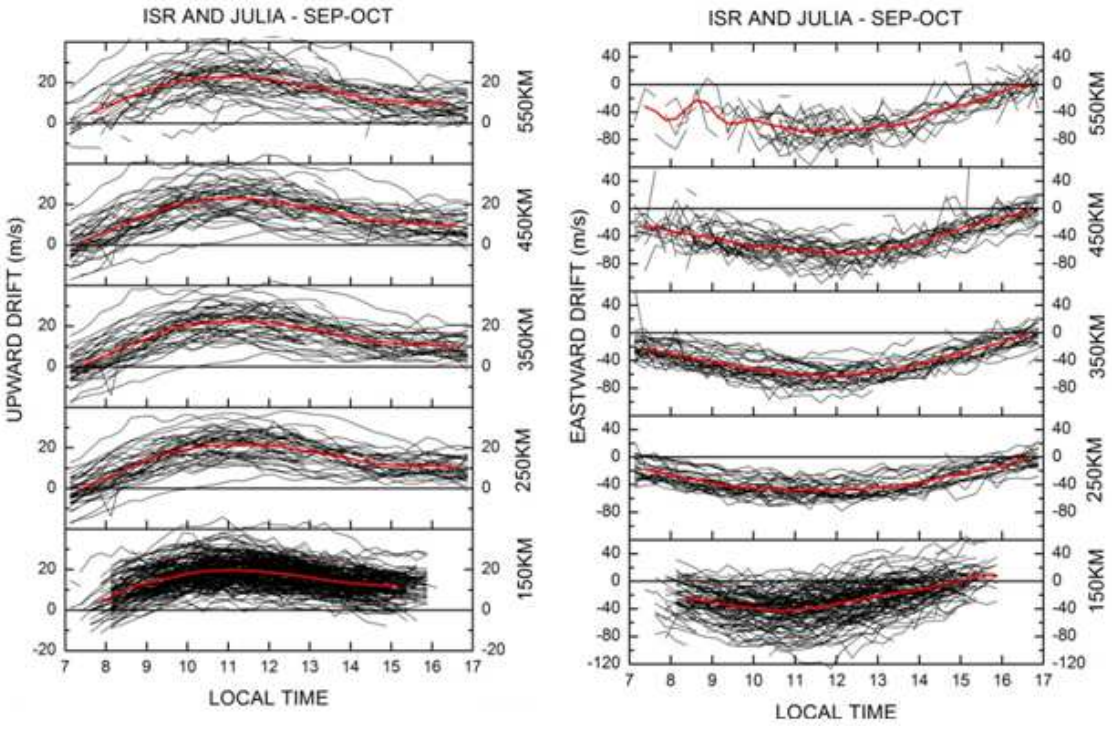

Figure 4.2. Examples of scatter plots of quiet-time ISR-JULIA vertical (left) and zonal (right) plasma drifts. The scatter of the 150 km data is largest in the zonal drifts.

daytime; but, instances of downward vertical drift and eastward zonal drifts can also be seen, particularly in JULIA data. The striking variability of 150 km zonal drifts can be seen in comparison to higher altitude ISR data. The vertical drifts show similar standard deviations for both E and F region, but in the case of zonal drifts, the standard deviation of the JULIA drifts is much larger than those of the F-region drifts.

4.2.1. Vertical Drifts

Figure 4.3 summarizes climatological vertical drifts for all six bimonthly periods over Jicamarca from 0700 LT to 1700 LT. In each panel, JULIA data at 150 km altitude is shown in red, whereas F-region data from ISR at 250 km (averaged from 200 to 300 km) is shown in green and at 400 km (averaged from 300 to 500 km) in blue. The average at 400 km corresponds to a larger altitude range because of two reasons: firstly, the signal-to-noise ratio starts decreasing at higher altitudes leading to increasing errors in the measurements; and secondly, because at altitudes above F region peak, the gradients are very small [*Pingree*

and Fejer, 1987].

The January-February data in all figures correspond to non Sudden Stratospheric Warming (nonSSW) periods, if not otherwise specified. The plots shown in Figure 4.3 have a 15 min time resolution smoothed further by three-point running averages. The early morning and late afternoon has statistically less data than in the middle of the day. In the January-February period, we have 15 days of ISR data and 154 days of JULIA data. In other periods, at F-region heights, we have used 22 days of ISR data in July-August to a maximum of 42 days of data in March-April. At 150 km, the data ranges from 71 days in March-April to 220 days in July-August. Figure 4.3 shows the higher peak value is attained at the higher altitudes, in most bimonthly periods, except during May-June and November-December. The highest peak value of around 23 m/s is reached in the equinoxial months at higher altitudes, whereas the lowest peak value of around 10 m/s is also seen at these altitudes in November-December. The time of peak drifts also differs from one bimonthly period to another: for example, the peak drift is attained at 1000 LT in January-February and the corresponding time in July-August is 1200 LT. Also different altitudes show peak values at different local times indicating change in gradients with local time and altitudes. This can be seen clearly between E-region and F-region data and even between F-region altitudes in January-February and March-April. The general trends of the altitudinal variations in the vertical drifts matches well with the results of *Pingree and Fejer* [1987]; that is, in the morning hours, we see a small positive gradient (drift values increases with altitude) from 150 to 600 km, which reverses in the afternoon. This reversal takes place at different local times in different seasons; as early as 0900 LT in November-December and as late as 1430 LT in July-August. The equinoxial months (March-April, September-October) show strong positive gradients in the middle of the day, whereas November-December shows negative gradients at the lower altitudes. The June solstice months (May-June, July-August) show opposite gradients in the afternoon with respect to the E region.

Figure 4.4 compares the altitudinal profiles of bimonthly averaged vertical plasma drifts. This Figure shows 30 min average altitudinal profiles with the standard errors of

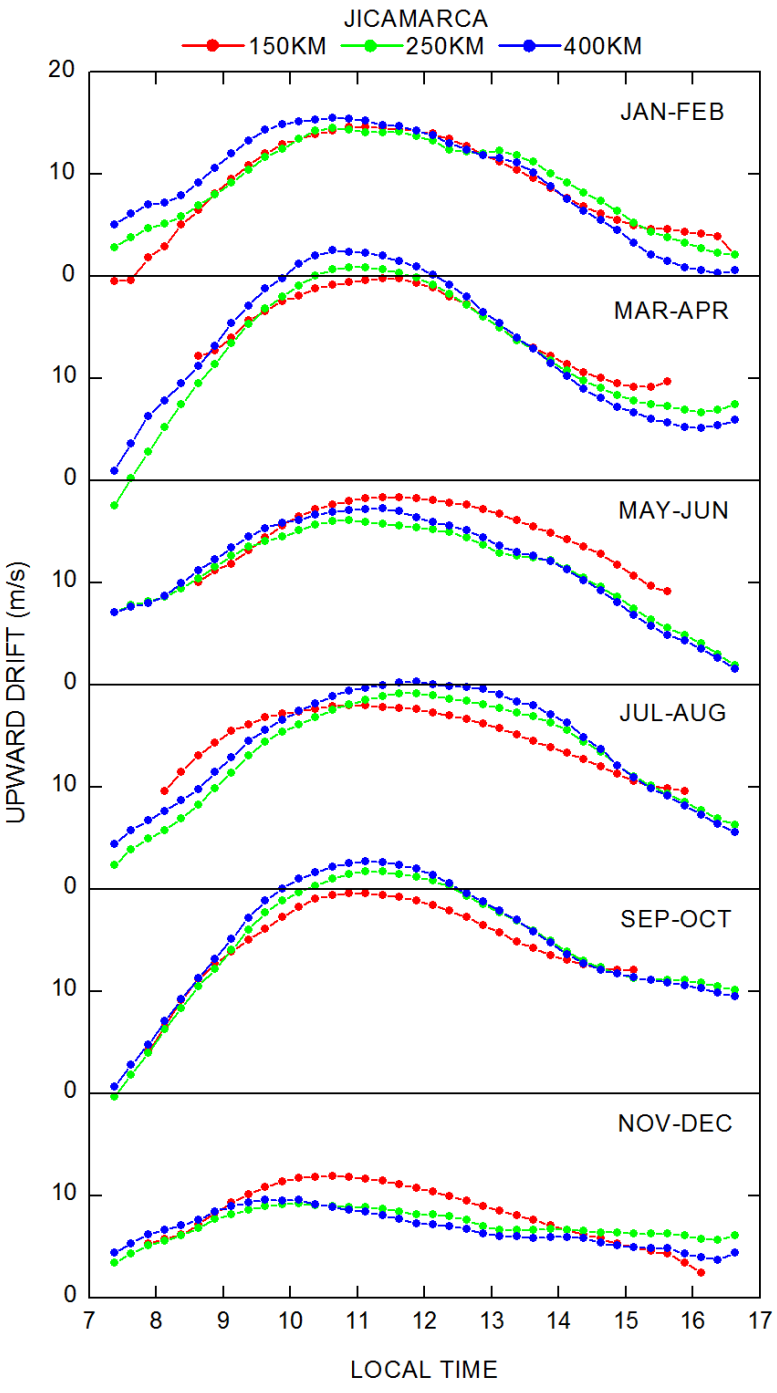

Figure 4.3. Bimonthly average Jicamarca vertical plasma drifts in 15 min local time bins.

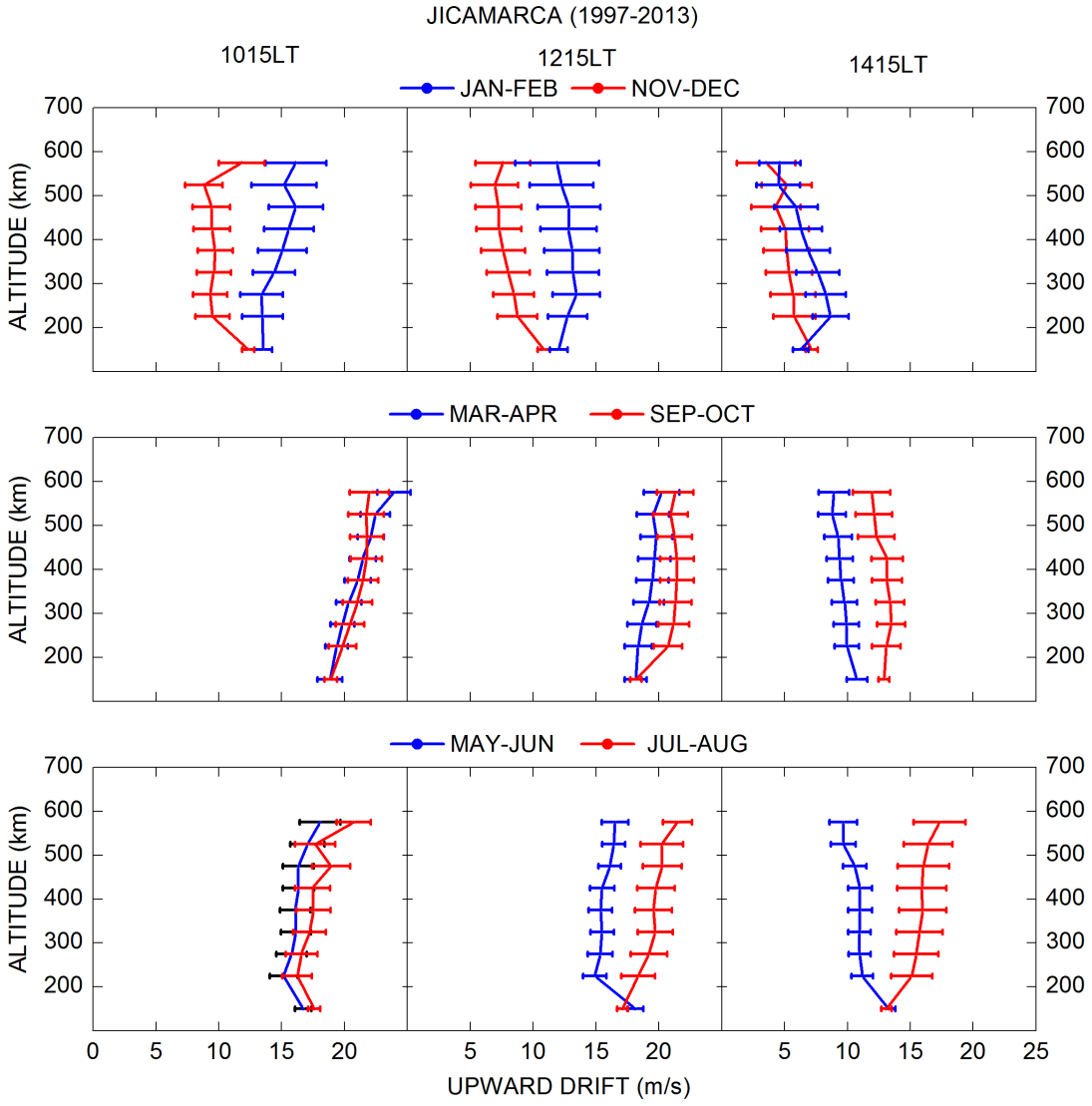

Figure 4.4. Altitudinal profiles of bimonthly 30 min averaged quiet-time vertical plasma drifts with the standard errors of their means.

their means (SEM) and 50 km altitude resolution at 1015 LT, 1215 LT, and 1415 LT. The January-February altitudinal profiles show only nonSSW periods. The morning hours show the drifts increasing with altitude except June solstice months and November-December. Above 200 km during March-April, these drifts increase at a rate of about 0.03 m/s/km at 1015 LT and at about 0.006 m/s/km in May-June. May-June does not show linearly decreasing drift values at low altitudes in the first half of the day. The afternoon gradients are small with values of about -0.005 m/s/km at 1415 LT in March-April and about

-0.01 m/s/km in January-February. We also observe the reversal from positive to negative gradients in July-August is very late in the afternoon compared to other bimonthly periods.

4.2.2. Zonal Drifts

Figure 4.5 shows bimonthly zonal drifts in different panels. The average solar flux for the data is around 110 sfu. The plots shown here have a 15 min time resolution and were smoothed further by three-point running averages. Like the vertical drifts, the early morning and late afternoon averages are based on less data than during the middle of the day. In January-February we have 9 days of ISR data and 105 days of JULIA data. In other periods, at F-region heights, we have used 17 days of ISR data in November-December to a maximum of 37 days of data in March-April. The JULIA data ranges from 42 days in March-April to 143 days in July-August.

The zonal plasma drifts show very small altitudinal variations in the morning hours and comparatively larger variations in the afternoon. The gradients are larger (-0.05 to -0.2 m/s/km) in the transition region from E to F region and smaller in the F region except during November-December, where they have small values throughout the day. Just like in the case of the vertical drifts, in Figure 4.5, we can also see the peak westward drifts are reached at higher altitudes. The highest peak value of 63 m/s occurs in September-October, whereas the lowest peak of 35 m/s occurs at 150 km in January-February. Also the local times of occurrence of the peak drifts are different at different altitudes. This is very pronounced in September-October, where the peak value at 150 km is reached at around 1030 LT, whereas for 400 km, the peak value is reached at around 1200 LT. The reversal of the zonal drifts from westward to eastward direction seems to take place earlier at the lower altitudes except during November-December and January-February. In January-February, the transition from westward to eastward drifts takes place almost simultaneously at all altitudes, whereas in November-December, the eastward turn of the westward drift takes place at higher altitudes first followed by E-region drifts.

To investigate this lower altitude transition region from E- to F-layer heights, Figure 4.6 shows the lower altitudinal region with higher spatial resolution. In this case, we have

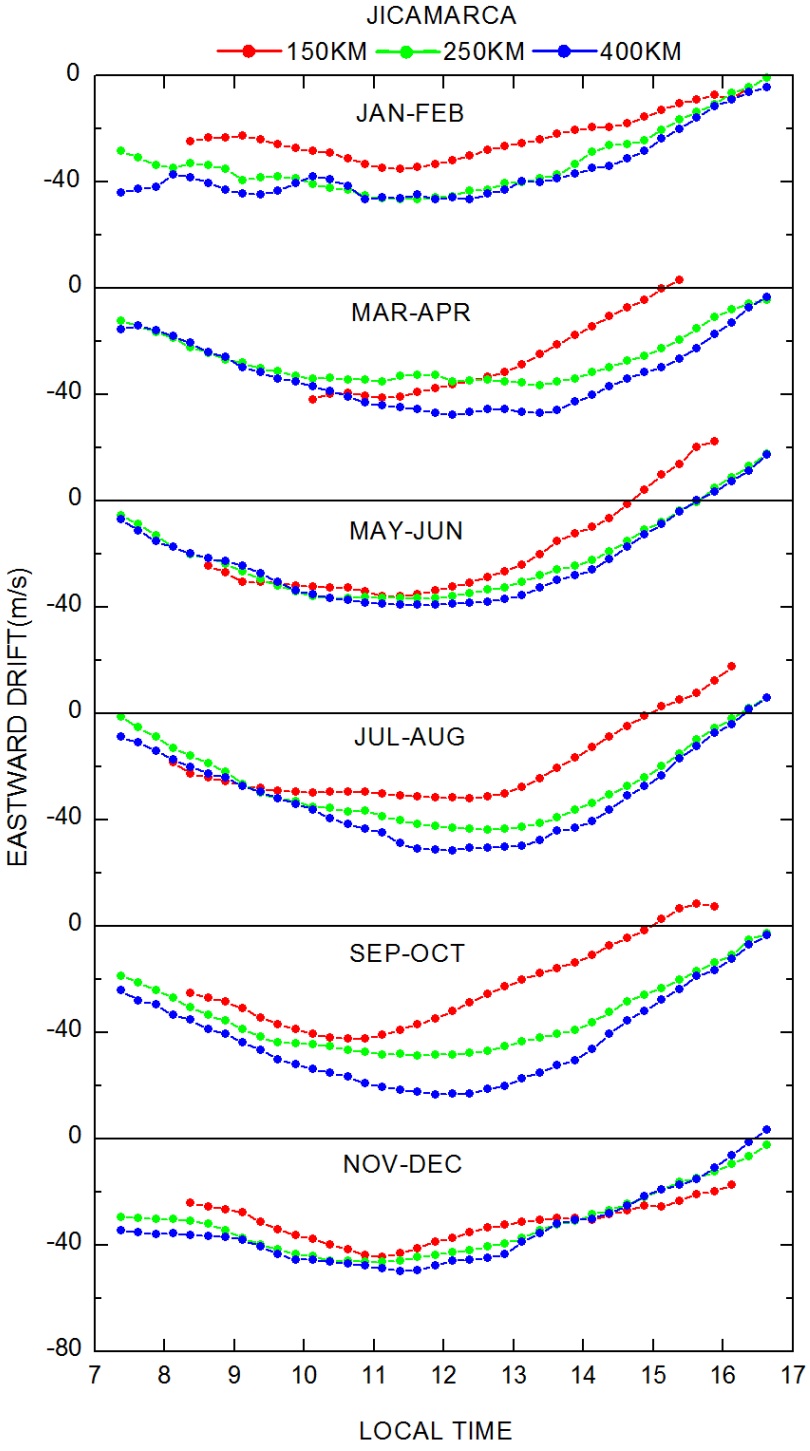

Figure 4.5. Bimonthly average Jicamarca zonal plasma drifts in 15 min local time bins.

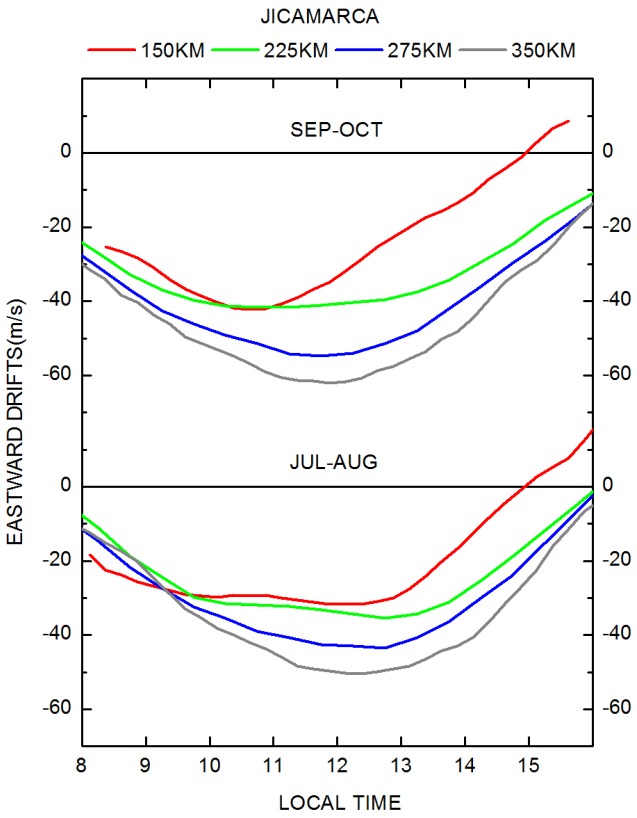

Figure 4.6. Altitudinal variation of zonal plasma drifts as a function of local time during September-October and July-August.

the JULIA 150 km zonal drifts and ISR 50 km altitudinal average data. We can clearly see the large change of the afternoon drifts at the lower altitudes in comparison to higher altitudes in F region.

Figure 4.7 compares the altitudinal profiles of bimonthly average zonal drifts. The altitudinal profiles shown in the figure are 30 min time averages with their standard errors of their means at 1015 LT, 1215 LT, and 1415 LT with an altitudinal resolution of 50 km. The general characteristics of the profiles are that the drifts increase fast in a westward direction at the lower altitudes and then increase slowly with increasing altitudes. The slopes are nonlinear at the lower altitudes with bigger values than at higher altitudes and with distinct breaks in the early hours in the equinoxial months. The slopes increase with local time and are larger in the afternoon hours, especially in the lower altitudes.

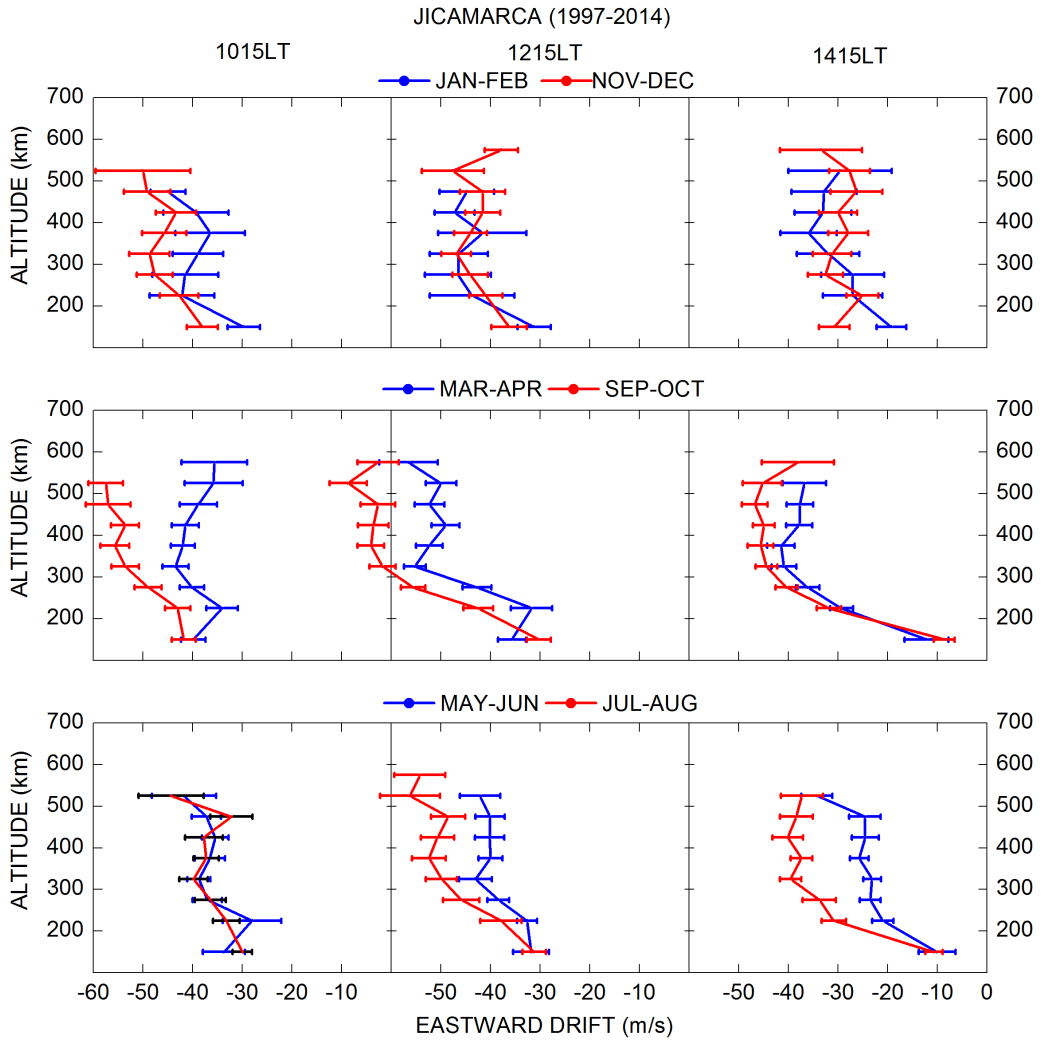

Figure 4.7. 30 min time-averaged zonal drifts height profiles of bimonthly periods are compared for morning, noon, and afternoon local times.

The January-February and November-December zonal drifts show very similar profiles, but the equinoxial months are quiet different, particularly in the morning hours. In January-February excluding morning hours, the drifts increase with slopes of about -0.09 m/s/km up to 325 km and then remain nearly constant with altitude. In March-April, the lower altitudes show nonlinear increase in westward zonal drifts with a slope of -0.1 m/s/km from 225 km to 325 km, whereas at higher altitudes above 325 km, the gradients are positive with a value of 0.03 m/s/km. In September-October, on the other hand, they follow the

general trend of increasing westward drifts with increasing altitudes and large slopes at lower altitudes. In the morning around 1015 LT, we can see a slope of about -0.05 m/s/km up to 375 km and then of about -0.02 m/s/km above 375 km. In the afternoon around 1415 LT, the slope is about -0.2 m/s/km up to 325 km and then increases with a slope of -0.01 m/s/km. July-August shows bigger negative slopes than May-June except in the morning hours. The slope in the afternoon hours in July-August can be up to about -0.2 m/s/km up to 325 km and then remains almost constant with altitude.

The bimonthly vertical and zonal JULIA and ISR drifts are compared in Figure 4.8 and 4.9, respectively. As can be seen, both the vertical and zonal bimonthly JULIA drifts do not differ much in the equinox months and June solstice, though in January-February, they show smaller zonal plasma drift values than November-December by 5-7 m/s. We notice in the F region, the November-December vertical drift values are smaller than the January-February drifts for most of the day. The zonal drifts during these two bimonthly periods are not much different. The vertical drifts during equinoxial months match closely only in the morning hours. March-April shows smaller values in the afternoon than the September-October drifts, whereas during the June solstice months, May-June shows smaller drift values than July-August for most of the day, except in the morning hours. For the zonal drifts, March-April shows smaller values than September-October until late afternoon, whereas, May-June shows smaller values than July-August in the afternoon hours in the F region.

4.2.3. Drifts During Sudden Stratospheric Warming (SSW) Periods

Sudden Statospheric Warming periods are times characterized by large scale changes in the temperature, wind, and circulation changes in the polar winter middle atmosphere caused by rapid growth of quasi-stationary planetary waves and their interaction with the stratospheric circulations [*Liu and Roble*, 2002; *Matsuno*, 1971]. This special meteorological process changes the plasma circulations in the ionosphere up to even equatorial latitudes. The vertical plasma drifts in E and F regions are known to change considerably during arctic winter SSW events [*Chau et al.*, 2009; *Fejer*, 2011; *Fejer et al.*, 2010; *Sridharan et al.*, 2009].

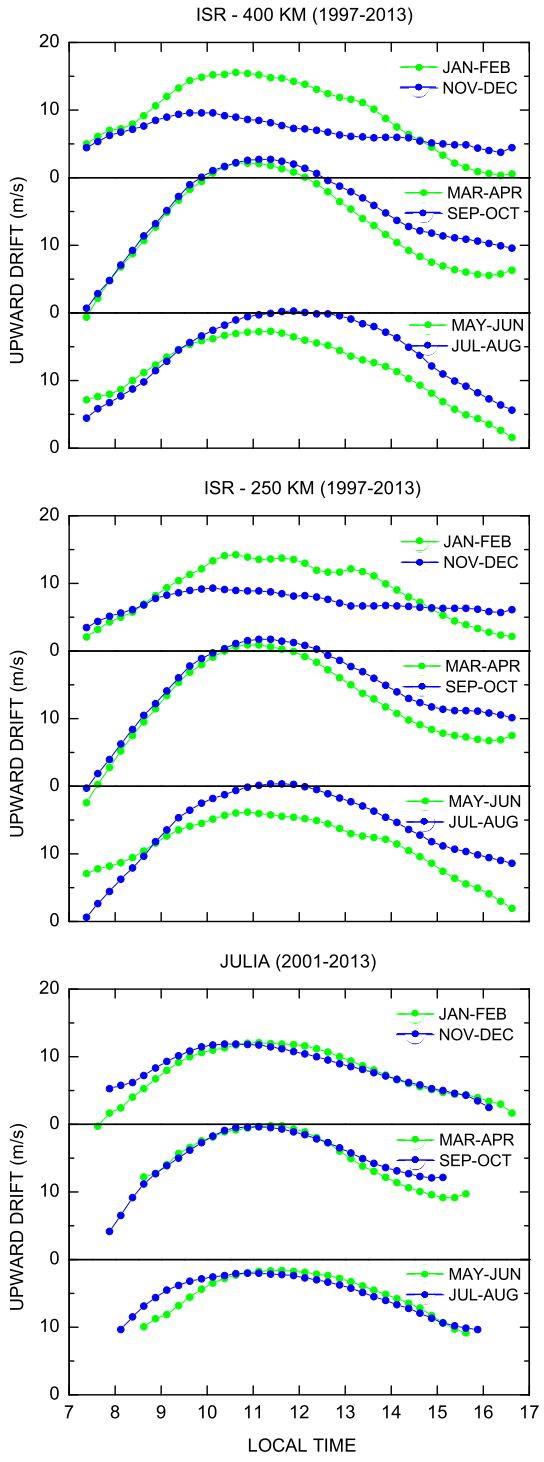

Figure 4.8. Comparison of different bimonthly vertical drift measurements.

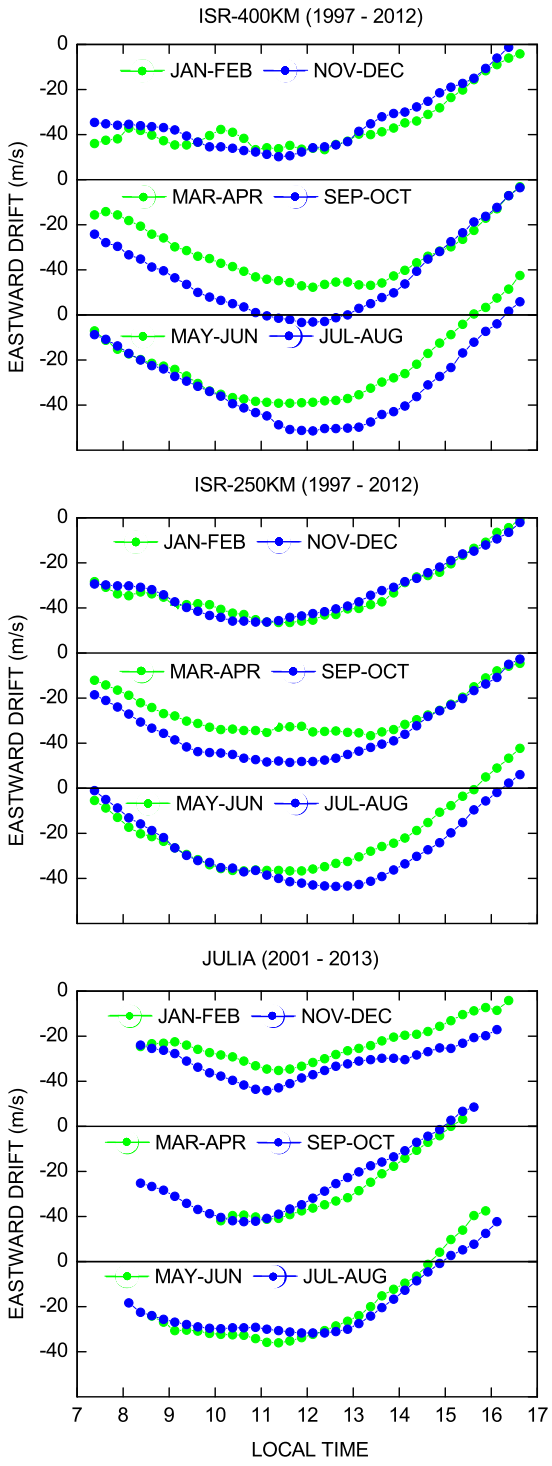

Figure 4.9. Comparison of different bimonthly zonal drift measurements.

Figure 4.10 compares altitudinal profiles for vertical drifts of SSW and nonSSW periods in the month of January-February. In this case, we have 15 days of ISR data during SSW period and 36 days during nonSSW period, JULIA has 54 days of SSW data and 154 days of nonSSW period data. The profiles shown are 30 min averages of the vertical drifts with their SEM and an altitudinal resolution of 50 km. We can see that though the general patterns in the slope throughout the day look similar, the vertical drifts differ in magnitudes. During SSW events the daytime drifts are highly suppressed (dependent on the phase of the moon), but show the same small positive gradients in the morning and negative gradients in the afternoon hours. The E-region drifts value does not change much during SSW and nonSSW periods, hence, creating a change in sign of the slope from E to F region during nonSSW period at afternoon hours and large negative slopes at lower altitudes during SSW periods throughout the day.

Figure 4.11 compares the 30 min averaged height profile of zonal drifts during SSW and nonSSW periods in January-February. The SSW has 30 and 21 days of ISR and JULIA data, respectively; whereas, the nonSSW has 9 and 105 days of ISR and JULIA data. We observe the slopes do not change much between these two periods. It is interesting to note the E-region drifts are larger in the morning and smaller in the afternoon than nonSSW periods. Also the SSW periods have larger variability than nonSSW periods throughout the day. Unlike vertical drifts, SSW events do not change the zonal drifts values much from nonSSW periods.

4.3. Discussion

In this chapter, we have presented the climatology of altitudinal variations of low-latitude daytime vertical and zonal plasma drifts. We have shown how these altitudinal variations change with local time. Highly variable zonal drifts at lower altitudes and occasional occurrence of drifts in opposite directions for both vertical and zonal drifts have also been observed.

The existence of altitudinal gradients were known for a long time [*Heelis et al.*, 1974; *Woodman*, 1970]. Using Jicamarca ISR data, *Murphy and Heelis* [1986] pointed out ne-

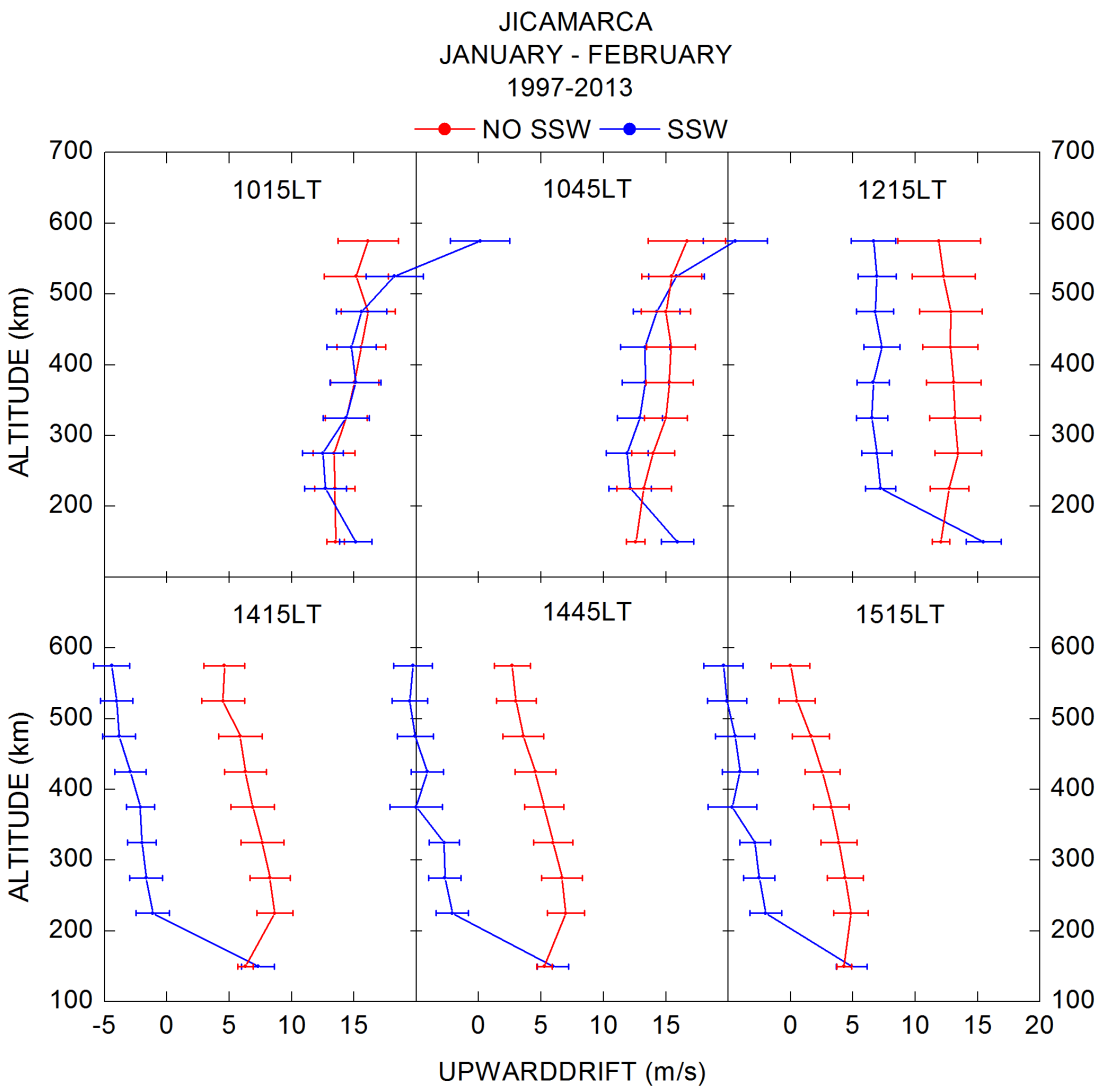

Figure 4.10. Comparison of height profiles of vertical plasma drifts during SSW and nonSSW periods over Jicamarca during January-February.

glecting these small gradients will violate the curl-free condition of electric field in the ionosphere. To satisfy the curl-free condition [*Fejer et al.*, 2014; *Murphy and Heelis*, 1986; *Pingree and Fejer*, 1987], the vertical drift gradients cannot be very large. The altitudinal gradients in the vertical drifts are balanced by the zonal gradients of the zonal drifts and are usually small because of the large zonal extent of the ionosphere compared to its vertical extent [*Chau and Woodman*, 2004]. It is important to mention that though the standard

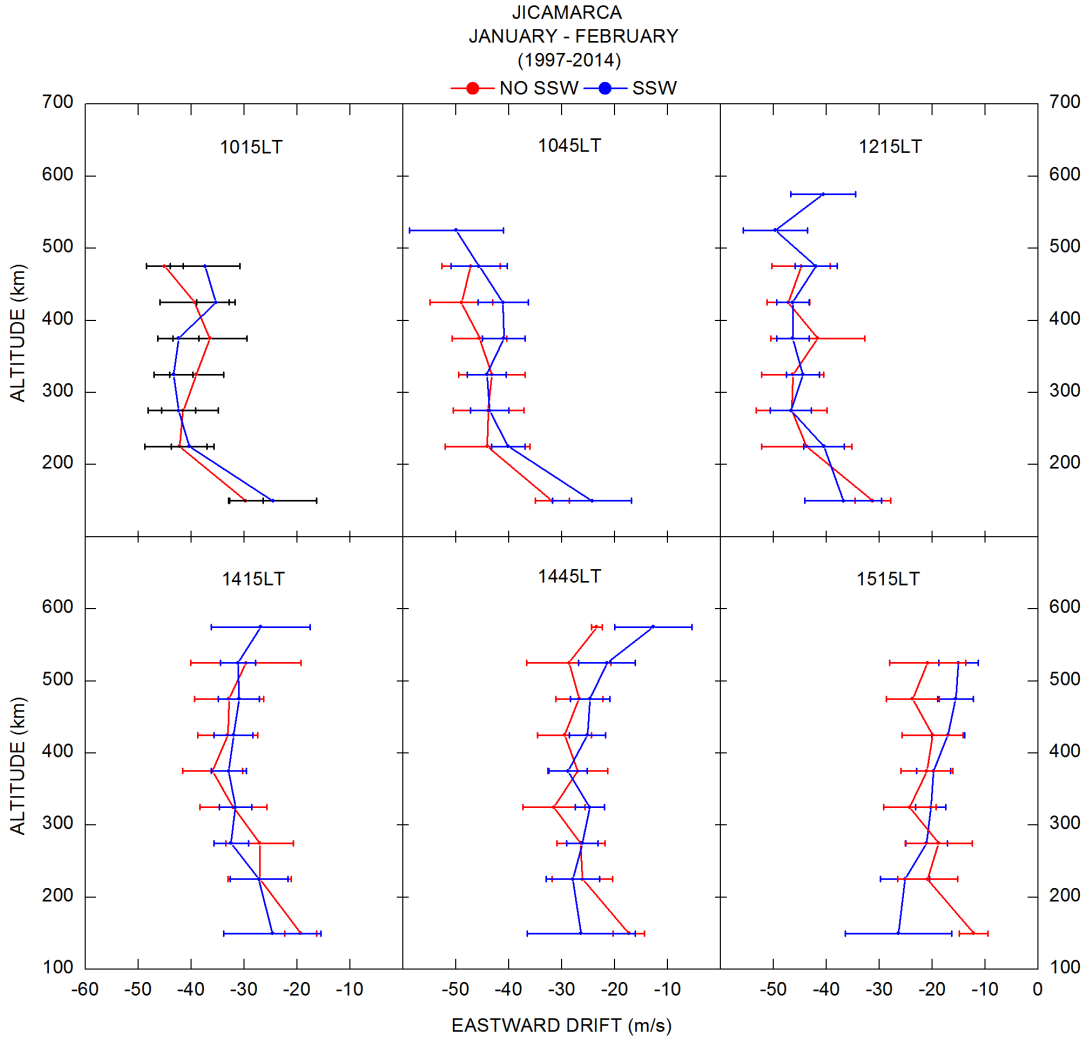

Figure 4.11. Comparison of height profiles of zonal plasma drifts during SSW and nonSSW periods over Jicamarca during January-February.

errors of the mean in Figures 4.4 and 4.7 are larger than the altitudinal gradients, Figure 4.1 clearly illustrates on any individual day, these altitudinal variations exist and should not be neglected.

The altitudinal variations in the vertical drift in Figure 4.4 mostly show the vertical drifts change very slowly with altitudes as has been reported by *Pingree and Fejer* [1987] and linearly from 150 km to 600 km except for a few occasional exceptions during January-February nonSSW periods and November-December. The morning positive gradients and

afternoon negative gradients are consistent with the findings of *Pingree and Fejer* [1987]. *Pingree and Fejer* [1987] showed a positive slope of about 0.02 m/s/km in March-April with 30 min average, which is very close to our climatological value of 0.03 m/s/km at 1015 LT. Our results are also consistent with the increasing ratio of zonal electric fields of E and F region from morning to afternoon as was found by *Prakash and Muralikrishna* [1981]. The linear change in drifts also indicates the electric field changes linearly with altitude (from E to F region) as suggested by *Chau and Woodman* [2004]. *Eccles* [1998a] developed a simple electric field model for low latitudes, which shows the gradients in vertical drifts as results of variations of neutral winds, E- and F-region conductivity, and their variation with longitude. The paper shows how different sources, like polarization fields from dynamo currents and conditions for curl-free electric fields contribute to the change in drift values with altitude. The electric field in their model depends on the distance squared from the center of the Earth, and as a result, should increase with altitude throughout the day. It is also dependent on the zonal winds, and as a result, any change in zonal winds can change the drift values (personal communication). *Fejer et al.* [2014] discusses altitudinal gradients of vertical plasma drifts and gives quantitative measurements of such gradients during evening time when they are larger than the daytime values. We will study these evening time gradients in the next chapter.

Alken [2009] developed a model for 150 km region vertical drifts using JULIA data for 0800 LT to 1600 LT and compared them with the vertical drifts from the *Scherliess and Fejer* [1999] model. Their results clearly show the JULIA vertical drifts' values show small difference from the F-region values throughout the day, which indicates to gradients in vertical drifts. It is important to note that they used 30 days running average of JULIA data. *Patra et al.* [2012] and *Rodrigues et al.* [2013] also reported similar differences between the 150 km vertical drifts and *Scherliess and Fejer* [1999] model. Along with longitudinal variations because of the various nonmigratory tides, this difference can be partly because of the altitudinal gradients, which were not considered in their studies.

Rodrigues et al. [2015] showed the difference between daytime E-region JULIA data and

F-region drifts from *Scherliess and Fejer* [1999] model are mostly negative in the morning and positive in the afternoon hours. Their results, done in latest solar minimum, very well match with the change in gradients from positive to negative shown in Figures 4.3 and 4.4 and discussed in *Pingree and Fejer* [1987] and *Chau and Woodman* [2004]. These gradients can also partly explain the negative drifts seen by C/NOFS satellite at higher altitudes, as reported by *Stoneback et al.* [2011] and also discussed in *Rodrigues et al.* [2015].

The equatorial electric fields and plasma drifts are controlled by E- and F-region dynamo caused by thermospheric neutral winds. These thermospheric winds are results of atmospheric tides generated because of absorption of solar radiation by the neutral atmosphere [*Fejer*, 2011; *Richmond*, 1995]. Using NCAR Thermosphere Ionosphere Electrodynamics General Circulations Model, *Fesen et al.* [2000] has shown the semidiurnal migrating 2,2 tidal mode affects the magnitude and phase of the daytime vertical drifts in the low-latitude ionosphere. An increase of semidiurnal component during daytime could result in increase of vertical drifts in the morning-noon hours and small or downward drifts in the afternoon [*Patra et al.*, 2014] and cause a semidiurnal variation in the low-latitude topside drifts [*Rodrigues et al.*, 2015]. Though the highly localized winds do not contribute to the electric fields [*Liu and Richmond*, 2013; *Maute et al.*, 2012], the migrating and nonmigrating tidal components can cause longitudinal variations in the drifts [*Patra et al.*, 2014]. The diurnal eastward propagating wave 3 (DE3) contributes strongly to the E and lower F region [*Hagan et al.*, 2007], and is responsible for wave 4 structure in zonal winds [*Häusler and Lühr*, 2009]. Simulations using TIEGCM [*Fesen et al.*, 2000; *Liu and Richmond*, 2013; *Liu et al.*, 2013] have shown the amplitudes, phase, and structures of these diurnal and semidiurnal migrating and nonmigrating tides can modulate the E- and F-region dynamos and cause changes in ionospheric responses. These model results showed these tides are highly variable, especially in the lower thermosphere [*Liu et al.*, 2013] and can cause the vertical drifts to change considerably [*Liu and Richmond*, 2013]. Further discussions on effect of tides on ionospheric responses are presented in *Patra et al.* [2014]; *Rodrigues et al.* [2015] and the references within.

For the low-latitude ionospheric zonal plasma drifts, *Fejer et al.* [1985] pointed out for integration time of 20 min or more, the daytime gradients change very slowly throughout the day. *Coley and Heelis* [1989] reported vertical structures of zonal winds from DE 2 satellite data during high solar activity. The variation of drifts with altitude, especially above F-region peak, indicates the decreasing wind speed with latitude [*Fejer et al.*, 1985; *Wharton et al.*, 1984]. During daytime, the E-region dynamo winds, which increase with latitude from the equator, dominate the F-region zonal drifts. The continuously present F-region dynamo then modifies the drift profiles on the top side [*Coley and Heelis*, 1989]. The F-region drifts are much smaller than the F-region neutral winds because of lower conductivity compared to E region where east-west drifts are more strongly coupled with the neutral winds at slightly higher latitudes [*Fejer et al.*, 1985; *Woodman*, 1971]. *Eccles* [1998a] developed a model based on electrodynamic quantities, which gives an estimate of the zonal plasma drifts from 150 km to 1500 km over low latitudes as equal to Pedersen conductivity weighted zonal winds. This model also suggests (Figure 2 in the paper) very strong negative gradients (increasingly westward with altitude) at the low altitudes up to 400 km, and then slowly increasing in westward direction at higher altitudes.

Coley and Heelis [1989] studied altitude profile of F-region zonal drifts in high solar activity period, and with a time average of two hours, they found the zonal drift to be almost height independent during 1400-1600 SLT. We see when the zonal drifts show a general pattern of very small gradients at higher altitudes, they are nonlinear at the lower altitudes as could be seen in Figure 4.7. This nonlinearity is most pronounced in equinoxial months of September-October when we can see large shear at the lower altitudes. These large nonlinear altitudinal variations are further illustrated in Figure 4.6. *Chau and Woodman* [2004] pointed out because of different gradients of E-region zonal winds before noon above and below 200 km, the 150 km drifts can be smaller than the ISR extrapolated drifts. Our data shows this very clearly in the morning hours of March-April and May-June. In the afternoon though, mostly nonlinear change in drift values are observed at lower altitudes. The high Pederson and Hall conductivity peaking at different altitudes, winds at different

altitudes with different conductivities driving currents with effects of diurnal and semi-diurnal tides forcing the E-region dynamo in the daytime makes the altitude under 200 km more variable in the daytime [*Heelis et al.*, 2012]. The conductivity decreases rapidly from 150 to 200 km during daytime and above 200 km, the Pedersen conductivity decreases very slowly up to about 400 km. The neutral winds also become more westward above 200 km [e.g., *Heelis et al.*, 2012], which can now drag the ions along with them. In recent studies *Fejer et al.* [2013] and *Coley et al.* [2014] found using C/NOFS data that the zonal drifts continue to show negative slope on the top-side ionosphere.

Using electrodynamic parameters *Chau and Woodman* [2004], from their personal communication with A. Richmond, suggested the nonlinearity in the bottom side using the following relationship connecting vertical plasma drifts (V_x), zonal plasma drifts (V_z), and local neutral wind (U_n):

$$\mathbf{V_x} \approx -\Big(\frac{\sum_H}{\sum_P}\Big)V_z + \int \frac{\Big(\sigma_P * U_n ds\Big)}{\sum_P}, \tag{4.1}$$

where σ_P is the Pederson conductivity and $\sum_H$ and $\sum_P$ represents the field line integrated Hall and Pederson conductivities. This equation results from the current continuity requirements, which demand if the zonal gradients of the zonal current density are very small, the field line integrated total outward current must vanish. The second term in right side represents the Pederson conductivity weighted field line-averaged neutral winds. V_x and V_z are assumed to be constant along the field line. They argued the Pederson conductivity weighted E-region winds contributed significantly to the integral on right side of equation 4.1 and can be significantly different than local neutral wind, U_n. V_x, thus represents the E-region zonal neutral winds at different latitudes. The fact the E-region drifts do not agree well with the F-region drifts suggests that either the E-region winds change significantly with latitude near the magnetic equator or the contribution from local neutral wind, U_n around 150 km is not negligible.

We have seen in Figure 4.7 and 4.8 that the average value of 150 km zonal drifts does not change much between the two bimonthly periods although they show higher day-to-day

variability compared to F-region drifts (Figure 4.2). So, large change in mean values takes place in the F region between the months compared, as reflected at higher altitudes in both the figures.

Occasional downward drifts for vertical drifts, particularly during low solar flux conditions, can be observed on certain days in Figure 4.2 as has also been reported by *Anderson et al.* [2002] in South American longitudes, *Patra et al.* [2012] in Indian and Indonesian longitudes, and *Rodrigues et al.* [2013] in the Brazilian longitude sector. This is more common in January-February, July-August, and November-December. We have also observed such exceptions in the case of 150 km zonal drifts on many occasions.

We could not study the solar flux variation of the altitudinal variations because of limited database, but previous studies [*Coley et al.*, 2014; *Fejer et al.*, 1981, 1985] have shown the daytime zonal drifts do not vary much with solar flux. Thus, we can claim the gradients shown here for zonal drifts should not change much with solar flux. This, however, needs to be investigated further in the future with actual observations with more data.

4.4. Summary

We have, for the first time, presented the climatology of the altitudinal variations of equatorial plasma drifts. The climatology of the F-region zonal drifts' altitudinal variations is also presented for the first time. We observed how the vertical drifts show positive gradients in the morning and become negative in the afternoon hours. Our results show that mostly, the slope from E- to F-region vertical drifts are linear as suggested by *Chau and Woodman* [2004]. Slopes in June solstice months are very small. We also observed during SSW periods, the slope of the vertical drifts do not change much from nonSSW periods.

The zonal drifts mostly show negative slope with larger nonlinear nature at the bottom side. The mean drift values at 150 km do not change much between the bimonthly periods. Equinoxial months show the largest nonlinear slopes at lower altitudes, particularly in afternoon hours. Also, unlike vertical drifts, the variability of the zonal winds at 150 km are higher than F-region drifts. As the zonal drifts do not change much with solar flux during the daytime, the altitudinal variations shown should be valid for any solar flux levels. Our

study also suggests SSW events do not affect zonal drifts much in terms of magnitude and altitudinal variability.

Including the altitudinal variations in the plasma drifts calculations is important to make the ionospheric electric field curl free. This chapter presented a detailed study of how these altitudinal variations change over local time and seasons. Incorporating these variations in ionospheric models will improve the space weather predictions and space-based navigation-communication systems.

CHAPTER 5
ALTITUDINAL DEPENDENCE OF EVENING EQUATORIAL F-REGION VERTICAL PLASMA DRIFTS [1]

Abstract

We use Jicamarca incoherent scatter radar measurements to study for the first time, the altitudinal variations of late afternoon and early night equatorial F-region vertical plasma drifts. We also present the initial vertical drift measurements over the altitudinal range from about 200 to 2000 km. These data show the afternoon drifts decrease weakly with altitude. Near their evening prereversal enhancements, the vertical drifts generally increase with altitude below about the F-layer peak, decrease with height near the F-layer peak and above, and are nearly height independent in the (solar flux dependent) topside ionosphere. The transition altitudes from height-decreasing to height-independent evening upward drifts decrease with altitude from solar maximum to solar minimum. After their reversal to downward, the vertical drifts do not change much with height. The altitudinal dependence of the evening vertical drifts has large day-to-day variability and is closely related to the time dependence of the zonal drifts, as expected from the curl-free electric field condition.

5.1. Introduction

Middle- and low-latitude quiet-time electric fields and plasma drifts are driven primarily by the dynamo action of thermospheric neutral winds [e.g., *Richmond*, 1995]. Equatorial F-region electrodynamic ($\mathbf{E} \times \mathbf{B}$) vertical drifts affect the altitudinal variation of low-latitude plasma density, composition, and thermospheric winds and also play a fundamental role in the generation and evolution of equatorial plasma structure and irregularities [e.g., *Fejer and Kelley*, 1980]. Therefore, the accurate specification of these plasma drifts is essential for realistic modeling of low-latitude ionospheric and thermospheric processes.

[1] This chapter was published by the AGU. Copyright 2014 American Geophysical Union. Fejer, B. G., D. Hui, J. L. Chau, and E. Kudeki (2014), Altitudinal dependence of evening equatorial F region vertical plasma drifts, J. Geophys. Res. Space Physics, 119, doi:10.1002/2014JA019949.. Reproduced by permission of the American Geophysical Union.

Low-latitude ionospheric plasma drifts have been studied extensively by using ground-based radar and ionosonde measurements [e.g.,*Abdu et al.*, 2006; *Fejer*, 2011; *Maruyama*, 1988; *Ramesh and Sastri*, 1995] and, more recently, also using satellite observations [e.g., *Fejer et al.*, 2008; *Kil et al.*, 2008; *Stoneback et al.*, 2011]. These measurements have determined the local time, seasonal, solar cycle, and longitudinal dependence of the low-latitude meridional (vertical at the equator) and zonal plasma drifts. Ionospheric electrodynamic circulation models have reproduced the general characteristics of equatorial vertical plasma drifts [e.g., *Eccles*, 1998a; *Fesen et al.*, 2000; *Millward et al.*, 2001], the sources of their variability [e.g., *Maute et al.*, 2012], and their ionospheric effects [e.g., *Huba et al.*, 2010; *McDonald et al.*, 2011] The incoherent scatter radar at the Jicamarca Radio Observatory (11.9^0 S, 76.8^0 W; dip latitude 1^0 N) has measured equatorial F-region vertical plasma drifts since 1970. Near the F-layer peak, these drifts do not have significant altitudinal variations except close to sunset and sunrise [*Woodman*, 1970]. Height-averaged (generally between about 250 and 600 km) Jicamarca vertical drift measurements have been used extensively in the study of the equatorial ionosphere [e.g., *Fejer*, 1991, 1997].

McClure and Peterson [1972] pointed out that although a constant vertical drift is usually a good approximation throughout the equatorial F region, positive and negative altitude gradients are frequently observed. *Murphy and Heelis* [1986] showed that the assumption of height-independent equatorial vertical plasma drifts is inconsistent with the curl-free electric field requirement and leads to significant (between about 30 to 60 min) decoupling between corotating magnetic flux tubes and flux tubes with typical equatorial zonal plasma drifts. *Pingree and Fejer* [1987] determined the average height variations of the Jicamarca F-region vertical drifts at altitudes between 200 and 650 km during equinox solar minimum conditions. They showed that, although the vertical drifts have large day-to-day variability, their average height gradients are consistent with a curl-free electric field at all local times. *Eccles* [1998a] used magnetic field line-integrated parameters to extend the work of *Murphy and Heelis* [1986], and to examine the major sources of low-latitude electric fields and the processes responsible for their height structure. *Chau and Woodman* [2004]

stressed the importance of the altitudinal dependence of the daytime Jicamarca vertical drifts by pointing out that the drifts from 150 km echoes are in much better agreement with the extrapolated (down) F-region drifts. Recently, *Klimenko et al.* [2012] concluded that time-dependent nonuniform in-height vertical plasma drifts at the magnetic equator can explain the occurrence of F_3 and multilayers during geomagnetic quiet times.

The evening prereversal enhancement is one of the most important features of the equatorial vertical drifts. This enhancement is produced by thermospheric wind driven F-region dynamo electric fields in the presence of rapidly decreasing E-region Pedersen conductivity across the dusk terminator [e.g., *Eccles*, 1998b; *Farley et al.*, 1986; *Heelis et al.*, 1974; *Rishbeth*, 1971]. *Sastri et al.* [1995] presented HF Doppler measurements from Trivandrum (8.2^0 N, 77^0 E; dip 0.6^0 N) and Kodaikanal (10.25^0 N, 77.5^0 E; dip 4^0 N) during winter solstice solar minimum conditions suggesting that, on the average, there is a positive height gradient in the vertical drift below the F-layer peak in the 1815 - 1925 LT sector. On the other hand, equatorial ionosonde observations over India and Brazil suggested that the evening vertical drift prereversal enhancements decrease with height (latitude) [*Abdu et al.*, 2009; *Hari et al.*, 1996]. *Fejer et al.* [1996] showed that in this local time sector, the Jicamarca vertical drifts increase with altitude below the F-layer peak during equinoctial and December solstice high solar flux periods.

F-region radar and satellite measurements also show the occurrence of a large shear in the zonal drifts after dusk, with westward drifts at the lowest altitudes and eastward at higher heights [e.g., *Kudeki et al.*, 1981; *Tsunoda et al.*, 1981]. This shear in the evening zonal drifts in local time was modeled initially by *Haerendel and Eccles* [1992] and *Eccles* [1998a]. The evening enhancement of the vertical drifts and the shear in the zonal drifts cause the so-called bottomside plasma drift vortex [e.g., *Kudeki and Bhattacharyya*, 1999]. Recently, the equatorial evening plasma vortex and the vertical drift prereversal enhancement were studied in detail by *Rodrigues et al.* [2012] and *Heelis et al.* [2012] using model simulations. *Heelis et al.* [2012] showed that F-region zonal wind-driven vertical currents in regions of largely reduced E-region Pedersen conductivities play fundamental roles in the

generation of the prereversal enhancement.

In this work, we present the first study of the altitudinal variation of late afternoon and early night equatorial vertical drifts. We also present the initial Jicamarca vertical drift measurements extending from the bottomside to well above the F peak. Our observations show significant changes in the height gradients of the vertical drifts near dusk, which are not evident in current low-latitude electrodynamic modeling studies. In the following sections, we first describe our novel high-altitude radar experiments and briefly the standard plasma drift measurements. Then, we examine the height profiles of the evening vertical drifts and discuss our results.

5.2. Measurements and Data Analysis

The Jicamarca incoherent scatter radar routinely measures F-region electrodynamic vertical and zonal plasma drifts. In these observations, the antenna beam is generally split into two beams, both perpendicular to the magnetic field, pointing about 2.5^0 to the east and 4.3^0 to the west of vertical. The experimental procedure was described in numerous publications [e.g., *Fejer*, 1991, 1997; *Woodman*, 1970]. These measurements are typically made with a time resolution of 5 min and a height resolution of 1525 km from about 200 and 900 km during high solar flux conditions and from about 200 and 600 km during low solar flux periods. The accuracy of the vertical and zonal drift measurements is about 12 m/s and 1020 m/s, respectively, during the day and larger at night, especially during late night low solar flux conditions. More accurate vertical drift measurements are made by pointing the full beam in the vertical direction perpendicular to the geomagnetic field. Specific details of the current experimental setup and drift data analysis were presented by *Kudeki et al.* [1999].

Jicamarca radar vertical drift observations over very large altitudinal ranges were first made during November 15-16, 2004 and March 19-20, 2013 by combining short- and long-pulse observational modes. The November 2004 measurements used a long 100 km uncoded pulse (instead of the standard 3-bit Barker code and 45-km pulse), an interpulse period (IPP) of 2000 km, and power measurements with two linear polarizations, so that the

transverse mode differential phase analysis [*Feng et al.*, 2003; *Kudeki et al.*, 2003] could be applied to also obtain electron density profiles. In this case, the data were sampled every 50 km (instead of 15-25 km), a special algorithm removed satellite echoes from 10-sec integrated data, and the incoherent scatter spectra were further integrated incoherently to get 5 min averages. The drifts were estimated using the nonlinear least square fitting procedure described by *Kudeki and Bhattacharyya* [1999], which provided an accuracy generally better than 2 and 6 m/s below and above 900 km, respectively. The March 2013 experiment used nearly identical observational parameters and data analysis except for an IPP of 1500 km and an altitudinal sampling of 75 km. In this case, the accuracy was generally better than about 2 m/s from about 300 to 1500 km.

5.3. Results

In this section, we describe initially the results of our high-altitude vertical drift observations. Then, we examine in more detail the height profiles of late afternoon and evening vertical drifts over the 200 and 900 km altitudinal range derived from standard Jicamarca F-region drift measurements.

High-Altitude Measurements

The Jicamarca radar measured vertical drifts up to about 2000 km with between 1640 to 2245 LT on November 15, 2004. This was a geomagnetic quiet period with a decimetric solar flux index of 106. Figure 5.1 shows selected drift profiles with 1σ error bars measured during 1700-2245 LT, and the corresponding climatological height-averaged (from about 250 to 700 km) drifts obtained from the *Scherliess and Fejer* [1999] climatological model for identical conditions. In this case, measurements were averaged over altitudinal ranges of 100 and 200 km below and above 1000 km, respectively, and the 5 min observations were smoothed using three- and seven-point running averages below and above 1000 km, respectively. The accuracy of these data generally decreases with altitude and from afternoon to early night as a result of decreasing signal-to-noise ratios and with the change of the angle between the antenna beam and the geomagnetic field [e.g., *Woodman and Hagfors*, 1969]. Equatorial

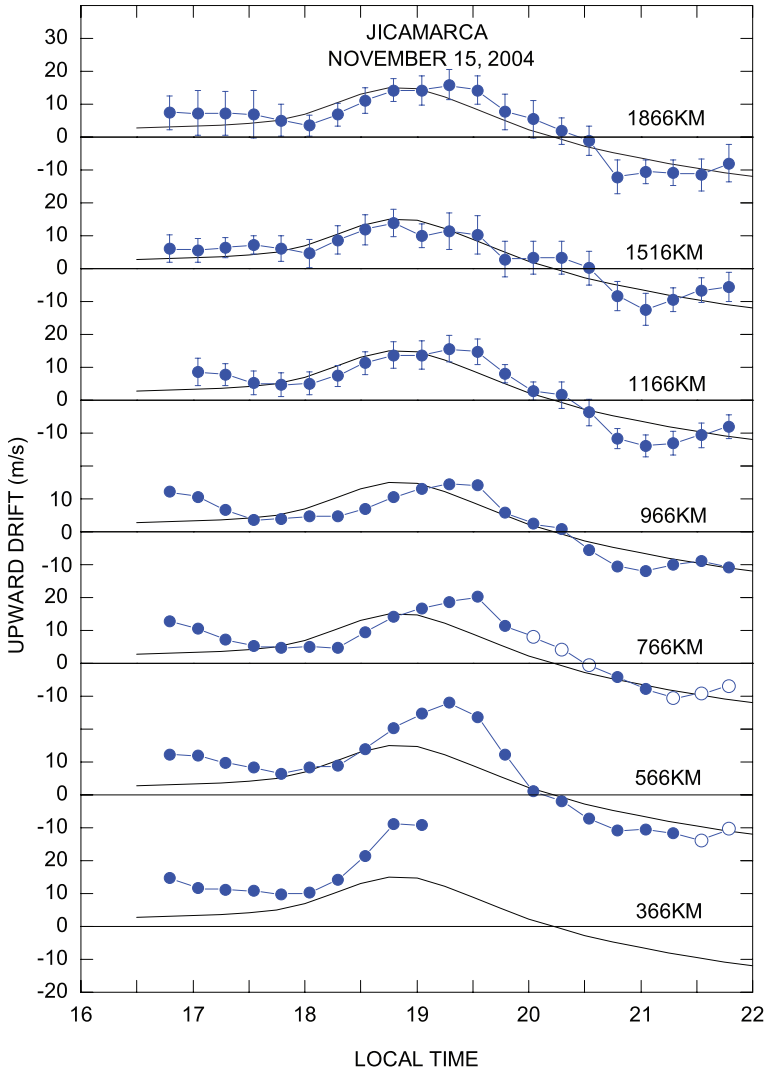

Figure 5.1. Equatorial vertical plasma drift profiles measured with the Jicamarca radar during 15 November 2004. Spread F echoes precluded low-altitude drift measurements after about 1930 LT. The open circles denote measurements under weak spread F conditions. The solid curves denote the height-averaged quiet-time climatological drifts.

spread F developed initially at 1900 LT from about 200 to 450 km. This unstable layer remained below 500 km until 2010 LT, when it expanded up to about 650 km at 2010 LT for about 30 min before moving down to about 500 km, except for a 30 min period starting at about 2140 when it reached up to about 700 km. Figure 5.1 shows that up to about 1800 LT the upward drifts decreased weakly with height from values of about 12 m/s at the lowest altitudes to about 8 m/s at the highest heights. With the development of the evening

prereversal enhancement between about 1800 and 2000 LT, the upward drifts increased more strongly at the lowest altitudes than above 1000 km where they reached nearly altitude-independent values. In this period, the peak upward drifts varied from about 30 m/s at the lowest altitudes, which is significantly larger than the climatological value, to about 12 m/s above 1000 km. After about 1930 LT, the upward drifts decreased systematically and did not change much with height. They reversed to downward at about 2015 LT showing again only small height dependence up to the end of the observational period.

Figure 5.2 presents typical late afternoon and evening 15 min averaged vertical drift height profiles during November 15. In this case, the data above 1000 km were smoothed using three-point running averages in altitude (i.e., 150 km). Figure 5.2 indicates that at 1718 LT the upward drifts decreased weakly with height up to about 1600 km. On the other hand, at 1858 LT, near the time of the peak prereversal enhancement, the drifts decreased strongly with height (at about 0.04 m/s/km) between about 400 km and 900 km and at a much smaller rate at higher altitudes. At this time, the peak electron density (inferred from the peak backscattered power) was below about 350 km, and spread F echoes were already present at lower heights. After the drift reversal to downward at about 2030 LT, the height profiles became noisier, as a result of lower signal-to-noise ratios, and the drifts decreased with height at much smaller rates (about 0.005 m/s/km) above about 500 km, as illustrated in the 2058 LT profile. In this case spread F echoes extend to altitudes of up to about 450 km.

Afternoon and evening vertical drifts were measured up to about 2000 km also during November 16, 2004, which was a geomagnetically quiet day with a solar flux index of 108. In this case, the afternoon drifts (not shown) again decreased weakly with height, but the evening and early night drifts were significantly different from those of the previous day and from the climatological values. In particular, they showed a late and unusually long (between about 1900 and 2100 LT) period of upward drifts. Figure 5.3 shows typical afternoon and early night 15 min averaged vertical drift profiles during this day. Here again, we smoothed the height profiles using three-point running averages. At 1808 LT, the drifts

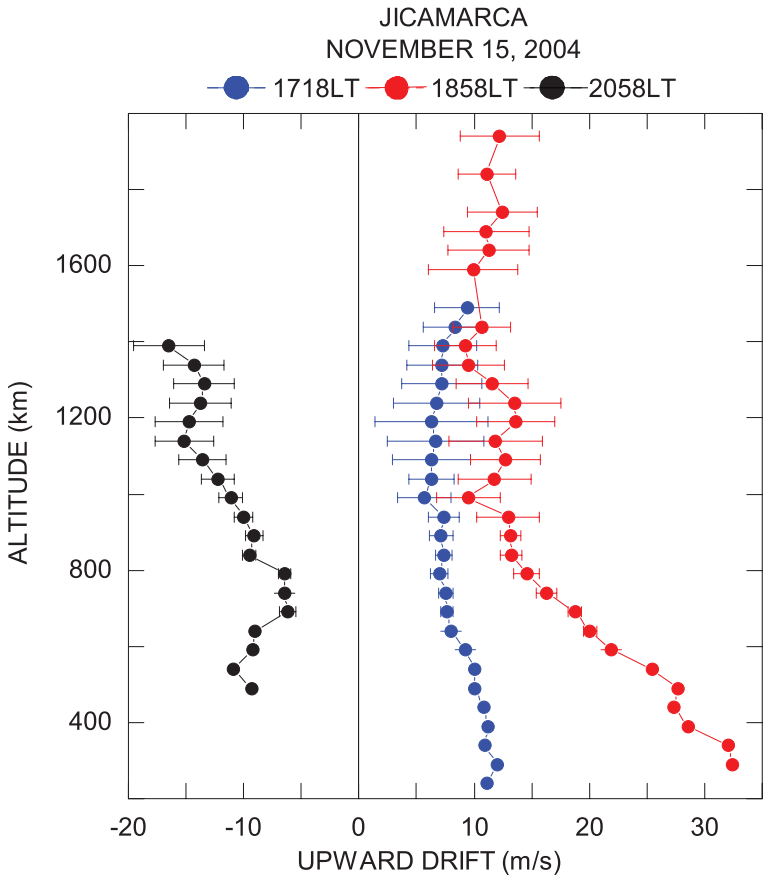

Figure 5.2. Examples of height profiles of evening vertical drifts over Jicamarca during 15 November 2004.

were upward below 600 km and downward at higher heights; they decreased on average, by about 0.03 m/s/km below about 800 km and at much smaller rate at higher altitudes. During the long period of early night upward drifts, their values decreased weakly with height between about 550 and 1200 km, as shown in the 2012 LT profile. At this time, spread F echoes were present below about 550 km.

The second campaign of high-altitude vertical drift measurements was carried out during March 19-20, 2013. These measurements were made with a 75 km height resolution to an altitude of 1500 km and a time resolution of 5 min. On March 19, vertical drifts were measured from 1400 and 2200 LT, except for an unfortunate data gap from 1850 to 2030 LT. This was a geomagnetic quiet day with a decimetric solar flux index of about 110. Figure 5.4 shows the local time variation of these drifts between 1600 and 1900 LT

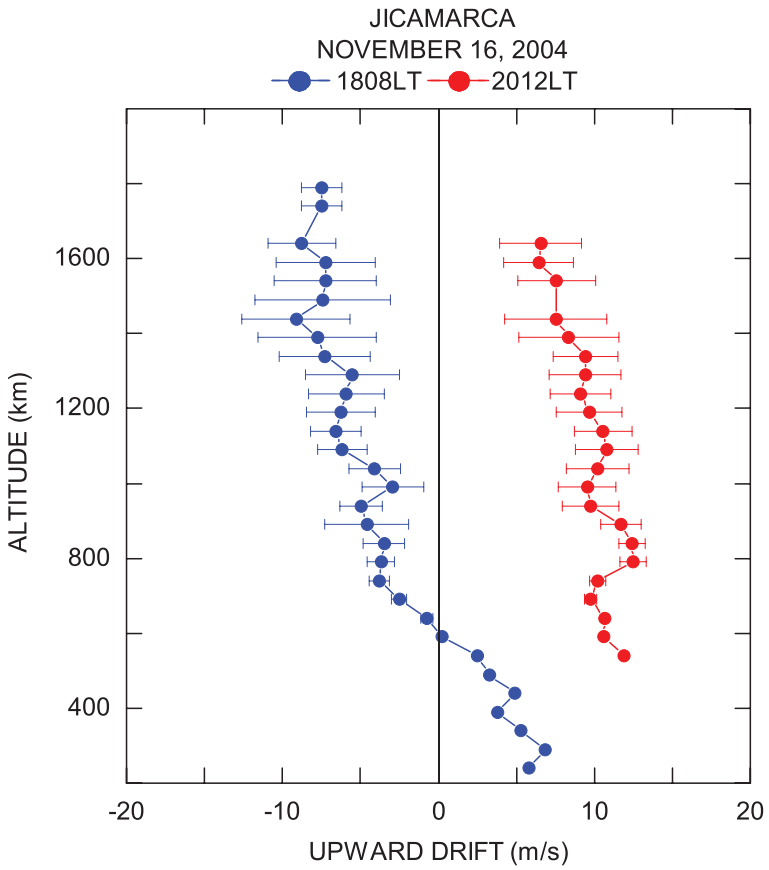

Figure 5.3. Examples of height profiles of evening vertical drifts over Jicamarca during 16 November 2004.

at selected altitudes obtained by three-point averages of the 5 min data up to 750 km and seven-point averages at higher altitudes, and the corresponding height-averaged climatological drifts. The accuracy of these measurements was generally better than 2 m/s. The afternoon data illustrate again the small typical decrease of the upward drifts with height. With the onset of the prereversal enhancement at about 1745 LT, the upward drifts started to increase at all heights up to about 1845 LT, but most strongly below about 700 km. The drift measurements after 2030 LT (not shown) did not change much with height above 400 km and were affected by spread F at lower altitudes. Figure 5.5 presents typical height profiles of the vertical drifts during the evening of March 19. In this case, the data above 600 km were obtained using three-point running averages in height. The profile at 1732 LT shows a relatively small decrease of the upward drifts with height. The second profile

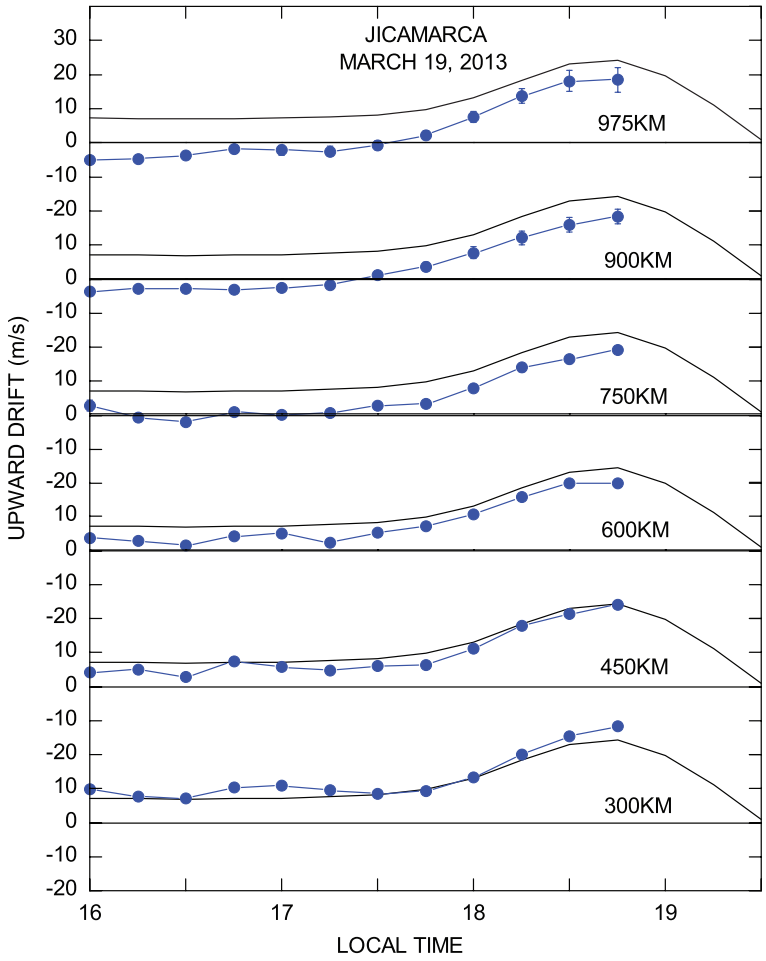

Figure 5.4. Equatorial vertical plasma drifts over Jicamarca during 19 March 2013. The solid curves denote the height-averaged quiet-time climatological drifts.

shows that in the early phase of the prereversal enhancement the upward drifts increased by nearly the same value at all altitudes. The profile at 1838 LT, at about the time of the prereversal enhancement peak, shows an increase of the upward drifts at the lowest altitudes, a nearly linear decrease between about 400 and 800 km, and essentially height independent values above about 800 km. Figure 5.5 also indicates that with the onset of the prereversal enhancement, the upward drifts had their largest increases at about 300 km. In this period, the peak electron density occurred at altitudes of about 300 km before about 1815 LT and at 375 km at about 1840 LT. Vertical drifts were measured up to about 1500 km also during March 20, 2013. This was a moderately disturbed day, especially near dusk, which resulted in significant departures from both the drift measurements on March 19 and

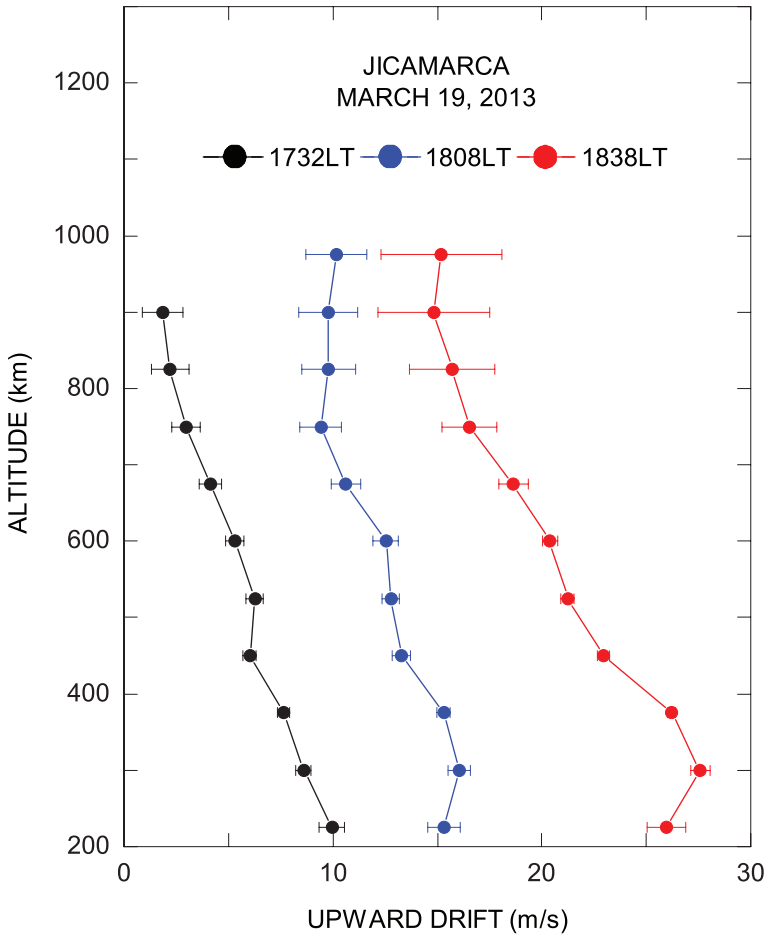

Figure 5.5. Selected height profiles of evening vertical drifts over Jicamarca during 19 March 2013.

from the quiet-time climatological values, as shown in Figure 5.6. These data were obtained using five-point running averages of the 5 min measurements. In this case, as usual, the afternoon drifts decreased weakly with altitude. At the typical time of the peak prereversal enhancement (about 1900 LT) the upward drifts were only 8 m/s at 300 km; they decrease linearly to zero up to about 600 km and did not change with height at higher altitudes up to about 1100 km. After their reversal to downward at about 1930 LT, the drifts did not change much with height up to the end of the observational period at 2200 LT.

Higher Resolution Measurements

We examined the altitudinal variations of late afternoon and evening vertical plasma

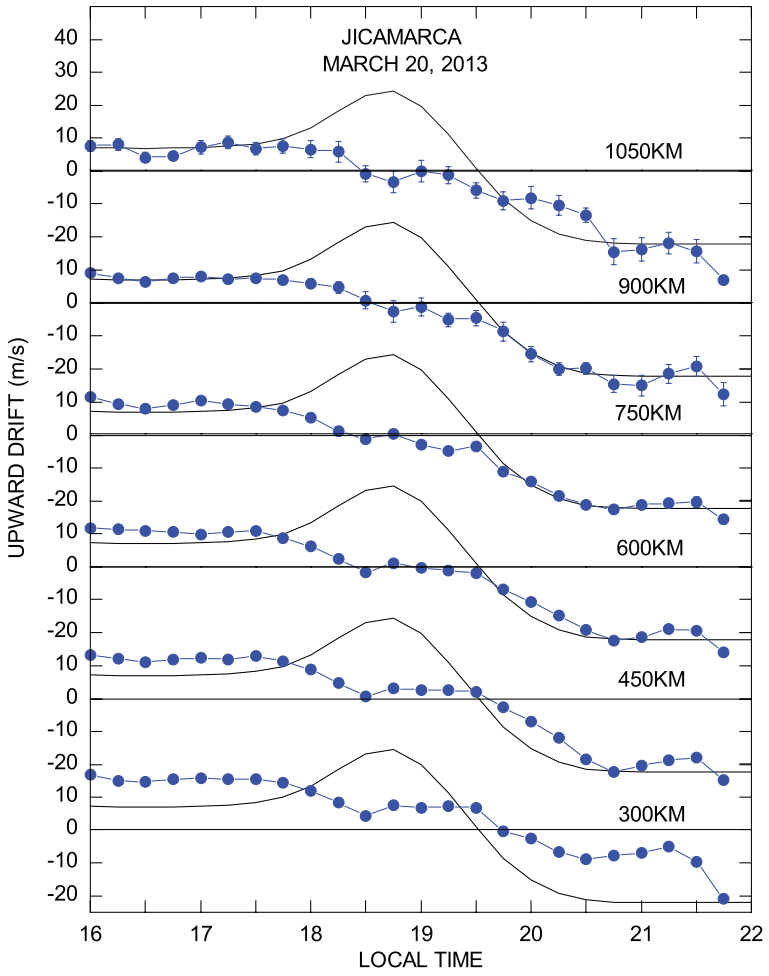

Figure 5.6. Afternoon and early night vertical plasma drifts over Jicamarca during 20 March 2013. This period was moderately disturbed. The solid curves denote the height-averaged quiet-time climatological drifts.

drifts near the F-layer peak in more detail using observations generally made during the so-called World Day campaigns, which have higher altitudinal resolution, but cover smaller altitudinal ranges. Of course, the higher altitudinal resolution also leads to larger drift variability, especially near solar minimum. We deleted drift measurements with errors larger than 2 m/s and in regions of equatorial spread F.

Figure 5.7 presents 10 min averaged vertical drift height profiles near dusk during September 18, 2001, which was a geomagnetically quiet period with a decimetric flux index of 204. These profiles are typical of equinox and December solstice high solar flux conditions. Spread F echoes were first observed at about 1910 LT and later covered an increasing

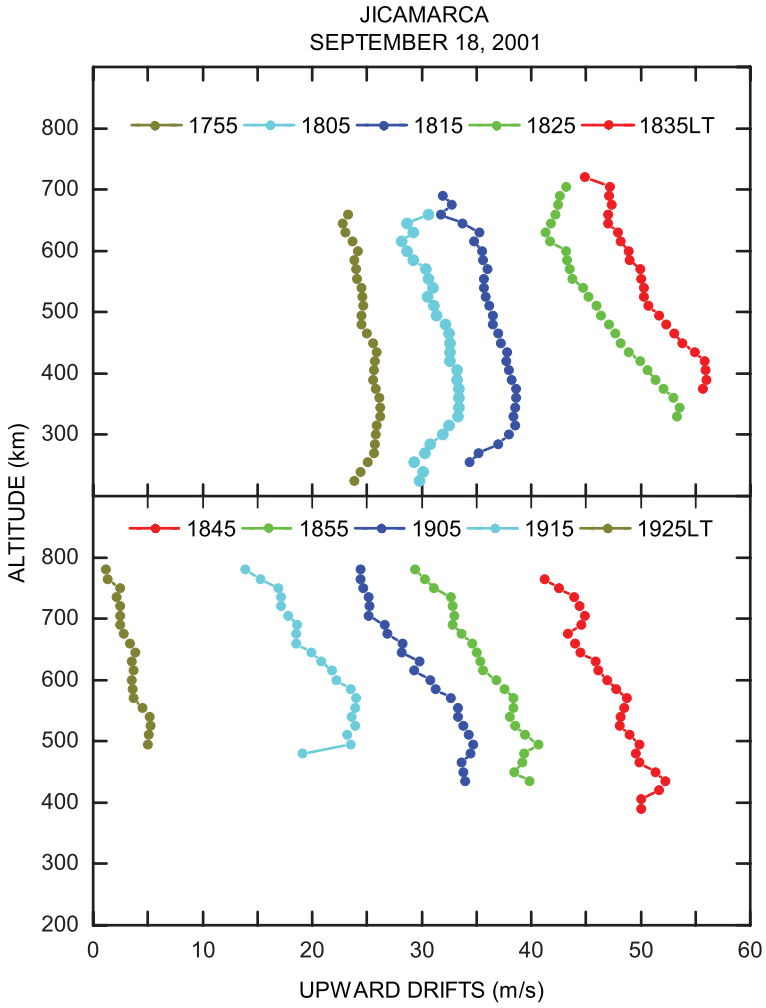

Figure 5.7. Altitudinal profiles of the Jicamarca vertical drifts during the evening of 18 September 2001. Low plasma densities and height-increasing equatorial spread F layer limited the range of bottomside drift measurements after about 1830 LT.

altitudinal range. On this evening, the peak electron density peak height was at about 350 km at 1800 LT; it increased to about 600 km at 1920 LT and to 495 km at 1915 LT. The top panel in Figure 5.7 shows the small height variation of the late-afternoon drifts, and the systematic increase of the upward drifts up to about 1840 LT with the development of positive and negative drift gradients below and above the peak drift heights. The bottom panel shows the upward drift rapidly decreasing with time at all altitudes. The last profile shows only small drift variations with height, which is generally the case about one hour after the peak prereversal drift enhancements.

Figure 5.8 shows late afternoon and early night vertical plasma drift profiles during April 17, 2001 when the decimetric solar flux index was 126. On this day, the onset of equatorial spread F occurred at about 1915 LT and strong geomagnetic activity started at about 1945 LT. The heights of peak power (density) were 300, 350, and 500 km at 1700, 1800, and 1900 LT, respectively. Figure 5.8 shows, again, small drift variations with height in the late afternoon. Near the peak prereversal velocity enhancement, the drift increased with height below about 400 km and decreased up to about 500 km. Close to their reversal the upward drifts increased with height above 500 km.

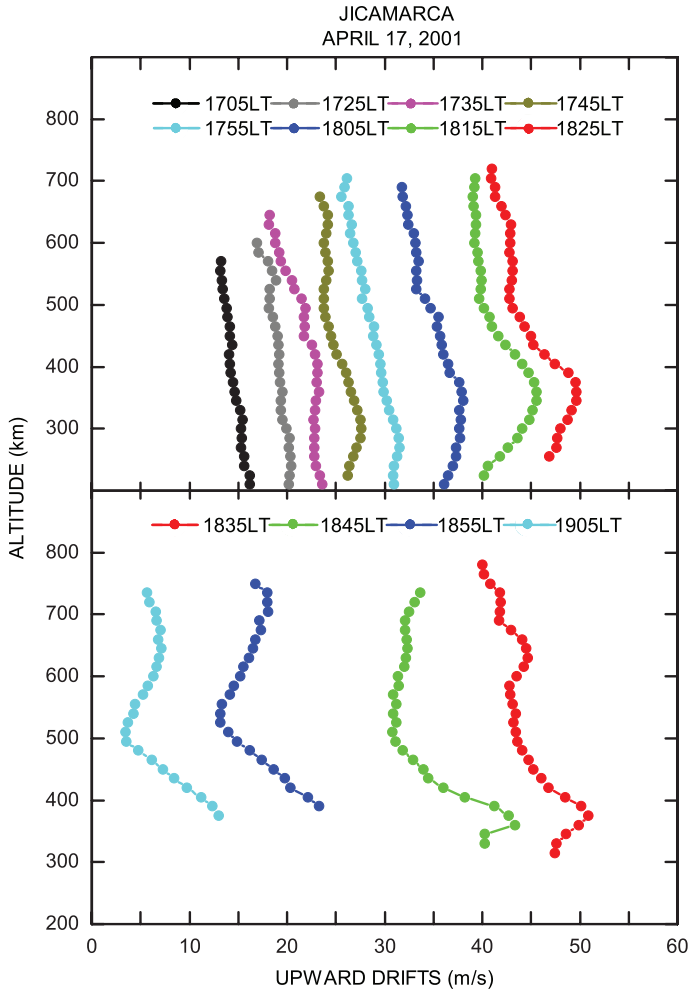

Figure 5.8. Altitudinal profiles of the Jicamarca vertical drifts during the evening of 17 April 2001. The topside velocity gradients changed at about 1850 LT.

Strongly height-increasing upward drifts over a large range of altitudes (up to about 800 km) are sometimes observed for up to about one hour after peak prereversal enhancements during December solstice and equinox moderate high solar flux conditions. One of these events is illustrated in Figure 5.9. This was a geomagnetically quiet period with a decimetric solar flux index of 165. This figure shows an increase of the upward drifts by about 0.06 m/s/km from about 400 to 700 km between 1855 and 1915 LT. On this day, these large velocity gradients were observed up to about 1930 LT, and the heights of peak electron density increased from 350 to 500 km between 1800 and 1930 LT.

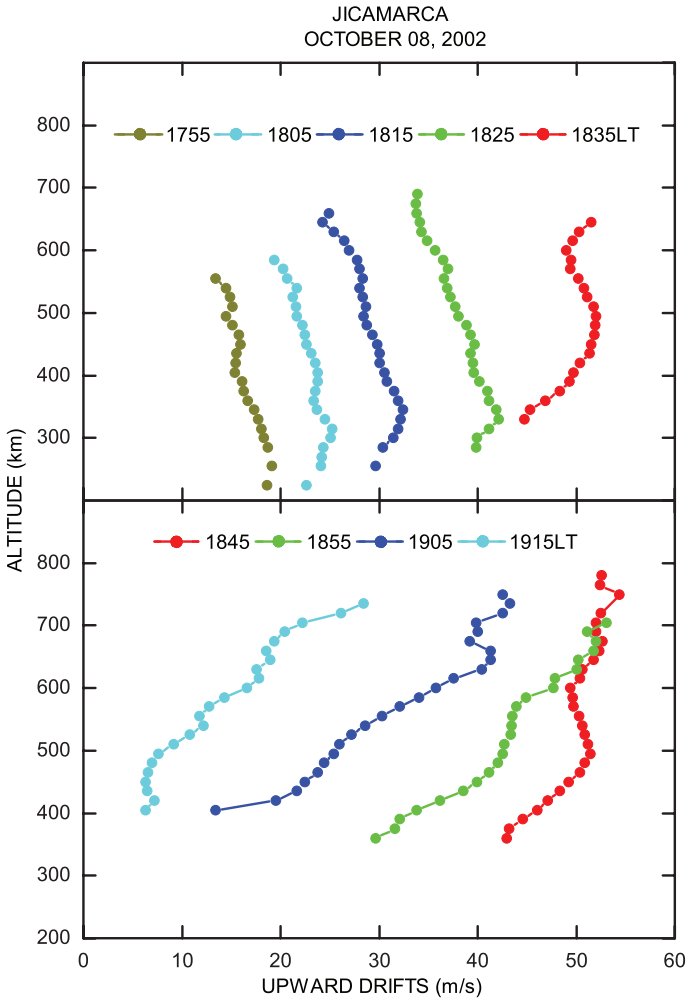

Figure 5.9. Altitudinal profiles of the Jicamarca vertical drifts showing strongly height-increasing drifts over an unusually large altitudinal range.

The general characteristics of late afternoon and evening vertical drift profiles during June solstice are generally consistent with those presented above. However, during this season, the height profiles and the peak prereversal enhancements have larger temporal, altitudinal and day-to-day variability, especially under low solar flux conditions. Figure 5.10 shows an example of very large variability of June solstice vertical drift profiles during moderate solar flux (decimetric index of about 175) magnetic quiet conditions. Figure 5.10 shows upward velocity peaks at altitudes of about 350 km on June 1 and below 220 km on June 3. The altitudes of peak electron densities at 1735, 1815, and 1855 LT were at about 320, 380, and 440 km on June 1 and at 340, 350, and 380 km on June 3, respectively. The velocity profiles on June 4 (not shown) were similar to those on June 3, but with a peak upward drift of 20 m/s at an altitude of about 250 km. The June 3 and 4 peak upward drift velocities were significantly larger than their height-averaged values.

We have illustrated above the large variability of the height profiles of the evening vertical drifts. This variability is largest near solar minima, when there is also very large variability on the occurrence, amplitude, and time of the prereversal enhancements [e.g., *Fejer and Scherliess*, 2001]. Figure 5.11 presents altitudinal drift profiles near the average time of the evening prereversal velocity enhancement during the January 18 - February 2, 2010 very low solar flux (F10.7 index of about 80) sudden stratospheric warming event [e.g., *Fejer*, 2011; *Fejer and Tracy*, 2013]. These profiles were obtained using three-point running height averages. During these days, the afternoon vertical drifts were also highly variable but, on the average, they decreased weakly with altitude. Figure 5.11 shows that, even in this period of extreme day-to-day variability, the altitudinal variation of these drifts have the general characteristics described above, i.e., increase at the lowest altitudes (below the F-layer peak), decrease near and above the F-layer peak and nearly constant values in the topside. This suggests that single height drift measurements and height-averaged values can significantly underestimate the peak prereversal velocity enhancements.

In this study, we have considered the altitudinal dependence of only quiet-time vertical plasma drifts. We note that during geomagnetically active conditions the equatorial vertical

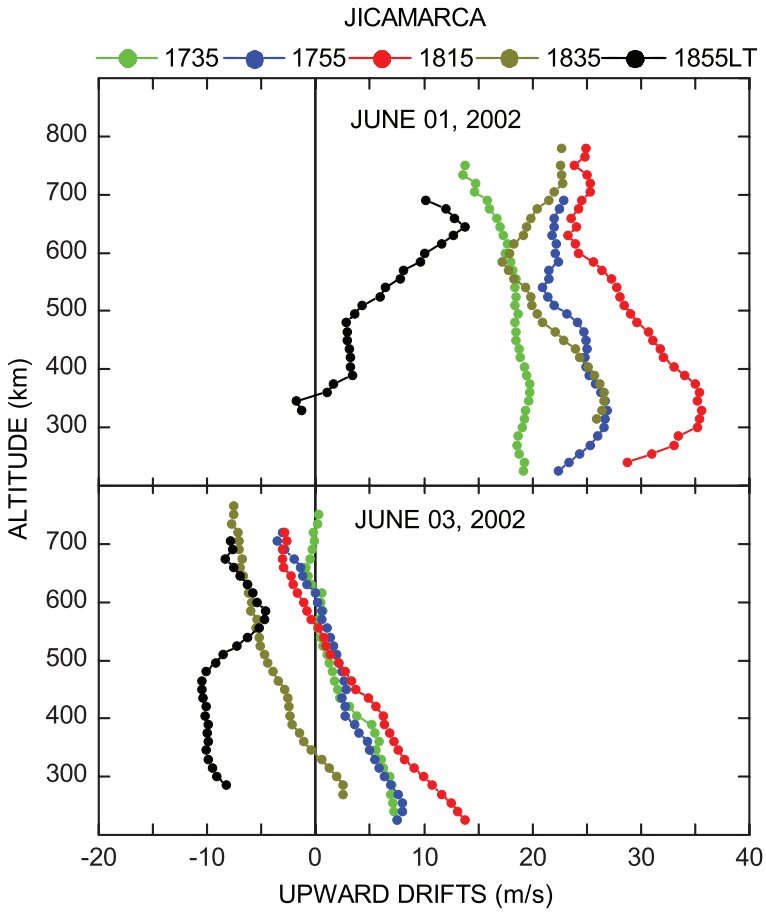

Figure 5.10. Altitudinal profiles of evening vertical drifts during June 2002.

plasma drifts are essentially height independent as a result of the very weak latitudinal variation of the low-latitude disturbance electric fields.

5.4. Discussion

We have shown that, although the late afternoon and early night equinoctial and December solstice equatorial vertical plasma drifts are quite variable, they have well-defined climatological altitudinal dependence. The late afternoon drifts have usually very small negative height gradients (about 0.005 m/s/km), which can extend to up to about 1800 km. Close to the peak prereversal velocity enhancements, the drifts briefly increase with height at the lowest altitudes, generally have relative large (up to about 0.02 - 0.04 m/s/km) negative gradients near and above the electron density peak, and do not change much with height

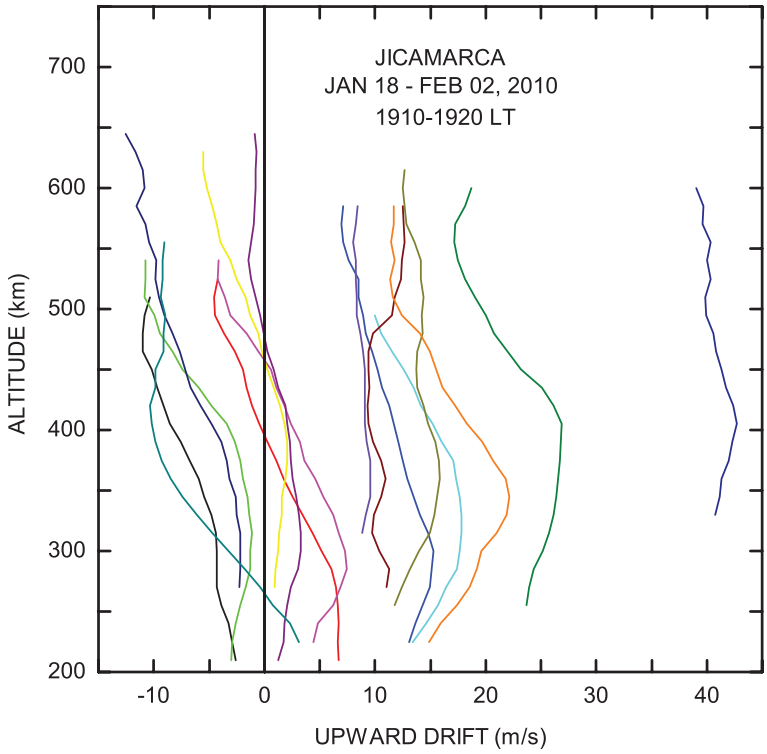

Figure 5.11. Height profiles of evening vertical drifts during December solstice very low solar flux conditions.

in the topside ionosphere (above about 800 km). In this local time sector, the transition height between decreasing and nearly altitude-independent upward drifts is about 800 km for moderate solar flux conditions and about 400 - 500 km near solar minima. As a result, during high solar flux periods, this transition height appears to be above the peak altitude (about 900 km) sampled during standard Jicamarca radar experiments. Unusually large increases in the upward drifts with height are sometimes observed over large altitudinal ranges (up to about 400 km) during periods of large and rapid drift decreases after their peak prereversal enhancements. These events occur most often during equinox and December solstice high solar flux conditions and last for about an hour. After the evening drift reversal (about 1930 - 2000 LT), the downward vertical velocities have, again, generally small altitudinal gradients. In this case, however, the frequent occurrence of equatorial spread F and the systematic smaller signal-to-noise ratios, decrease the altitudinal range of reliable ambient drift radar measurements. The June solstice evening drifts have the largest altitudinal and

day-to-day variability. The evening prereversal enhancement peaks during this season can occur at altitudes as low as about 200 km.

The altitudinal dependence of the late afternoon and evening F-region vertical drifts described above can generally be explained using the theoretical results derived by *Murphy and Heelis* [1986]. This study showed that near the magnetic equator, for a static dipole magnetic field in the meridional plane and symmetric vertical (v_r) and zonal (v_ϕ) drifts about the equator (i.e., $\partial/\partial\theta = 0$), the curl-free electric field condition, curl $\mathbf{E}$ = curl ($\mathbf{v} \times \mathbf{B}$), gives:

$$\frac{1}{r}\left(\frac{\partial v_\phi}{\partial \phi}\right) - 2\frac{v_r}{r} + \left(\frac{\partial v_r}{\partial r}\right) = 0, \tag{5.1}$$

where r = R + z, where r is the radial distance, R is the radius of the Earth, and z is the height. Here, it is also assumed that the magnetic flux density is longitude independent and that its variation perpendicular to the magnetic meridional plane is negligible. *Murphy and Heelis* [1986] pointed out that the altitudinal variation of the vertical drifts is largely coupled to the longitudinal gradient (or temporal variation, if longitude and local time are interchangeable) of the zonal drifts. *Pingree and Fejer* [1987] showed that, on the average, the Jicamarca low solar flux equinoctial vertical drifts between 250 and 650 km increased with height in the morning and decreased from about noon to about 2200 LT, when the eastward drifts reached their peak values. They also reported that the height averaged altitudinal gradient was largest (about 0.02 m/s/km) near dusk. Since the second term in equation (1) was only about 0.006 m/s/km, the observed altitudinal dependence was mostly related to the temporal variation of the F-region zonal plasma drifts. We note, however, that during equinoctial and December solstice high solar flux periods close to the peak prereversal enhancements, this term can reach values of about 0.02 m/s/km. *Pingree and Fejer* [1987] also pointed out that their measurements were not accurate enough to determine any change in the velocity gradient with altitude.

The main characteristics of the altitudinal structure of our measured evening vertical drifts reported above are also consistent with the results derived from the curl-free condition

with the assumption that temporal variation of the zonal drifts is a good proxy for their longitudinal variation. The small decrease of the late afternoon upward drift with height is consistent with the small local time variation (i.e., longitudinal gradient) of the nearly season- and solar-cycle independent afternoon zonal drifts [e.g., *Fejer*, 1991; *Fejer et al.*, 2005]. The increase of the upward velocity with height in the bottomside of the F layer near dusk can largely be explained as resulting from the decrease of the corresponding zonal drifts, as illustrated in Figure 5.12. In this case, the errors on the vertical drifts were smaller than 2 m/s. The errors in the zonal drifts were about 10 m/s up 2000 LT in the upper height range, while in the lower height range they were about 10 m/s up to 1925 LT, about 25 m/s from 1930 to 1945 LT and about 80 m/s later. On this day, the afternoon vertical drifts decreased weakly with height consistent with the small height-independent increase in the corresponding eastward drifts. Figure 5.12 shows that, as expected from the curl-free condition, the height increasing and decreasing average vertical drifts between 1920 and 1940 were associated with decreasing and increasing eastward drifts, respectively. The development of the low-altitude height-increasing upward drifts is associated with the growth phase of the shear in the zonal plasma flow below the F-layer peak. The resulting bottomside plasma flow vortex extends to higher altitudes until the reversal of the vertical velocity. Our data suggest that this bottomside vortex is essentially a permanent feature of the equatorial evening ionosphere. The large rapid increase in the errors of the zonal drift measurements in the bottomside of the F layer often make it difficult to follow the development of this vortex.

The other general features of the evening vertical drift height structure can also be explained as resulting mostly from the local time/longitudinal variation of the corresponding zonal drifts. In this local time sector, the zonal drifts are eastward, their amplitudes increase, and their peak values occur at earlier local times with increasing solar flux [e.g., *Fejer et al.*, 2005], resulting in faster drift variations during high solar flux periods than during low flux times. On the other hand, the peak prereversal enhancements also strongly increase with solar flux [e.g., *Fejer*, 1991]. Therefore, close to the peak prereversal enhancements, the curl-

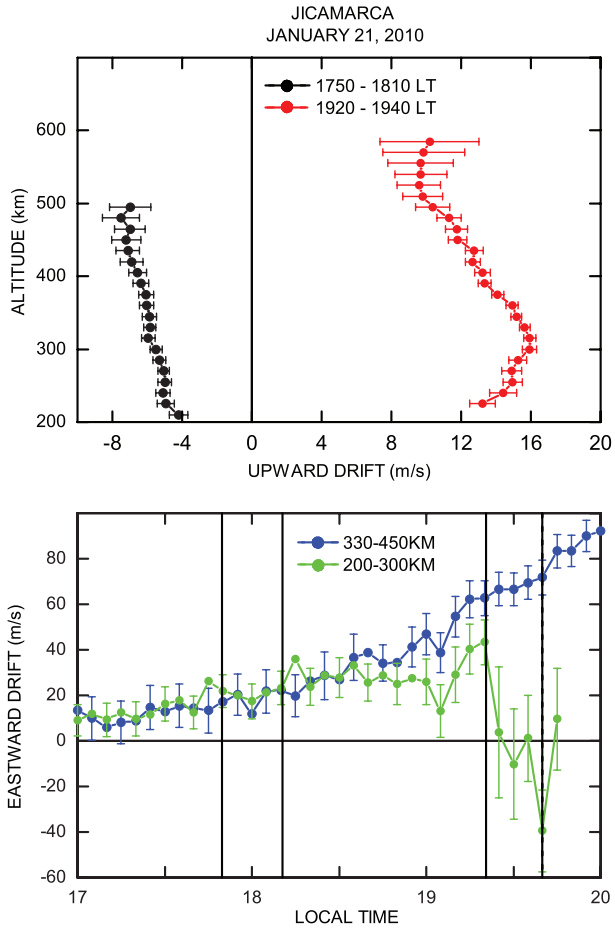

Figure 5.12. Height profiles of evening vertical drifts during December solstice very low solar flux conditions.

free conditions are consistent with the largely season and solar cycle-independent decreases of the upward drifts with height (on the order of 0.020.04 m/s/km) near the layer peak and above. The occasional occurrence of height-increasing vertical drifts over a large range of altitudes near dusk is likely due to early fast decreases of the eastward drifts. These events occur primarily during December solstice and equinox high solar flux periods. During the evening of October 8, 2002 shown in Figure 5.9, for example, the eastward drifts near the F region and above decreased rapidly after 1855 LT.

Satellite measurements indicate that close to the times of the peak prereversal enhancements of the vertical drifts, the topside equatorial eastward drifts decrease with height [e.g., *Coley and Heelis*, 1989; *Coley et al.*, 2014; *Pacheco et al.*, 2011]. This leads to slower

zonal drift variations in the topside ionosphere than near the F-layer peak and, therefore, to weaker altitudinal variations in the vertical drifts. *Coley et al.* [2014] showed that the time rate of change of the topside equatorial evening zonal drifts measured by the C/NOFS satellite decreases with solar flux. This is consistent with lower transition height between nearly independent and altitude decreasing upward drifts for lower solar flux conditions.

Numerous theoretical and numerical models have been used to study the electrodynamics of the low-latitude ionosphere, but they have provided only very limited information on the height dependence of evening equatorial vertical drifts. *Eccles* [1998a,b] showed that the primary causes of low-latitude zonal and vertical electric field structure are polarization electric fields resulting in meridional wind system-driven divergencies of the zonal Pedersen currents, and curl-free electric field effects. This study also pointed out that magnetic field-aligned integrated Pedersen conductivity plays a dominant role on the altitudinal variation of the equatorial vertical drifts. The evening prereversal velocity enhancements predicted this model decrease with altitude and disappear near an altitude of 1000 km; the corresponding eastward drifts also decrease in the topside ionosphere. This model does not predict the occurrence of height-increasing upward drifts in the bottom of the F layer, and nearly height-independent prereversal velocity enhancements extending at least up to about 1800 km. Recently, *Heelis et al.* [2012] examined the effect of zonal winds in the development of the equatorial vertical drift prereversal enhancement. This simulation study predicted that the equatorial vertical plasma drifts decrease slowly with altitude from 100 to 500 km. *Rodrigues et al.* [2012] used numerical simulations to study the development of the evening plasma drift vortex. Clearly, more detailed simulation studies are needed for the understanding of the complex altitudinal dependence of the equatorial vertical drifts and their important effects on the evening low-latitude ionosphere.

5.5. Summary

We have presented the first detailed study of the altitudinal dependence of late afternoon and early night equatorial F-region vertical plasma drifts and reported the first Jicamarca vertical drift measurements extending up to about 2000 km. Our results indi-

cate that even though the vertical drifts have large spatial and temporal variability in this local time sector, their height structure have well-defined general characteristics that can largely be explained by the curl-free electric field condition.

The late afternoon drifts usually decrease weakly with altitudes up to about 1800 km under moderate solar flux conditions. Near the time of the evening prereversal velocity peak, the upward drifts generally increase with height in the bottomside of the F layer, they decrease near and above the electron density peak, and are nearly height independent in the (solar flux dependent) topside ionosphere. The transition height between decreasing and nearly altitude-independent drifts increases with solar flux and appears to be above the peak altitude (above about 900 km) by the Jicamarca radar during high solar flux conditions. The evening upward drifts occasionally increase with height over unusually large altitudinal ranges (e.g., 300 - 400 km) for about an hour after their peak values during equinox and December solstice high solar flux conditions. At the reversal of the vertical drifts to downward, they again have generally small altitudinal gradients. The June solstice evening drifts are highly variable and sometimes have prereversal peaks at altitudes as low as about 200 km.

We have shown that the late afternoon and evening F-region vertical drift profiles can generally be explained by the curl-free electric field condition using the local time dependence of the zonal drifts as a proxy for the zonal drift longitudinal dependence. The typical height profiles near the evening prereversal enhancements, with upward drifts increasing in the bottomside and decreasing near the layer peak and above, for example, are associated with eastward drift decreasing and increasing with time in the lower and upper F region, respectively. In this case, the lower altitude height-increasing upward drifts are also associated with the sheared zonal drifts and the development of the plasma flow vortexes. In the topside ionosphere the evening vertical drifts do not change much with height, which is consistent with the weaker temporal dependence of the correspondingly weaker zonal drifts. The dependence of the amplitude and time of the peak eastward peak drifts on season and solar cycle also produces clear signatures on the vertical drift profiles. Our results suggest

the height profiles of the equatorial vertical plasma drifts are longitude dependent and their prereversal enhancement peaks are sometimes underestimated by single point satellite and ground-based measurements.

The results reported above indicate that single point ground-based and satellite vertical drift measurements provide an incomplete description of the electrodynamics of the evening equatorial ionosphere. C/NOFS satellite measurements show significant longitudinal variation on the low-latitude F-region zonal plasma drifts at all local times [e.g., *Coley et al.*, 2014; *Fejer et al.*, 2013]. These results, together with more realistic magnetic field models, could be used for more detailed information on the altitudinal structure of the vertical drifts. The longitudinal dependence of the zonal drifts also suggests the altitudinal variation of the evening vertical drifts and their electrodynamic effects (e.g., latitudinal variation of total electron content) should have significant longitudinal dependence.

CHAPTER 6
SUMMARY AND CONCLUSIONS

This chapter summarizes the main results from the previous two chapters that are based on our studies. Future work to enhance this present work and suggestions to how to use this study are also included.

6.1. Summary

We have studied the variation of E- and F-region plasma vertical and zonal drifts with altitudes over low latitudes. The study is split into daytime when the changes of the drifts with altitude are small, particularly in the case of vertical drifts, and around dusk, when their altitudinal gradients change very rapidly because of fast changes in the electrodynamic properties.

During the day, we have shown, the upward drifts increase with altitude in the morning hours, which gradually change to decreasing with altitude in the afternoon hours. The westward drifts, on the other hand, show large nonlinear decreases at the bottom side and smaller decreases at higher altitudes. An important part of this work is the study of the relationship between E- and F-region drifts during the day by combining ISR and JULIA data. A linear relationship between the E and F region, suggested by *Chau and Woodman* [2004], is seen consistently in cases of vertical drifts, but do not hold in cases of zonal drifts, particularly at the lower altitudes. We also notice at times, the zonal plasma drifts exhibit opposite altitudinal variations at the lower and upper altitudes.

The June solstice months show small altitudinal variations for both vertical and zonal plasma drifts. Largest altitudinal variations are seen in the equinoxial months for the zonal drifts, especially in the lower altitudes in the afternoon. We also notice, for both components, the drifts peak at different altitudes at different local times. The change of increases of the vertical drift with height in the morning hours to decreases in the afternoon takes place at different local times in different seasons. Our observations show during the morning hours in May-June and November-December, the linear relationship between E-

and F-region vertical drifts do not hold. We believe this because of the effect of the neutral winds at the 150 km region. The afternoon reversal from westward to eastward zonal drifts seems to take place at lower altitudes at an earlier time except November-December.

This study also shows climatological drifts at E and F regions at different altitudes in bimonthly bins. We focused mainly on zonal drifts, as there have not been many such studies. Our bimonthly data show much larger variations in the mean drifts values at F-region heights than in the 150 km region. The zonal drifts, however, unlike vertical drifts, show larger day-to-day variability near 150 km than at F-region altitudes.

We studied the variation of plasma drifts during SSW periods. Our observations show the altitudinal variations of the vertical plasma drifts do not change during SSW periods from nonSSW periods. The SSW period zonal drifts and their altitudinal variations also do not change much from nonSSW periods.

Since the database of zonal drifts was not large enough to study altitudinal variations as a function of solar flux, we used a single bin of 110 sfu. However, since the daytime zonal drifts do not change much with solar flux, these climatological altitudinal profiles should be valid for different solar flux levels.

We have presented, for the first time, the evening time altitudinal profiles of vertical drifts from 200 km up to an altitude of about 2000 km. While the altitudinal variations of vertical drifts have large spatial and temporal variability, they have well defined general characteristics, which are functions of solar flux. The drifts increase with altitudes below F-region peak, decrease with increasing altitudes above that up to a certain height and then become almost height independent at higher altitude. This oppositely directed plasma flow about F-region peak gives rise to a vortex-like pattern in the plasma flow, which is a permanent feature of the post sunset sector. The transition altitude from height dependent to height independent increases with solar flux conditions. The upward vertical drifts do not show much height dependence after reversal to downward direction.

We have also discussed these altitudinal profiles of evening time vertical drifts can be largely explained by curl-free electric field conditions in low latitudes and is balanced by

local time dependence as a proxy for longitudinal derivatives of zonal drifts. The decreasing zonal drifts below F-region peak and increasing zonal drifts around and above F-region peak are responsible for such vertical drifts altitude profiles. The season-dependent time and amplitude of peak eastward drifts influences the prereversal enhancement peaks and vertical drift profiles. These drift profiles change with season, solar cycle, and longitudes.

We pointed out why single point measurements of the plasma drifts are not sufficient to understand the rapidly changing electrodynamics of these drifts in the dusk sector. The knowledge of longitude-dependent drifts, along with corresponding neutral winds and accurate magnetic field models, would help understand the physical processes responsible for vertical structure of these drifts.

6.2. Suggestions for Future Work

We have shown climatology of altitudinal profiles vertical and zonal drifts from 150 to about 600 km during day time, but could not study how these profiles changes with solar flux. With a larger data base of vertical and zonal drifts in the future, the solar flux dependence of the altitudinal profiles can be studied. The zonal drifts, which show large nonlinear altitudinal changes in the bottom side, need to be studied in relation to neutral winds. The longitudinal behavior of the bottom-side drifts also remains to be done. Occasionally we have observed negative vertical drifts and eastward zonal drifts at 150 km altitude regions even during quiet times. Similar observations have been reported by many for vertical drifts during the daytime from different longitude sectors. No clear drivers for such anomalous drifts have been established. Further investigations of such exceptional drift patterns and their possible driving by local neutral winds will be an excellent addition to this work. This study mainly focused on daytime and post sunset plasma drift variations with altitude. A similar in-depth study into the altitude variations in the nighttime and especially in the dawn sector will complement our work very well.

Finally, the most important follow up would be to incorporate these altitudinal variations in ionospheric models. This would certainly improve predictions of the ionospheric weather for space-based systems.

REFERENCES

Abdu, M. (1997), Major phenomena of the equatorial ionosphere-thermosphere system under disturbed conditions, *J. Atmos. Sol. Terr. Phys.*, *59*(13), 1505–1519.

Abdu, M. A., K. N. Iyer, R. T. de Medeiros, I. S. Batista, and J. H. A. Sobral (2006), Thermospheric meridional wind control of equatorial spread F and evening prereversal electric field, *Geophys. Res. Lett.*, *33*(7), L07106, doi:10.1029/2005GL024835.

Abdu, M., et al. (2009), Conjugate point equatorial experiment (COPEX) campaign in Brazil: Electrodynamics highlights on spread F development conditions and day-to-day variability, *J. Geophys. Res.*, *114*(A4).

Alken, P. (2009), A quiet time empirical model of equatorial vertical plasma drift in the Peruvian sector based on 150 km echoes, *J. Geophys. Res.*, *114*(A2), A02308, doi:10.1029/2008JA013751.

Anderson, D., and R. Roble (1981), Neutral wind effects on the equatorial F-region ionosphere, *J. Atmos. Sol. Terr. Phys.*, *43*(8), 835–843.

Anderson, D., A. Anghel, K. Yumoto, M. Ishitsuka, and E. Kudeki (2002), Estimating daytime vertical **EXB** drift velocities in the equatorial F-region using ground-based magnetometer observations, *Geophys. Res. Lett.*, *29*(12), 37–1–37–4, doi:10.1029/2001GL014562.

Balsley, B. B. (1964), Evidence of a stratified echoing region at 150 kilometers in the vicinity of the magnetic equator during daylight hours, *J. Geophys. Res.*, *69*(9), 1925–1930, doi:10.1029/JZ069i009p01925.

Bernard, R., and A. Spizzichino (1971), Semi-diurnal wind and temperature oscillations in the E-region observed by the nancay incoherent scatter experiment, *J. Atmos. Sol. Terr. Phys.*, *33*(9), 1345–1352.

Bilitza, D., W. Hoegy, L. Brace, and R. Theis (1988), Evaluation of the international reference ionosphere with the large AE-C and DE 2 data bases, *Adv. in Space Res.*, *8*(4), 209–212, doi:http://dx.doi.org/10.1016/0273-1177(88)90242-6.

Blanc, E., B. Mercandalli, and E. Houngninou (1996), Kilometric irregularities in the E and F regions of the daytime equatorial ionosphere observed by a high resolution hf radar, *Geophys. Res. Lett.*, *23*(6), 645–648, doi:10.1029/96GL00415.

Carpenter, D. L., and C. G. Park (1973), On what ionospheric workers should know about the plasmapause-plasmasphere, *Rev. Geophys.*, *11*(1), 133–154, doi:10.1029/RG011i001p00133.

Chakrabarty, D., R. Sekar, R. Narayanan, T. K. Pant, and K. Niranjan (2004), Thermospheric gravity wave modes over low and equatorial latitudes during daytime, *J. Geophys. Res.*, *109*(A12), A12309, doi:10.1029/2003JA010169.

Chapagain, N. P., M. J. Taylor, and J. V. Eccles (2011), Airglow observations and modeling of F region depletion zonal velocities over Christmas Island, *J. Geophys. Res.*, *116*(A2).

Chapman, S. (1956), The electrical conductivity of the ionosphere: A review, *Il Nuovo Cimento (1955-1965)*, *4*, 1385–1412.

Chapman, S., and R. Lindzen (1970), Atmospheric tides, 200 pp., D. Reidel, Dordrecht, Netherlands.

Chau, J. L., and E. Kudeki (2013), Discovery of two distinct types of equatorial 150 km radar echoes, *Geophys. Res. Lett.*, *40*(17), 4509–4514, doi:10.1002/grl.50893.

Chau, J. L., and R. F. Woodman (2004), Daytime vertical and zonal velocities from 150-km echoes: Their relevance to F-region dynamics, *Geophys. Res. Lett.*, *31*(17), L17801, doi:10.1029/2004GL020800.

Chau, J. L., B. G. Fejer, and L. P. Goncharenko (2009), Quiet variability of equatorial **EXB** drifts during a sudden stratospheric warming event, *Geophys. Res. Lett.*, *36*(5), L05101, doi:10.1029/2008GL036785.

Coley, W. R., and R. A. Heelis (1989), Low-latitude zonal and vertical ion drifts seen by DE 2, *J. Geophys. Res.*, *94*(A6), 6751–6761, doi:10.1029/JA094iA06p06751.

Coley, W. R., J. P. McClure, and W. B. Hanson (1990), Equatorial fountain effect and dynamo drift signatures from AE-E observations, *J. Geophys. Res.*, *95*(A12), 21,285–21,290, doi:10.1029/JA095iA12p21285.

Coley, W. R., R. A. Stoneback, R. A. Heelis, and M. R. Hairston (2014), Topside equatorial zonal ion velocities measured by C/NOFS during rising solar activity, *Ann. Geophys.*, *32*(2), 69–75, doi:10.5194/angeo-32-69-2014.

Cowling, T. G. (1945), The electrical conductivity of an ionized gas in a magnetic field, with applications to the solar atmosphere and the ionosphere, *Proc. R. Soc.*, *183*(995), 453–479, doi:10.1098/rspa.1945.0013.

Eccles, J. V. (1998a), A simple model of low-latitude electric fields, *J. Geophys. Res.*, *103*(A11), 26,699–26,708, doi:10.1029/98JA02657.

Eccles, J. V. (1998b), Modeling investigation of the evening prereversal enhancement of the zonal electric field in the equatorial ionosphere, *J. Geophys. Res.*, *103*(A11), 26,709–26,719, doi:10.1029/98JA02656.

England, S. L., S. Maus, T. J. Immel, and S. B. Mende (2006), Longitudinal variation of the E-region electric fields caused by atmospheric tides, *Geophys. Res. Lett.*, *33*(21), L21105, doi:10.1029/2006GL027465.

Evans, J. V. (1978), Incoherent scatter contributions to studies of the dynamics of the lower thermosphere, *Rev. Geophys.*, *16*(2), 195–216, doi:10.1029/RG016i002p00195.

Farley, D. T., E. Bonelli, B. G. Fejer, and M. F. Larsen (1986), The prereversal enhancement of the zonal electric field in the equatorial ionosphere, *J. Geophys. Res.*, *91*(A12), 13,723–13,728, doi:10.1029/JA091iA12p13723.

Fawcett, C. D. (1999), An investigation of equatorial 150-km irregularities. Ph.D. thesis, Univ. of Ill., Urbana-Champaign.

Fejer, B. G. (1991), Low latitude electrodynamic plasma drifts : a review, *J. Atmos. Sol. Terr. Phys.*, *53*(8), 677–693, doi:http://dx.doi.org/10.1016/0021-9169(91)90121-M.

Fejer, B. G. (1997), The electrodynamics of the low-latitude ionosphere: Recent results and future challenges, *J. Atmos. Sol. Terr. Phys.*, *59*(13), 1465–1482, The Ninth International Symposium on Equatorial Aeronomy, doi:http://dx.doi.org/10.1016/S1364-6826(96)00149-6.

Fejer, B. G. (2011), Low latitude ionospheric electrodynamics, *Space Sci. Rev.*, *158*(1), 145–166.

Fejer, B. G., and M. C. Kelley (1980), Ionospheric irregularities, *Rev. Geophys.*, *18*(2), 401–454, doi:10.1029/RG018i002p00401.

Fejer, B. G., and L. Scherliess (2001), On the variability of equatorial F-region vertical plasma drifts, *J. Atmos. Sol. Terr. Phys.*, *63*(9), 893–897, doi:http://dx.doi.org/10.1016/S1364-6826(00)00198-X.

Fejer, B. G., and B. D. Tracy (2013), Lunar tidal effects in the electrodynamics of the low latitude ionosphere, *J. Atmos. Sol. Terr. Phys.*, *103*(0), 76–82, doi:http://dx.doi.org/10.1016/j.jastp.2013.01.008.

Fejer, B. G., D. T. Farley, R. F. Woodman, and C. Calderon (1979), Dependence of equatorial F region vertical drifts on season and solar cycle, *J. Geophys. Res.*, *84*(A10), 5792–5796, doi:10.1029/JA084iA10p05792.

Fejer, B. G., D. T. Farley, C. A. Gonzales, R. F. Woodman, and C. Calderon (1981), F region east-west drifts at Jicamarca, *J. Geophys. Res.*, *86*(A1), 215–218, doi:10.1029/JA086iA01p00215.

Fejer, B. G., E. Kudeki, and D. T. Farley (1985), Equatorial F region zonal plasma drifts, *J. Geophys. Res.*, *90*(A12), 12,249–12,255, doi:10.1029/JA090iA12p12249.

Fejer, B. G., E. R. de Paula, S. A. Gonzlez, and R. F. Woodman (1991), Average vertical and zonal F region plasma drifts over Jicamarca, *J. Geophys. Res.*, *96*(A8), 13,901–13,906, doi:10.1029/91JA01171.

Fejer, B. G., E. R. de Paula, R. A. Heelis, and W. B. Hanson (1995), Global equatorial ionospheric vertical plasma drifts measured by the AE-E satellite, *J. Geophys. Res.*, *100*(A4), 5769–5776, doi:10.1029/94JA03240.

Fejer, B. G., E. R. de Paula, L. Scherliess, and I. S. Batista (1996), Incoherent scatter radar, ionosonde, and satellite measurements of equatorial F region vertical plasma drifts in the evening sector, *Geophys. Res. Lett.*, *23*(14), 1733–1736, doi:10.1029/96GL01847.

Fejer, B. G., J. R. Souza, A. S. Santos, and A. E. Costa Pereira (2005), Climatology of F region zonal plasma drifts over Jicamarca, *J. Geophys. Res.*, *110*(A12), A12310, doi: 10.1029/2005JA011324.

Fejer, B. G., J. W. Jensen, and S.-Y. Su (2008), Quiet time equatorial F region vertical plasma drift model derived from ROCSAT-1 observations, *J. Geophys. Res.*, *113*(A5), A05304, doi:10.1029/2007JA012801.

Fejer, B. G., M. Olson, J. Chau, C. Stolle, H. Lühr, L. Goncharenko, K. Yumoto, and T. Nagatsuma (2010), Lunar-dependent equatorial ionospheric electrodynamic effects during sudden stratospheric warmings, *J. Geophys. Res.*, *115*(A8).

Fejer, B. G., B. D. Tracy, and R. F. Pfaff (2013), Equatorial zonal plasma drifts measured by the C/NOFS satellite during the 2008−2011 solar minimum, *J. Geophys. Res.*, *118*(6), 3891–3897, doi:10.1002/jgra.50382.

Fejer, B. G., D. Hui, J. L. Chau, and E. Kudeki (2014), Altitudinal dependence of evening equatorial F region vertical plasma drifts, *J. Geophys. Res.*, *119*(7), 5877–5890, 2014JA019949, doi:10.1002/2014JA019949.

Feng, Z., E. Kudeki, R. F. Woodman, and J. Chau (2003), Transverse-beam incoherent scatter radar measurements of F region plasma densities at Jicamarca, *Radio Sci.*, *38*(4), 1071, doi:10.1029/2002RS002722.

Fesen, C. G., G. Crowley, R. G. Roble, A. D. Richmond, and B. G. Fejer (2000), Simulation of the pre-reversal enhancement in the low latitude vertical ion drifts, *Geophys. Res. Lett.*, *27*(13), 1851–1854, doi:10.1029/2000GL000061.

Forbes, J., and F. Vial (1989), Monthly simulations of the solar semidiurnal tide in the mesosphere and lower thermosphere, *J. Atmos. Sol. Terr. Phys.*, *51*(78), 649–661, International Middle Atmosphere Program Symposium, doi:http://dx.doi.org/10.1016/0021-9169(89)90063-9.

Forbes, J. M., and F. Vial (1991), Semidiurnal tidal climatology of the E region, *J. Geophys. Res.*, *96*(A2), 1147–1157, doi:10.1029/90JA02187.

Haerendel, G., and J. V. Eccles (1992), The role of the equatorial electrojet in the evening ionosphere, *J. Geophys. Res.*, *97*(A2), 1181–1192, doi:10.1029/91JA02227.

Hagan, M. E., J. M. Forbes, and F. Vial (1993), Numerical investigation of the propagation of the quasi-two-day wave into the lower thermosphere, *J. Geophys. Res.*, *98*(D12), 23,193–23,205, doi:10.1029/93JD02779.

Hagan, M. E., A. Maute, R. G. Roble, A. D. Richmond, T. J. Immel, and S. L. England (2007), Connections between deep tropical clouds and the Earth's ionosphere, *Geophys. Res. Lett.*, *34*(20), L20109, doi:10.1029/2007GL030142.

Hanson, W. B., and R. J. Moffett (1966), Ionization transport effects in the equatorial F region, *J. Geophys. Res.*, *71*(23), 5559–5572, doi:10.1029/JZ071i023p05559.

Hari, S. S., K. S. Viswanathan, K. S. V. Subbarao, and B. V. Krishna Murthy (1996), Equatorial E and F region zonal electric fields in the postsunset period, *J. Geophys. Res.*, *101*(A4), 7947–7949, doi:10.1029/95JA03855.

Hartman, W. A., and R. A. Heelis (2007), Longitudinal variations in the equatorial vertical drift in the topside ionosphere, *J. Geophys. Res.*, *112*(A3), A03305, doi: 10.1029/2006JA011773.

Häusler, K., and H. Lühr (2009), Nonmigrating tidal signals in the upper thermospheric zonal wind at equatorial latitudes as observed by champ, *Ann. Geophys.*, *27*(7), 2643–2652, doi:10.5194/angeo-27-2643-2009.

Heelis, R., P. Kendall, R. Moffett, D. Windle, and H. Rishbeth (1974), Electrical coupling of the E- and F-regions and its effect on F-region drifts and winds, *Planet. Space Sci.*, *22*(5), 743–756, doi:http://dx.doi.org/10.1016/0032-0633(74)90144-5.

Heelis, R. A., G. Crowley, F. Rodrigues, A. Reynolds, R. Wilder, I. Azeem, and A. Maute (2012), The role of zonal winds in the production of a pre-reversal enhancement in the vertical ion drift in the low latitude ionosphere, *J. Geophys. Res.*, *117*(A8), A08308, doi:10.1029/2012JA017547.

Hines, C. O. (1965), Dynamical heating of the upper atmosphere, *J. Geophys. Res.*, *70*(1), 177–183, doi:10.1029/JZ070i001p00177.

Huang, C.-S., F. J. Rich, O. de La Beaujardiere, and R. A. Heelis (2010), Longitudinal and seasonal variations of the equatorial ionospheric ion density and eastward drift velocity in the dusk sector, *J. Geophys. Res.*, *115*(A2).

Huba, J. D., G. Joyce, J. Krall, C. L. Siefring, and P. A. Bernhardt (2010), Self-consistent modeling of equatorial dawn density depletions with SAMI3, *Geophys. Res. Lett.*, *37*(3), L03104, doi:10.1029/2009GL041492.

Hudson, R. D. (1971), Critical review of ultraviolet photoabsorption cross sections for molecules of astrophysical and aeronomic interest, *Rev. Geophys.*, *9*(2), 305–406, doi: 10.1029/RG009i002p00305.

Immel, T. J., H. U. Frey, S. B. Mende, and E. Sagawa (2004), Global observations of the zonal drift speed of equatorial ionospheric plasma bubbles, *Ann. Geophys.*, *22*(9), 3099–3107, doi:10.5194/angeo-22-3099-2004.

Johnson, C. Y. (1969), Ion and neutral composition of the ionosphere., *Annals of the IQSY*, *5*, 197–213.

Kato, S. (1957), Prevailing wind in the ionosphere and geomagnetic sq variations, *J. Geomagn. Geoelectr.*, *9*(4), 215–217.

Kato, S. (1980), *Dynamics of the upper atmosphere*, 1, Springer Science & Business Media.

Kelley, M. C. (2009), *The Earth's Ionosphere: Plasma Physics & Electrodynamics*, vol. 96, Academic Press, San Diego, Calif.

Kil, H., E. R. Talaat, S.-J. Oh, L. J. Paxton, S. L. England, and S.-Y. Su (2008), Wave structures of the plasma density and vertical **EXB** drift in low-latitude F region, *J. Geophys. Res.*, *113*(A9), A09312, doi:10.1029/2008JA013106.

Klimenko, M., V. Klimenko, and A. Karpachev (2012), Formation mechanism of additional layers above regular {F2} layer in the near-equatorial ionosphere during quiet period, *J. Atmos. Sol. Terr. Phys.*, *9091*(0), 179–185, doi:http://dx.doi.org/10.1016/j.jastp.2012.02.011.

Krishna Murthy, B. V., S. S. Hari, and V. V. Somayajulu (1990), Nighttime equatorial thermospheric meridional winds from ionospheric h'F data, *J. Geophys. Res.*, *95*(A4), 4307–4310, doi:10.1029/JA095iA04p04307.

Kudeki, E., and S. Bhattacharyya (1999), Postsunset vortex in equatorial F-region plasma drifts and implications for bottomside spread-F, *J. Geophys. Res.*, *104*(A12), 28,163–28,170, doi:10.1029/1998JA900111.

Kudeki, E., and C. D. Fawcett (1993), High resolution observations of 150 km echoes at Jicamarca, *Geophys. Res. Lett.*, *20*(18), 1987–1990, doi:10.1029/93GL01256.

Kudeki, E., B. G. Fejer, D. T. Farley, and H. M. Ierkic (1981), Interferometer studies of equatorial F region irregularities and drifts, *Geophys. Res. Lett.*, *8*(4), 377–380, doi: 10.1029/GL008i004p00377.

Kudeki, E., C. D. Fawcett, W. L. Ecklund, P. E. Johnston, and S. J. Franke (1998), Equatorial 150-km irregularities observed at Pohnpei, *Geophys. Res. Lett.*, *25*(21), 4079–4082, doi:10.1029/1998GL900069.

Kudeki, E., S. Bhattacharyya, and R. F. Woodman (1999), A new approach in incoherent scatter F region **EXB** drift measurements at Jicamarca, *J. Geophys. Res.*, *104*(A12), 28,145–28,162, doi:10.1029/1998JA900110.

Kudeki, E., R. F. Woodman, and Z. Feng (2003), Incoherent scatter radar plasma density measurements at Jicamarca using a transverse-mode differential-phase method, *Geophys. Res. Lett.*, *30*(5), 1255, doi:10.1029/2002GL015496.

Liu, H.-L., and A. D. Richmond (2013), Attribution of ionospheric vertical plasma drift perturbations to large-scale waves and the dependence on solar activity, *J. Geophys. Res.*, *118*(5), 2452–2465, doi:10.1002/jgra.50265.

Liu, H.-L., and R. G. Roble (2002), A study of a self-generated stratospheric sudden warming and its mesosphericlower thermospheric impacts using the coupled TIME-GCM/CCM3, *J. Geophys. Res.*, *107*(D23), ACL 15–1–ACL 15–18, 4695, doi:10.1029/2001JD001533.

Liu, H.-L., V. A. Yudin, and R. G. Roble (2013), Day-to-day ionospheric variability due to lower atmosphere perturbations, *Geophys. Res. Lett.*, *40*(4), 665–670, doi:10.1002/grl.50125.

Lühr, H., M. Rother, K. Häusler, P. Alken, and S. Maus (2008), The influence of nonmigrating tides on the longitudinal variation of the equatorial electrojet, *J. Geophys. Res.*, *113*(A8), A08313, doi:10.1029/2008JA013064.

Maeda, K. (1952), Dynamo-theoretical conductivity and current in the ionosphere, *J. Geomagn. Geoelectr.*, *4*(2), 63–82, doi:10.5636/jgg.4.63.

Maeda, K., and S. Kato (1966), Electrodynamics of the ionosphere, *Space Sci. Rev.*, *5*(1), 57–79.

Maruyama, T. (1988), A diagnostic model for equatorial spread F, 1, Model description and application to electric field and neutral wind effects, *J. Geophys. Res.*, *93*(A12), 14,611–14,622, doi:10.1029/JA093iA12p14611.

Matsuno, T. (1971), A dynamical model of the stratospheric sudden warming, *J. Atmos. Sci.*, *28*(8), 1479–1494.

Matsushita, S. (1969), Dynamo currents, winds, and electric fields, *Radio Sci.*, *4*(9), 771–780, doi:10.1029/RS004i009p00771.

Maute, A., A. D. Richmond, and R. G. Roble (2012), Sources of low-latitude ionospheric **EXB** drifts and their variability, *J. Geophys. Res.*, *117*(A6), A06312, doi:10.1029/2011JA017502.

Maynard, N., T. Aggson, F. Herrero, and M. Liebrecht (1988), Average low-latitude meridional electric fields from de 2 during solar maximum, *Tech. rep.*, DTIC Document.

McClure, J. P., and V. L. Peterson (1972), Plasma transport in the equatorial F region, *Radio Sci.*, *7*(5), 539–547, doi:10.1029/RS007i005p00539.

McDonald, S. E., C. Coker, K. F. Dymond, D. N. Anderson, and E. A. Araujo-Pradere (2011), A study of the strong linear relationship between the equatorial ionization anomaly and the prereversal **EXB** drift velocity at solar minimum, *Radio Sci.*, *46*(6), RS6004, doi:10.1029/2011RS004702.

Millward, G., I. Müller-Wodarg, A. Aylward, T. Fuller-Rowell, A. Richmond, and R. Moffett (2001), An investigation into the influence of tidal forcing on F region equatorial vertical ion drift using a global ionosphere-thermosphere model with coupled electrodynamics, *J. Geophys. Res.*, *106*(A11), 24,733–24,744.

Moffett, R., J. Murphy, and G. Bailey (1975), Storm-time increases in the ionospheric total electron content, *Nature*, *253*, 330–331.

Murphy, C. H., and G. V. Bull (1968), Ionospheric winds over Yuma, Arizona, measured by gun-launched projectiles, *J. Geophys. Res.*, *73*(9), 3005–3015, doi:10.1029/JA073i009p03005.

Murphy, J., and R. Heelis (1986), Implications of the relationship between electromagnetic drift components at mid and low latitudes, *Planet. Space Sci.*, *34*(7), 645–652, doi:http://dx.doi.org/10.1016/0032-0633(86)90042-5.

Nicolls, M. J., and M. C. Kelley (2005), Strong evidence for gravity wave seeding of an ionospheric plasma instability, *Geophys. Res. Lett.*, *32*(5), doi:10.1029/2004GL020737.

Pacheco, E. E., R. A. Heelis, and S.-Y. Su (2011), Superrotation of the ionosphere and quiet time zonal ion drifts at low and middle latitudes observed by Republic of China Satellite-1 (ROCSAT-1), *J. Geophys. Res.*, *116*(A11), A11329, doi:10.1029/2011JA016786.

Patra, A. K., P. P. Chaitanya, N. Mizutani, Y. Otsuka, T. Yokoyama, and M. Yamamoto (2012), A comparative study of equatorial daytime vertical **EXB** drift in the Indian and Indonesian sectors based on 150 km echoes, *J. Geophys. Res.*, *117*(A11), A11312, doi:10.1029/2012JA018053.

Patra, A. K., P. P. Chaitanya, Y. Otsuka, T. Yokoyama, M. Yamamoto, R. A. Stoneback, and R. A. Heelis (2014), Vertical **EXB** drifts from radar and C/NOFS observations in the Indian and Indonesian sectors: Consistency of observations and model, *J. Geophys. Res.*, *119*(5), 3777–3788, doi:10.1002/2013JA019732.

Pingree, J. E., and B. G. Fejer (1987), On the height variation of the equatorial F region vertical plasma drifts, *J. Geophys. Res.*, *92*(A5), 4763–4766, doi:10.1029/JA092iA05p04763.

Prakash, S., and P. Muralikrishna (1981), E and F region electric fields over dip equator, *J. Geophys. Res.*, *86*(A4), 2095–2098, doi:10.1029/JA086iA04p02095.

Ramesh, K., and J. Sastri (1995), Solar cycle and seasonal variations in F-region vertical drifts over Kodaikanal, India, *Ann. Geophys.*, *13*(6), 633–640, doi:10.1007/s00585-995-0633-7.

Rich, F., and S. Basu (1985), *Ionospheric physics, Handbook of Geophysics and the Space Environment*, Air Force Geophysics Laboratory, Bedford, Mass.

Richmond, A. D. (1995), Ionospheric electrodynamics, in, *Handbook of Atmospheric Electrodynamics*, *2*, edited by H. Volland, pp.249–290, CRC Press, Boca Raton, FL.

Richmond, A. D., S. Matsushita, and J. D. Tarpley (1976), On the production mechanism of electric currents and fields in the ionosphere, *J. Geophys. Res.*, *81*(4), 547–555, doi:10.1029/JA081i004p00547.

Rishbeth, H. (1971), Polarization fields produced by winds in the equatorial F-region, *Planet. Space Sci.*, *19*(3), 357–369, doi:http://dx.doi.org/10.1016/0032-0633(71)90098-5.

Rishbeth, H. (1977), Dynamics of the equatorial F-region, *J. Atmos. Sol. Terr. Phys.*, *39*(910), 1159–1168, doi:http://dx.doi.org/10.1016/0021-9169(77)90024-1.

Rishbeth, H. (1997), The ionospheric E-layer and F-layer dynamos a tutorial review, *J. Atmos. Sol. Terr. Phys.*, *59*(15), 1873–1880, doi:http://dx.doi.org/10.1016/S1364-6826(97)00005-9.

Rishbeth, H. (1998), How the thermospheric circulation affects the ionospheric F2-layer, *J. Atmos. Sol. Terr. Phys.*, *60*(14), 1385–1402, doi:http://dx.doi.org/10.1016/S1364-6826(98)00062-5.

Rishbeth, H., and O. K. Garriott (1969), *Introduction to Ionospheric Physics*, 331 pp., Academic Press, New York, NY.

Rodrigues, F. S., G. Crowley, R. A. Heelis, A. Maute, and A. Reynolds (2012), On TIE-GCM simulation of the evening equatorial plasma vortex, *J. Geophys. Res.*, *117*(A5), A05307, doi:10.1029/2011JA017369.

Rodrigues, F. S., E. B. Shume, E. R. de Paula, and M. Milla (2013), Equatorial 150 km echoes and daytime F region vertical plasma drifts in the Brazilian longitude sector, *Ann. Geophys.*, *31*(10), 1867–1876, doi:10.5194/angeo-31-1867-2013.

Rodrigues, F. S., J. M. Smith, M. Milla, and R. A. Stoneback (2015), Daytime ionospheric equatorial vertical drifts during the 2008−2009 extreme solar minimum, *J. Geophys. Res.*, *120*(2), 1452–1459, 2014JA020478, doi:10.1002/2014JA020478.

Sabben, D. V. (1962), Ionospheric current systems caused by non-periodic winds, *J. Atmos. Sol. Terr. Phys.*, *24*(11), 959 – 974, doi:http://dx.doi.org/10.1016/0021-9169(62)90143-5.

Sagawa, E., T. J. Immel, H. U. Frey, and S. B. Mende (2005), Longitudinal structure of the equatorial anomaly in the nighttime ionosphere observed by image/fuv, *J. Geophys. Res.*, *110*(A11), A11302, doi:10.1029/2004JA010848.

Sastri, J. H., V. K. M. Varma, and S. R. P. Nayar (1995), Height gradient of F region vertical drift in the evening equatorial ionosphere, *Geophys. Res. Lett.*, *22*(19), 2645–2648, doi:10.1029/95GL02668.

Scherliess, L., and B. G. Fejer (1999), Radar and satellite global equatorial F region vertical drift model, *J. Geophys. Res.*, *104*(A4), 6829–6842, doi:10.1029/1999JA900025.

Scherliess, L., D. C. Thompson, and R. W. Schunk (2008), Longitudinal variability of low-latitude total electron content: Tidal influences, *J. Geophys. Res.*, *113*(A1), A01311, doi:10.1029/2007JA012480.

Schunk, R., and A. Nagy (2009), *Ionospheres: Physics, Plasma Physics, and Chemistry*, Cambridge University Press, New York, NY.

Sheehan, R. E., and C. E. Valladares (2004), Equatorial ionospheric zonal drift model and vertical drift statistics from UHF scintillation measurements in South America, *Ann. Geophys.*, *22*(9), 3177–3193.

Sobral, J. H., et al. (2011), Midnight reversal of ionospheric plasma bubble eastward velocity to westward velocity during geomagnetically quiettime: Climatology and its model validation, *J. Atmos. Sol. Terr. Phys.*, *73*(11), 1520–1528.

Sridharan, S., S. Sathishkumar, and S. Gurubaran (2009), Variabilities of mesospheric tides and equatorial electrojet strength during major stratospheric warming events, *Ann. Geophys.*, *27*(11), 4125–4130, doi:10.5194/angeo-27-4125-2009.

Stoneback, R. A., R. A. Heelis, A. G. Burrell, W. R. Coley, B. G. Fejer, and E. Pacheco (2011), Observations of quiet time vertical ion drift in the equatorial ionosphere during the solar minimum period of 2009, *J. Geophys. Res.*, *116*(A12), A12327, doi:10.1029/2011JA016712.

Su, Y.-J., J. M. Retterer, O. de La Beaujardire, W. J. Burke, P. A. Roddy, R. F. Pfaff, G. R. Wilson, and D. E. Hunton (2009), Assimilative modeling of equatorial plasma depletions observed by C/NOFS, *Geophys. Res. Lett.*, *36*(18), L00C02, doi:10.1029/2009GL038946.

Torr, D. G. (1979), Ionospheric chemistry, *Rev. Geophys.*, *17*(4), 510–521, doi:10.1029/RG017i004p00510.

Tsunoda, R. T., R. C. Livingston, and C. L. Rino (1981), Evidence of a velocity shear in bulk plasma motion associated with the post-sunset rise of the equatorial F-layer, *Geophys. Res. Lett.*, *8*(7), 807–810, doi:10.1029/GL008i007p00807.

Valladares, C. E., R. Sheehan, S. Basu, H. Kuenzler, and J. Espinoza (1996), The multi-instrumented studies of equatorial thermosphere aeronomy scintillation system: Climatology of zonal drifts, *J. Geophys. Res.*, *101*(A12), 26,839–26,850, doi:10.1029/96JA00183.

Volland, H. (1997), Atmospheric tides, in *Tidal Phenomena, Lecture Notes in Earth Sciences*, vol. 66, pp. 221–246, Springer Verlag, Berlin-Heidelberg.

Wharton, L., N. Spencer, and H. Mayr (1984), The Earth's thermospheric superrotation from dynamics explorer 2, *Geophys. Res. Lett.*, *11*(5), 531–533.

Woodman, R. (1970), Vertical drift velocities and east-west electric fields at the magnetic equator, *J. Geophys. Res.*, *75*(31), 6249–6259, doi:10.1029/JA075i031p06249.

Woodman, R. (1971), East-west ionospheric drifts at the magnetic equator(E region electromagnetic east-west drift velocity measurement at magnetic equator by incoherent scatter radar), *Space Research XII*, pp. 969–974.

Woodman, R., and F. Villanueva (1995), Comparison of electric fields measured at F region heights with 150 km irregularity drift measurements, Ninth International Symposium on Equatorial Aeronomy, Bali, Indonesia.

Woodman, R. F., and T. Hagfors (1969), Methods for the measurement of vertical ionospheric motions near the magnetic equator by incoherent scattering, *J. Geophys. Res.*, *74*(5), 1205–1212, doi:10.1029/JA074i005p01205.

APPENDIX

Figures 1.1, 2.1, 2.2, 3.1, 3.2, 3.3, 3.4, 3.5 and 3.6 are reprinted with permission.

Gmail by Google

Debrup Hui <debruphui@gmail.com>

AUTHOR - Request to reuse my coauthored paper in my PhD dissertation

Wiley Global Permissions <permissions@wiley.com> Thu, Jun 25, 2015 at 9:43 AM
To: Debrup Hui <debruphui@gmail.com>

Dear Debrup Hui,

Thank you for your email.

Permission is granted for you to use the material requested for your thesis/dissertation subject to the usual acknowledgements (author, title of material, title of book/journal, ourselves as publisher) and on the understanding that you will reapply for permission if you wish to distribute or publish your thesis/dissertation commercially.

You should also duplicate the copyright notice that appears in the Wiley publication in your use of the Material. Permission is granted solely for use in conjunction with the thesis, and the material may not be posted online separately.

Any third party material is expressly excluded from this permission. If any material appears within the article with credit to another source, authorisation from that source must be obtained.

Best Wishes

Emma Willcox

Permissions Coordinator

WILEY

CURRICULUM VITAE

Debrup Hui

Education

PhD in Physics, 2015, Utah State University, USA

Dissertation Title: *Altitudinal Variability of Quiet-time Plasma Drifts in the Equatorial Ionosphere.*

MS in Electrical Engineering, 2011, Utah State University, USA

Technical Report Title: *A Model for Rapid Charging Events on International Space Station.*

MS in Physics, 2009, University of Texas at Arlington, USA

Thesis Title: *Moment Calculations for Low Energy ions in Jupiters Magnetotail from NASA's New Horizons Mission.*

MS in Electronic Science, 2003, University of Calcutta, India

Thesis Title: *Patterning of metal films on Glass Substrate by means of Optical Lithography and Selective Etching.*

BS in Electronics, 2001, North Eastern Hill University, India

Journal Publications

Fejer, B. G., D. Hui, J. L. Chau, and E. Kudeki (2014), Altitudinal dependence of evening equatorial F region vertical plasma drifts, J. Geophys. Res. Space Physics, 119, 58775890, doi:10.1002/2014JA019949.

DasGupta, A., A. Das, D. Hui, K. K. Bandyopadhyay, and M. R. Sivaraman (2006), Ionospheric perturbation observed by the GPS following the December 26th, 2004 Sumatra-Andaman earthquake, Earth Planet. Space, 35, 929959.

Research Profile

Jan 2012 present	Graduate Research Assistant at CASS, USU
Jun 2011 - Aug 2011	Research Data Analyst at CASS, USU
Aug 2009 Dec2010	Graduate Research Assistant at ECE, USU
Jan 2008 - Aug 2009	Graduate Research Assistant at Physics, UT, Arlington.
Jun 2007 Aug 2007	Research Fellow in the S. K. Mitra Center for Research in Space Environment, University of Calcutta.
Apr 2006 - May 2007	Project Fellow in the Center for Advance Studies in Radiophysics and Electronics, University of Calcutta.
May 2004 Mar 2006	Project Assistant in the S. K. Mitra Center for Research in Space Environment, University of Calcutta.